Mixed Micelle System: Equilibrium and Kinetics

Anniina Salonen

A thesis submitted for the degree of Doctor of Philosophy
to the
University of Edinburgh

2005

Abstract

Lipid–detergent systems are interesting to study, as the two amphiphiles have very different spontaneous curvature, however readily form mixed micelles in solution. These micelles can be shorter cylindrical micelles or long worm–like micelles. For such a system the size of the micelles varies strongly with solute conditions, being dependent on the total amount of amphiphile in solution, as well as, the lipid to detergent ratio in the micelles.

Although the broad phase behaviour of such systems has been studied and is relatively well understood, there are still many open questions remaining. Some of the questions that motivated the work presented are: how the length and composition of the micelles varies within the micellar region, and how the micelles grow?

The biologically interesting system under study is lecithin and bile salt, where the equilibrium sizes were experimentally determined for different samples within the micellar region. A model, combining the length of the micelles, with the concentrations of lecithin and bile salt in the system is presented, and is used to calculate the composition of the micelles at equilibrium.

The kinetics of the growth of the micelles after a pertubation causing a shift in the equilibrium size has not been studied in detail before. The kinetics of the system are studied using a stopped flow setup, which I specifically designed for neutron scattering experiments. The stopped flow setup allows for the measurement to start 200ms after the initial mixing of the two liquids, after dilution of a solution the micelles relax to a new longer length. The kinetics of this relaxation were studied as a function of the initial and final size of the micelles, as well as, the ionic strength of the solution.

The micelles were found to grow through coalescence, where the rate of growth seems to be constant for different sizes of micelles and the time taken for the relaxation depends on the difference between the final and initial lengths of the micelles. The rate of growth is strongly influenced through changing the ionic strength of the solution, indicating the importance of an electrostatic barrier to the fusion of micelles.

Declaration

I declare that this thesis has been composed entirely by myself and has not been submitted in any previous application for a degree. The work reported has been carried out by me unless otherwise indicated.

Anniina Salonen

Acknowledgements

There are several people without whose support and encouragement the work would never have been possible.

Firstly, I would like to thank my supervisor Stefan Egelhaaf for his enthusiasm and advice throughout the thesis.

I would also like to thank Peter Schurtenberger for allowing me to spend the time as part of his group in Fribourg building the stopped flow setup, for the discussions and help with the neutron scattering experiments. Many thanks to Jacques Leng and Anna Stradner for their patient help with the stopped flow experiments, as well as Joachim Kohlbrecher, Steven van Petegem and Roland May as the instrument responsibles at PSI and ILL.

I have enjoyed working both in Edinburgh and in Fribourg, where I have learnt a lot from everyone around. I would specifically like to thank Mike Cates and Veronique Trappe for useful discussions.

I would also like to acknowledge Oskar Huttusen Säätiö for their financial support in the last three years.

Special thanks to all my friends, especially Mike and Seona for all their support, but mainly for helping me completely forget about work. Seona, also thank you for all the help at the end of the thesis. A huge thank you to François for discussions, advice and for making sure I get to the end.

Lopuksi, kiitokset Äidille, Isälle ja Murulle; olette ihania.

Contents

List of symbols used

a_0 Optimum headgroup area per molecule

a_B Surface area occupied by a bile salt molecule

a_L Surface area occupied by a lecithin molecule

b Kuhn length of micelle

B_1 Fit parameter for the concentration dependence of the length of mixed micelles

B_3 Fit parameter for the concentration dependence of the length of mixed micelles

BS Molar concentration of bile salt

C_0 Mean spontaneous curvature of a surfactant film

C_B Spontaneous curvature of bile salt

C_L Spontaneous curvature of lecithin

c_S Ionic strength of solution (added salt + buffer + bile salt)

c_{Si} Initial ionic strength of solution for kinetic experiments

c_{Sf} Final ionic strength of solution for kinetic experiments

$c(t, L)$ Length distribution of worm–like micelles

CMC Critical micellar concentration

D Detergent concentration in solution (typically bile salt)

D Diffusion constant of cylindrical micelles (only chapter 8)

d_i Initial dilution for kinetic experiments

d_f Final dilution for kinetic experiments

d'_f Nominal final dilution for kinetic experiments

e Electronic charge

E DLVO interaction energy between two approaching worm–like micelles

E_{ec} Endcap energy of a micelle

$E_d(h, \phi)$ Interaction energy between two approaching monolayers of arbitrary curvature

GCDC Glycochenodeoxycholic acid sodium salt

H Hamaker constant

h Distance between two interacting monolayers

k Boltzmann's constant

k^- Backward rate constant of a reaction

k^+ Forward rate constant of a reaction

L Length of a cylindrical or worm–like micelle

$\overline{L}$ Mean length of a cylindrical or worm–like micelle

L_0 Initial length of worm–like micelle (before pertubation to equilibrium)

L_∞ Final length of worm–like micelle

l_c Critical chain length of surfactant molecule

L_{mid} Length of cylindrical part of micelle (i.e. excluding endcaps)

L_{tot} Total length density of middle parts of micelle = $n_{mic}L_{mid}$

LEC Molar concentration of lecithin

$\overline{m}$ Mean aggregation size

N_A Avogadro's number

$\overline{N}_g$ Number of free counterions in solution

$\overline{N}_{g0}$ Flocculation concentration

n_{mic} Number density of micelles

p Dimensionality of aggregates

PC Phosphatidylcholine

PEEK™ A Victrex®polymer

PTFE PolyTetraFluoroEthylene

PVDF PolyVinyliDene Fluoride

Q_{tot} Bile salt to lecithin ration in solution BS/LEC = $1/R_{tot}$

Q_e $1/R_e$

Q_e^m $1/R_e^m$

Q_e^{SOL} $1/R_e^{SOL}$

Q_e^{SAT} $1/R_e^{SAT}$

R Minor axis radius of elliptical cross–section of worm–like micelle

R_{av} Average radius of cylindrical cross–section

R_{tot} Lecithin to bile salt molar ratio in solution (aggregates + bulk solution) LEC/BS

R_e Lecithin to bile salt molar ratio in aggregates (micelles or vesicles)

R_e^m Lecithin to bile salt molar ratio in micelles

R_e^{SOL} Lecithin to bile salt molar ratio in micelles required to solubilise vesicles

R_e^{SAT} Lecithin to bile salt molar ratio at saturation i.e. when some mixed micelles are formed

S Reaction surface

SANS Small angle neutron scattering

T Temperature

t_0 Time constant in the kinetics of worm–like micelles

t_R Time resolution in kinetic experiments

TC Taurocholic acid sodium salt

TCDC Taurochenodeoxycholic acid sodium salt

v_B Volume of a bile salt molecule

v_L Volume of a lecithin molecule

$V_a(h)$ Van der Waals attraction between two surfaces per unit area

V_e^σ Electrostatic repulsion with constant charge between two surfaces per unit area

V_e^ψ Electrostatic repulsion with constant potential between two surfaces per unit area

x Dimensionless concentration variable $(X_{tot} - X_1)/X_1$

X_N Concentration of surfactant molecules in an aggregate of N molecules

X_{tot} Total concentration of surfactant

X_1 Concentration of surfactant monomers

α_e Energy gain of adding a bile salt molecule onto the endcap of a micelle

α_m Energy gain of adding a bile salt molecule onto the cylindrical part of a micelle

γ Surface energy

$\frac{\delta L}{\delta t}$ Rate of increase of the average length of worm–like micelles

ϵ Ellipticity of cross–section

κ_D Debye length

λ Number of lecithin molecules per length of cylindrical axis of a micelle

μ Chemical potential

μ Correction factor for kinetics of ionic surfactants (only section 2.5)

σ Polydispersity in the size of micelles

σ Surface charge density on a micellar surface = $e\phi_r/a_B$

$\frac{\sigma L}{L}$ Polydispersity in the length of the micelles

ϕ_r Surface fraction covered by surfactant molecules on surface r

Φ Total volume fraction of amphiphiles in solution (i.e. lecithin + bile salt)

Φ_b Volume fraction of bile salt in bulk (including monomers and simple micelles)

Φ_e Volume fraction of bile salt in endcaps

Φ_m Volume fraction of bile salt in cylindrical parts

ψ_e Electrostatic potential on the surface of the endcap per kT

ψ_m Electrostatic potential on the surface of the cylindrical part of a micelle per kT

ρ_B Number density of bile salt molecules in micelles

ρ_L Number density of lecithin molecules in micelles

τ_{rep} Characteristic time scale for the reptation of polymers

τ_{break} Characteristic time scale for the breaking of worm–like micelles

τ_{uf} Ultrafast relaxation time constant for simple micelles

τ_f Fast relaxation time constant for simple micelles

τ_s Slow relaxation time constant for simple micelles

$\tau_e s$ Extremely slow relaxation time for simple micelles

τ_{s1} Slow relaxation time constant due to monomer exhange

τ_{s2} Slow relaxation time constant due to coalescence of micelles

τ Characteristic time constant for the growth (shrinking) of worm–like micelle

τ_{coal} Rate of coalescence of micelles per volume

0.1 Neutron Scattering

λ Wavelength of radiation

θ Angle of scattering

q Scattering wave vector

r Separation between scatterers

ω Angular frequency of radiation

$E(q,t)$ Scattered amplitude of the radiation

$I(q,t)$ Scattered intensity of radiation

N Number of scatterers per unit volume

$\rho(0)$ Scattering length density of scatterers at q = 0

$P(q)$ Form factor of the scattering particles

$S(q)$ Structure factor of the scattering particles

a Scattering length

M Molecular mass

V Volume of molecule

ρ Scattering length density

$B_g = I_{Cd}$ General background scattering intensity

$I_X(q,\lambda)$ Measured intensity

$C(\lambda)$ Instrument dependent parameter

T_X Transmission of the sample

e_X Path length of radiation through sample

σ_X Differential scattering cross–section per unit volume

$B(\theta)$ Scattering by the walls of scattering cell

PSI Paul Scherrer Institute

SANS-I Small angle instrument at PSI

ILL Institute Laue Langevin

D22 Small angle instrument at ILL

Chapter 1

Introduction

1.1 Amphiphilic Molecules

Although the word amphiphile or surfactant might not be familiar to people not acquainted with chemistry or soft matter physics, these molecules are found everywhere around us: food products, cosmetics, technology, biological systems.

As the name suggests 'amphi-' from Greek meaning both and 'phile' from *philos* loving, these molecules love both polar liquids like water, and unpolar liquids like oil. This is because they are composed of two parts, one water–loving and the other water–hating (oil–liking) as shown in figure 1.1.

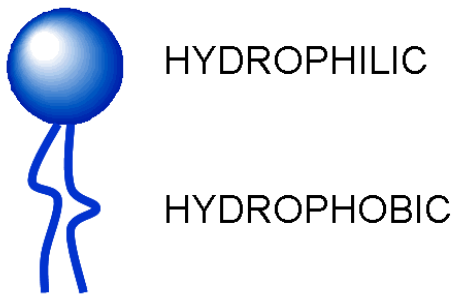

Figure 1.1: Hydrophobic and hydrophilic parts of the amphiphile.

Their unique properties arising from their two part structure mean that they like to sit at the interface between oil and water (hence the name SURFace ACTive), where they can have the hydrophobic parts in oil and the hydrophilic parts in water. In milk it is amphiphilic molecules that stabilise the fat in the water. This principle is also the basic idea behind the workings of soaps and shampoos, where the hydrophobic parts will seek the grease and oil and the surfactant will encase the oil and carry it away with the water.

An important property of surfactants is that they are able to self–assemble to form many different types of aggregate. As an example, when added to water they will want to protect the hydrophobic parts. Some of the aggregates that surfactants can form in water are shown in figure 1.2 from spherical micelles (A) to long cylindrical micelles (B) to bilayers (C) and inverted micelles (D).

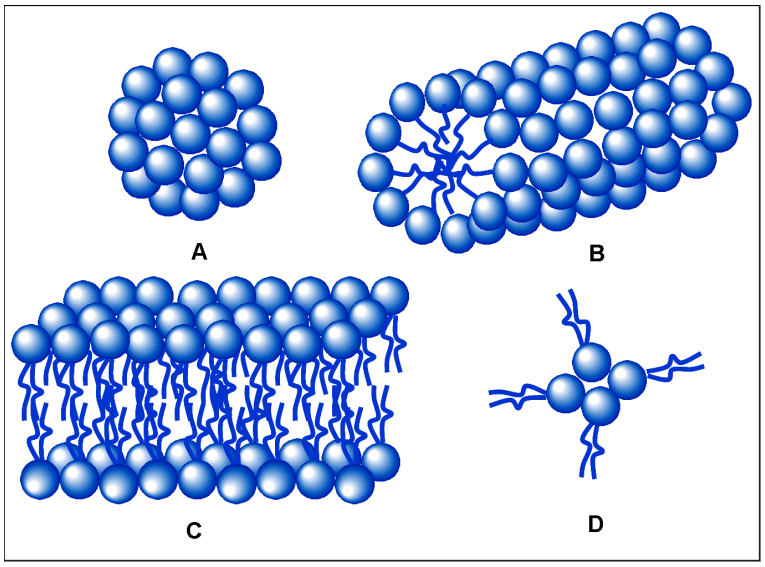

Figure 1.2: Aggregates formed by amphiphiles in water.

If the bilayers become large enough they can bend to close up on themselves and form double layered vesicles. In fact biological cells are basically vesicles, however composed of many different amphiphiles with many other molecules included in the bilayers.

The types of aggregate that are formed can be controlled through external parameters or through the use of a mixture of two or more amphiphiles, with different preferred aggregates. The

subject of this thesis is to study the equilibrium and kinetic behaviour of mixtures of two amphiphiles: lecithin and bile salt. These two readily form micelles, which are found in human bile, where one of their functions is to carry around cholesterol and other lipids.

There is interest in lipid–detergent systems, as not only do they form micelles together but under suitable conditions can also form vesicles. There is growing interest in using vesicles and micelles as drug carriers, which means that understanding their formation and behaviour is of importance. The lecithin–bile salt system is also of academic interest as it serves as a model mixed micelles system.

However, despite a lot of work, there are still many unanswered questions on the formation of these mixed micelles, their composition and in the understanding of the size dependence. It is important to understand the basic physics behind these systems as this can lead to more efficent products.

Aside from the equilibrium behaviour, the kinetic processes in the systems are even less understood. When solution conditions or the concentration of amphiphiles change the micelles can change their shape and size. In biological systems the outer conditions often change, such as when bile salt is secreted in the bile it is in a concentrated environment, but upon entering into circulation, it is diluted. The processes of growth for mixed micelle systems are still largely unexplored.

It is trying to understand how these micelles form, what determines the shape of micelle that they form, and what the processes of growth of the micelles upon change in the external conditions, that form some of the questions motivating the work of this thesis.

1.2 Outline of Thesis

Chapter 2 starts with an introduction into the background of amphiphile behaviour in water and aggregates made of a single surfactant type, discussing the equilibrium and kinetic behaviour of the systems. Chapter 3 discusses the equilibrium and kinetics of two–component aggregates, mainly lipid–surfactant systems. The basics of small angle neutron scattering (SANS) and data treatment are explained in chapter 4, with a brief overview of the data fitting routines used. The

preparation of the experimental samples is detailed in chapter 5. Carrying out time resolved experiments into the kinetics of the micellar growth requires a stopped flow setup, where two liquids can be mixed and consequently the changes in the system followed. There does not exist a suitable stopped flow for SANS experiments, so one was designed and constructed. The construction and commissioning of the stopped flow setup for use with the SANS experiments is explained in chapter 6. The equilibrium experiments are discussed in chapter 7, starting with the results from SANS experiments followed by the description of a model to calculate the composition of the micelles (i.e. how the lecithin and bile salt partition in the micelles and in solution). The model is then compared to data from literature. Kinetic experiments and results using the stopped flow setup are detailed in chapter 8. Chapters 9 and 10 conclude the thesis and outline some ideas for future work.

Chapter 2

Surfactant Aggregation: Single Component Aggregates

Hydrophobic molecules are substances that - although soluble in many non-polar solvents (such as alcohols or oil), are barely soluble in water. Molecules that like the polar solvents (such as water) are called hydrophilic.

Amphiphiles consist of a hydrophobic (or 'water hating') and a hydrophilic ('water loving') part such as shown in figure 2.1. Commonly the hydrophilic part is referred to as the 'head' and the hydrophobic as the 'tail', where the tails are made of hydrocarbons. The effect of adding amphiphilic molecules into water is shown in figure 2.1 [1].

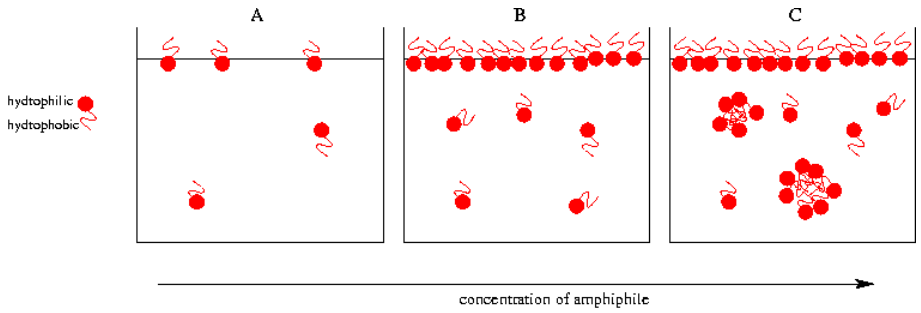

Figure 2.1: Addition of amphiphile to water.

Starting with a low concentration of surfactant (figure 2.1 A.), the surfactant partitions between

the surface and solution, as on the surface it can get its tails out of water. Increasing the amount of surfactant in solution, and as the surface becomes crowded (figure 2.1 B.), at a certain concentration the surfactants will start to self-assemble – again to keep the hydrophobic tails out of contact with water (figure 2.1 C.). The aggregates formed will have the hydrophobic tails together shielded by the hydrophilic head-groups, which will remain in contact with water. In figure 2.1 simple micelles are shown. The concentration around which micelles start to form is called the critical micellar concentration (CMC).

However, micellisation cannot be explained purely in terms of the hydrophobic effect, as the attractive forces arising from the surface tension between the hydrophobic parts and water are called. In surfactant systems there are various competing terms in the free energy of the formation of the micelles. There is a surface term, which includes the interactions of the head-groups (attractive - arising from the hydrophobic effect, and repulsive - electrostatic, hydration or steric hindrance) and a packing term, (depends largely on the geometry of the micelles) which requires the resulting shape to exclude water from the interior, whilst accommodating the hydrophilic groups on the surface. Some of the different forms of micelle are shown in figure 1.2: spherical micelles, long cylindrical (or worm–like) micelles, flat bilayers and inverted structures, with decreasing spontaneous curvature. Average spontaneous curvature of the aggregate is defined as the average curvature of the aggregate, hence for spherical micelles the spontaneous curvature is 1/radius of micelle and it goes down to zero for flat bilayers.

The surfactant monomers are only weakly bonded together, so changing the solution conditions will not only change the interactions between the aggregates, but also the interactions within. This means that it is crucial to understand why the structures form in the first place before reflecting and developing theories on their subsequent behaviour.

2.1 Partitioning of surfactant between surface and water

The partitioning of the surfactant molecules between an aqueous solution and another fluid (air,oil) phase has been modelled by Diamant and Andelman [2] through free energy arguments, where the entropy of mixing between bulk and surface, as well as the interactions on the surface

are taken into account. When the kinetics of adsorption onto the surface are much faster than the diffusion of the molecules, local equilibrium can be assumed. This holds for non-ionic surfactants or ionic surfactants with added salt. A Davies isotherm [3] can be used to describe the equilibrium partitioning between the volume fraction of surfactants in bulk solution Φ_b (away from the surface) and the area fraction ϕ_r covering the surface,

$$\phi_r = \frac{\Phi_b}{\Phi_b + e^{-(\alpha+\psi_0)/kT}} \tag{2.1}$$

where α is energy gain of adding a surfactant molecule onto the surface and ψ_0 the potential on the surface (electrostatic potential for ionic surfactants). All the surfactant in the bulk is assumed to exist as monomers. The particular values of α and ψ_0 depend on the surfactants used and the interfacial surface.

2.2 Thermodynamic model for micelle formation

The properties of micelle formation can be studied in terms of separation of the amphiphiles into different phases, in solution and in aggregates (of different sizes). Equilibrium thermodynamics require that the chemical potential of a type of molecule in different phases be equal. This means that the chemical potential (μ) of the surfactant in monomers and in aggregates must be equal in equilibrium, which can be denoted as [4]:

$$\begin{aligned} \mu = \quad & \underbrace{\mu_1^0 + kT \ln X_1}_{\text{monomers}} = \quad \underbrace{\mu_2^0 + \tfrac{1}{2}kT \ln \tfrac{1}{2}X_2}_{\text{dimers}} \quad = \underbrace{\mu_3^0 + \tfrac{1}{3}kT \ln \tfrac{1}{3}X_3}_{\text{trimers}} = ... \end{aligned} \tag{2.2}$$

This can be written alternatively as

$$\mu = \mu_N = \mu_N^0 + \frac{kT}{N} \ln \frac{X_N}{N} = \text{const} \quad N = 1, 2, 3, ... \tag{2.3}$$

where μ_N is the mean chemical potential of a molecule in an aggregate of N monomers, μ_N^0 is the standard part of the chemical potential of a molecule in an aggregate of aggregation number

N (i.e. mean interaction free energy of individual molecules) and X_N is the concentration of molecules in aggregates of N molecules. Here $N = 1$, μ_1^0 and X_1 refer to the molecules in solution i.e. monomers.

Using the monomeric form as a reference state, equation 2.3 can be rewritten as

$$X_N = N(X_1 e^{(\mu_1^0 - \mu_N^0)/kT})^N. \tag{2.4}$$

The conservation of concentration leads to an expression for the total surfactant concentration C

$$C = \sum_{N=1}^{\infty} X_N. \tag{2.5}$$

The equilibrium of the aggregates (equation 2.4) and the conservation relation (equation 2.5) completely define the system.

If, it is assumed that μ_N^0 does not depend on N (i.e. $\mu_1^0 = \mu_2^0 = .. = \mu_N^0$) equation 2.4 would result in $X_N = NX_1^N$. As $X_1 < 1$, so $X_N \ll 1$, and most of the molecules would remain in solution as monomers. Thus the requirement for aggregate formation is that there exist a difference in the chemical potentials of the surfactants in solution and surfactants in the micelles.

The condition for the formation of larger aggregates is $\mu_N^0 < \mu_1^0$. It can be shown [4] that the interaction free energy of the molecules (μ_N^0) can be expressed in terms of the 'bulk' energy of a molecule in an infinite aggregate (μ_∞^0), the intermolecular interactions (α), and through arguments of unbonded end/surface monomers: the dimensionality of the aggregates p as

$$\mu_N^0 = \mu_\infty^0 + \frac{\alpha kT}{N^p}, \tag{2.6}$$

where p = 1 for one dimensional linear aggregates (such as cylindrical micelles) and decreases to 1/2 for disks or sheets, and to 1/3 for spheres.

2.2.1 Critical Micellar Concentration

The equilibrium in the chemical potentials equation 2.4, the conservation of concentration equation 2.5 and the condition for aggregate formation equation 2.6 can be combined as

$$X_N = N(X_1 \mathrm{e}^{\alpha(1-1/N^p)})^N \tag{2.7}$$

For low monomer concentrations (such that $X_1\mathrm{e}^{\alpha} \ll 1$) $X_1 > X_2 > X_3 > ... > X_N$ for all α and most of the surfactant molecules are in the monomeric state.

For disks or spheres equation 2.7 approximates to $X_N = N[X_1\mathrm{e}^{\alpha}]^N\mathrm{e}^{-\alpha N^p}$. This means that there will exist very few aggregates of appreciable size. Above the CMC, there is a phase transition to an aggregate of infinite size.

However for cylindrical aggregates (p = 1) $X_N = N[X_1\mathrm{e}^{\alpha}]^N\mathrm{e}^{-\alpha}$, this independence of the second exponential on N leads to a broad distribution of micellar sizes where at very large N the concentration of aggregates approaches zero [4]. This will be explored in further detail in the following section.

2.2.2 Size distribution of micelles

At low and high surfactant concentration regimes (with p = 1) the expectation value of the size of the aggregates $< N >$ can be calculated using the total concentration of surfactant C, and the monomer concentration X_1 as a reference state as [4]

$$< N >= \sqrt{1 + 4C\mathrm{e}^{\alpha}}. \tag{2.8}$$

When C is small (i.e. below the CMC) this can be approximated as 1 and all the surfactant molecules exist as monomers in solution. At large concentrations $< N >\approx 2\sqrt{C\mathrm{e}^{\alpha}}$, leading to a $C^{1/2}$ dependence for the size of the aggregates.

Through similar arguments the density distribution of the aggregates can be given by [4]

$$X_N/N = \text{Const.} \quad \mathrm{e}^{-N/M} \quad \text{for} \quad N > M, \tag{2.9}$$

where M (=$\sqrt{C\mathrm{e}^{\alpha}}$) is the size of aggregates with the highest number density.

The average size of the micelles increases with increased concentration ($C^{1/2}$ dependence), which is called 'concentration induced growth'. The concentration of large aggregates decays exponentially for increasing N with a characteristic decay number M. This leads to a very broad distribution in the sizes of the cylindrical micelles.

2.3 Determination of the shape of the micelles

Having discussed the formation of the micelles, it has still not been explained how the shape of the micelles is chosen. The particular conformations are determined by a delicate balance of forces; the two opposing forces at the interface of the hydrophobic core and the hydrophilic head group govern the self-assembly of the molecules. The attractive hydrophobic forces want to minimise the surface area of the interface, so as to protect the hydrophobic groups, whilst the repulsive headgroup interactions want to maximise the distance between headgroups.

The hydrophobic effect can be represented by a positive surface energy per headgroup area, and its contribution to μ_N^0 written as γa, where γ is the surface energy (or tension), and a is the headgroup area. Typical values range from 20mJm^{-2} to 50mJm^{-2} [4].

The repulsion between the headgroups arises from hydration, steric and ionic (if the headgroups are charged) effects. These repulsive contributions are too difficult to formulate explicitly, but they are expected to be inversely proportional to the headgroup area i.e. a^{-1} [4].

Therefore, the total interfacial free energy per molecule in an aggregate may be written, to first order, as

$$\mu_N^0 = \gamma a + \frac{K}{a}, \tag{2.10}$$

where K is a constant. It is assumed that both forces (the interfacial attraction and the headgroup repulsion) act in the same plane at the hydrophobic-hydrophilic interface. The minimum

energy is hence found when $\delta\mu_N^0/\delta a = 0$, which gives,

$$\mu_N^0(\text{min}) = 2\gamma a_0, \qquad a_0 = \sqrt{K/\gamma}, \tag{2.11}$$

where a_0 is the optimum headgroup area per molecule i.e. the area required by the headgroup on a micellar surface. The total interfacial energy can now be written in terms of a_0 as

$$\mu_N^0 = 2\gamma a_0 + \frac{\gamma}{a}(a - a_0)^2 \tag{2.12}$$

where the unknown constant K has been eliminated. This implies that the interactions have a minimum at a_0 around which the energy varies parabolically. These equations ignore various second-order effects which can become very important (for further information see [4].)

2.3.1 Packing in surfactant assemblies

As explained previously surfactants assemble into a variety of structures. Geometric or 'packing' properties can be used to understand the shape of the favoured structures, as any structure will need to shield the hydrocarbon tails from contact with water, whilst fitting all the hydrophilic heads on the surface of the micelle. The packing properties will be discussed in terms of the following parameters: optimal headgroup area a_0, volume v of the hydrophobic part and the critical chain length l_c (roughly the length beyond which the hydrophobic tail cannot extend whilst still being considered fluid).

The critical length l_c can be approximated as the fully extended molecular length of the hydrocarbon chain, however in practice l_c should be less than this. The length and volume of the hydrophobic part can be estimated for hydrocarbons (with a linear, saturated C-H chain) from the number of hydrocarbons n in the amphiphile according to [1]

$$\begin{aligned} l_c &\leq\approx (1.54 + 1.265n)\text{Å} \\ v &\approx (27.4 + 26.9n)\text{Å}^3. \end{aligned} \tag{2.13}$$

There are many different geometries of aggregates which could fulfil the above packing constraints. However, the actual shape chosen is determined by a balance between entropy, which favours small aggregates, and energy considerations: smaller structures might only be possible with a headgroup area greater than a_0, which would be energetically unfavourable.

The geometric parameters can be combined into a dimensionless packing parameter, $P = v/a_0 l_c$ [4], which can be used to determine the exact shape of the micelles formed. The criteria for different shapes will be explained below.

Spherical Micelles

To form spherical micelles, the optimal surface area must be large enough and the volume of the hydrophobic part small enough that the radius of the micelle will not exceed the critical chain length. For a spherical micelle with an aggregation number of N and radius R, the total volume and surface area are given by:

$$\begin{aligned} Nv &= \frac{4\pi}{3}R^3 \\ Na_0 &= 4\pi R^2. \end{aligned} \tag{2.14}$$

The radius R (= $\frac{3v}{a_0}$) must be less than l_c and hence the packing parameter P must be

$$P = \frac{v}{a_0 l_c} \leq \frac{1}{3}. \tag{2.15}$$

Surfactants with small tails and/or large headgroups will pack into spherical micelles. This includes surfactants with charged headgroups where the repulsion leads to an increase in the optimal headgroup area a_0.

Cylindrical Micelles

Using similar arguments of surface area and volume of cylindrical micelles leads to packing parameters $\frac{1}{3} < \frac{v}{a_0 l_c} < \frac{1}{2}$. This means that surfactants with smaller headgroups than ones

discussed above will form cylindrical micelles where the surface area to hydrophobic volume ratio is smaller. The size dependence (or length dependence) and equilibrium properties of cylindrical micelles are further discussed in section 2.4.

Bilayers, Vesicles and Inverted Structures

Amphiphiles that form bilayers or vesicles (bilayers that have closed up on themselves) have even smaller headgroups and/or larger hydrophobic parts (such as lecithin with two hydrophobic tails), such that $\frac{1}{2} < \frac{v}{a_0 l_c} < 1$. There are many different ways in which the bilayers can join up to form very complicated three-dimensional structures depending on the amphiphiles used and the solution conditions [5].

At packing numbers greater than 1 inverted structures are formed, such as shown in figure 1.2 (D).

2.3.2 Spontaneous Curvature

Another way of looking at the formation of aggregates of different shapes is using Helfrich's descriptions in terms of spontaneous curvature, where the arguments are based on the bending of fluid sheets [5]. The mean spontaneous curvature C_0 of a surfactant film is defined as

$$C_0 = \frac{1}{R_1} + \frac{1}{R_2}, \tag{2.16}$$

where R_1 and R_2 are the main radii of curvature of the surface. This means that for a sphere with radius R_s, $C_0 = 2/R_s$, for a cylinder with a cross-sectional radius of R_c and as the longitudinal component has zero curvature $C_0 = 1/R_c$. Bilayers are flat, with no curvature and hence $C_0 = 0$.

The discussion on the effects of the curvature on the shape of the surfactant aggregates is briefly discussed for systems consisting of two amphiphiles of competing curvatures (such as lecithin and bile salt) in section 3.2.1.

2.4 Cylindrical and worm–like micelles

Cylindrical or worm–like micelles encompass all the micelles which arise from packing fractions between 1/3 and 1/2; from short rod-like micelles to entangled solutions of long polymer-like micelles. The micelles can be considered as consisting of long cylindrical middle parts with two more curved (spherical) end–caps. The creation of these highly curved end–caps is energetically costly for a micelle, where the surfactants would prefer to stay in a cylindrical shape.

At increasing concentrations of surfactants in solution, larger micelles are expected (due to growth through mass-action effects). Spherical micelles cannot do this without creating a hole in the middle, however, cylindrical micelles can, and do, grow longer.

The longer worm–like micelles are often discussed in the language of polymer physics [6], and are sometimes called living polymers, as the micelles are continuously breaking up and joining together. This means that their molecular weight distribution is in thermal equilibrium, and the size distribution of worm–like micelles has been calculated by Cates and Candau [7].

The fusion of two micelles (L_1 + L_2 = L_{1+2}) will result in an energy gain through the loss of two endcaps (two micelles have four endcaps whereas the resulting micelle only has two). The resulting gain in energy is equivalent to the energy cost of creating two endcaps $2E_{ec}$ (except in sign), where E_{ec} is the energy cost of creating an endcap. The endcap energy depends on the average spontaneous curvature and can increase to very high values when the spontaneous curvature is low (obviously if the spontaneous curvature becomes too small the surfactants will assemble as bilayers or vesicles instead). If the endcap energy is sufficiently large the micelles can become very long with average lengths of micrometres [8].

However this gain in endcap energy is balanced by a loss in translational entropy; two micelles moving independently are replaced by one. Using a mean-field (or Flory-Huggins) approach these two competing terms can be taken into account [7] and the number density of chains of length L, $c(L)$ can be described as

$$\begin{aligned} c(L) &\propto e^{-L/\overline{L}}, \\ \overline{L} &\simeq \sqrt{\Phi e^{E_{ec}/kT}}, \end{aligned} \tag{2.17}$$

where $\overline{L}$ is the mean length of the micelles, and Φ is the total volume fraction defined by $\Phi = \sum_L Lc(L)$. Equation 2.17 is directly comparable to equation 2.8 (at high concentrations) as $L \propto N$ and $\bar{L} \propto M$ and α relates to the endcap energy of the micelles E_{ec}. The surfactant molecules in aggregates are still free to move, and the micelles can fuse or break apart, which means that the exact size of a micelle changes in time. It is also assumed that the micelles do not close upon themselves to make ring-like micelles. At low concentrations the result coincides with the law of mass action for inflexible micellar rods [7].

There has been some disagreement with experimental results on the power of $\Phi^{1/2}$ term. It has been found to agree with data for systems which exhibit weak growth [9]. But, the power can change dramatically for ionic surfactants with low added salt concentrations, where the charge distribution on the micelles might have to be taken into consideration [10]. It has been found that charged cylindrical micelles exhibit three regimes of growth of the aggregates, where the growth law changes for increasing concentrations of surfactant and/or electrolyte and only at higher surfactant concentrations is a power-law-type growth obtained [11].

As the micelles grow to longer lengths, with finite bending rigidity, their flexibility becomes more measurable [12]. The elastic energy cost dE_{ee} of bending a length element dL of a cylinder to curvature C is

$$dE_{ee} = \frac{1}{2} K C^2 dL, \tag{2.18}$$

where K is the rigidity modulus. This results in a characteristic length as a measure of the flexibility l_c, called the persistence length

$$l_c = \frac{K}{kT}. \tag{2.19}$$

The persistence length separates the shorter length scale over which the micelle is essentially a rigid rod and the longer length scale where it is more like a flexible polymer with the conformation corresponding to a random walk. This separation of length-scales, which holds for sufficiently long flexible micelles, allowed for the early measurement of the rigidity and length of micelles using neutron scattering methods [13, 14]. There exist more advanced models for analysis of neutron scattering data of worm–like micelles for which see chapter 4.

The dynamics of worm–like micellar solutions have also been studied based on the reptation model developed for polymers [6]. After a small pertubation to the system, the polymers can relax by diffusion along a tube created by the presence of the other polymers, also called 'reptation'. The relaxation has a characteristic time scale τ_{rep}, dependant on the length of the polymers and their diffusion constant.

In addition to relaxation through reptation the micelles can also break or recombine, leading to another characteristic time scale τ_{break}, describing the lifetime of a micelle of mean length [7].

If $\tau_{break} \gg \tau_{rep}$ then the resulting relaxation is simply controlled by τ_{rep}, but as τ_{break} decreases a single exponential decay to equilibrium is expected with $\tau = (\tau_{break}\tau_{rep})^{1/2}$ [15]
.

This theory was extended by Cates *et al*. [15] to stiff rod-like micelles, which can undergo angular relaxation and translational diffusion, in addition to reversible breaking and reptation, after a pertubation. The angular relaxation and translational diffusion are found to depend on the breaking time of the micelles, with different regimes found for fast and slow breaking times of the micelles.

2.5 Kinetics of Micellar Formation

Even at equilibrium the micelles are dynamic units, which as such form and break continuously, and this means that they are very sensitive to changes in solution properties. There has been a lot of interest in the kinetics of micellar formation, i.e. when micelles are subjected to a change in conditions how do they relax to their equilibrium state.

It is generally believed that, although there are various mechanisms through which micelles could relax after a pertubation, there are two dominating routes of relaxation observed experimentally [16]:

- monomer exchange
- coalescence or breakup of micelles

The growth (or shrinking) of the micelles through monomer exchange can be denoted as

$$X_1 + X_{n-1} \rightleftharpoons X_n, \tag{2.20}$$

i.e. the increase (decrease) in the number of micelles X_n, made up of n surfactant molecules, can be achieved by the incorporation (ejection) of monomers, whose concentration is X_1.

The coalescence or fission of micelles can be written as

$$X_n + X_m \rightleftharpoons X_{n+m}. \tag{2.21}$$

Where X_{n+m} is a micelle created through the fusion of two smaller micelles X_n and X_m, and in reverse, X_n and X_m are created from the fission of a micelle of X_{n+m}.

The kinetics of the micellar processes have been extensively studied since the 1960's using various techniques (NMR, EPR, T-jump, P-jump, etc. [17] and references within). Experimentally four different relaxation regimes have been found, with very different characteristic time constants τ: ultrafast τ_{uf} [18, 19], fast τ_f [17], slow τ_s [17] and extremely slow τ_{es} [20].

The ultrafast regime is observed with surfactant molecules with high CMCs. The relaxation has a time constant τ_{uf} of about 10^{-10}s, and is attributed to reactions of monomers with the submicellar structures (aggregation number < 10) which are present in higher concentrations of surfactants with high CMCs [18].

The fast regime and the slow regime were the first relaxation processes discovered and have been studied both experimentally and theoretically in more detail [17, 21, 22, 23]. These will

be discussed further later on, but they arise from the initial adjustment of the monomer concentration (fast) and the attainment of equilibrium micellar size through changes in the proper micelles (slow). The characteristic time constant for the fast regime τ_f is in the range of microseconds, and for the slow regime τ_s in the range of milliseconds.

The extremely slow relaxation regime (τ_{es} from seconds to hours) is observed with relaxation after large deviations from equilibrium [20]. After a suitable change in conditions where the CMC of the surfactant is decreased, the excess monomers quickly transfer into the existing micelles. This results in micelles in excess of the equilibrium size with only a small population of monomers and oligomers. Hence the equilibration of these large micelles through monomer exchange is very slow [20, 24].

In the next section the slow and fast relaxation regimes will be examined in more detail, starting from a model where only the possibility of growth (breakup) through monomer exchange is assumed. This is then extended to include reactions between the micelles, through fusion and fission.

2.5.1 Aniasson-Wall Model

An initial theoretical explanation for the formation of micelles was put forward by Aniasson and Wall (Stepwise association model [21, 22]) where it was assumed that after a perturbation micelles can only grow through monomer exchange.

The fast and slow relaxation processes can be schematically described as shown in figure 2.2 (adapted from [25].)

The fast relaxation process is attributed to the change in the monomer concentration of the system, the exchange of monomers between the bulk and the micelles is very fast. Hence this step toward equilibrium occurs within μs. During the process the mean aggregation number of the micelles changes, but the actual number of the micelles does not.

For the slow process it is instructive to look at the system as two subsystems (monomers and micelles) joined together by a region with a low concentration of micelles (aggregation numbers between X_1 and X_m). The total number and aggregation number of the micelles now have

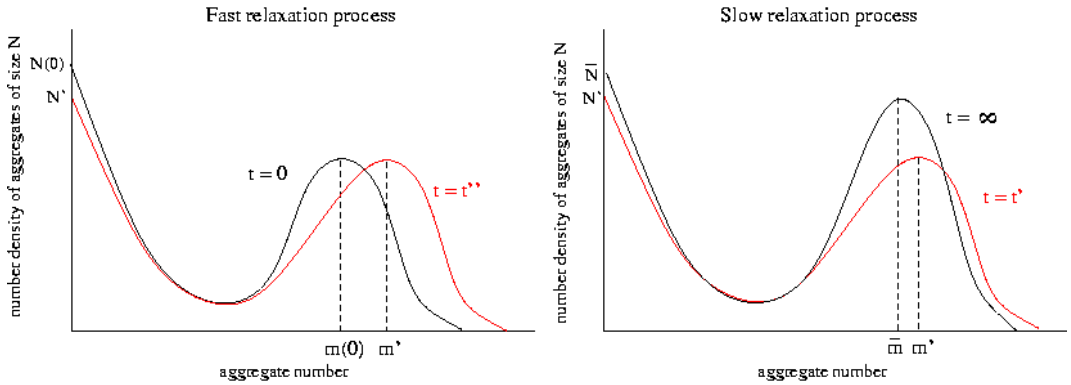

Figure 2.2: The relaxation processes in a micellar system

to be changed, and this can only occur through complete breakdown or formation of the micelles through the middle part of the distribution (where the concentration is very small). This multi-step process takes a much longer time than the rearrangement of monomers, leading to a longer relaxation time.

Theoretically the time constants for the two relaxation processes can be found using an analogy between heat conduction and the rearrangement process [21, 22]. The system is regarded as two reservoirs (monomers and micelles) connected by a region with high resistance (very few aggregates). The fast relaxation process can be described as initial pseudo-equilibrium in the two reservoirs followed by a slow movement through the connecting 'tube' with finite resistance (slow relaxation).

Through comparison with flow equations the theoretical form for τ_f can be found [23] in terms of the concentration of surfactant and the backward rate constant of equation 2.20 k^-

$$\frac{1}{\tau_f} = \frac{k^-}{\sigma^2} + \frac{k^- x}{N}, \tag{2.22}$$

where σ is the polydispersity in the size of the micelles, and N the average aggregation number of the micelles, x is a dimensionless concentration variable given by $(X_{tot} - \overline{X}_1)/\overline{X}_1$ where X_{tot} is the total concentration of surfactant, and $\overline{X}_1$ is the equilibrium concentration of monomers.

From equation 2.22 a linear dependence between τ_f^{-1} and X_{tot} is expected and indeed reasonable agreement with experiments is found [23], although the experiments were carried out with ionic surfactants and the analysis is strictly only valid for non-ionic surfactants [25].

Lessner *et al*. [25] extended the analysis to include ionic surfactants. For ionic surfactants it is assumed that the counterions move much more easily than the surfactants and adjust almost instantly to the movement of the latter. The fast relaxation time constant was now found to be

$$\frac{1}{\tau_f} = \frac{k^-}{\sigma^2} + (1+\mu)\frac{k^- x}{N}, \tag{2.23}$$

similar to equation 2.22, but with an extra term (1 + μ) where μ is a variable dependent on the number of free monomers, the number of free counterions and the effective degree of dissociation in the aggregates.

This result has been applied to different surfactant systems and found to be in good agreement with the ionic strength dependence of the fast time constant [25].

The predictions of the Aniasson-Wall model for the slower relaxation time were only in qualitative agreement with experimental data [26]. In particular the observation of an unexplained minimum in τ_s for ionic surfactants with increasing ionic strength, led Lessner *et al* [25, 27] to propose a new model. They assumed two possible relaxation paths for the slower relaxation time, and extended it for use with ionic or non-ionic surfactants. It was assumed that, as well as relaxation through monomer exchange (equation 2.20), the micelles could fuse or fission (equation 2.21), whilst the interactions are treated using the DLVO theory [5]. This means that at higher added ionic strengths the repulsion between the ionic micelles would be effectively screened and the micelles could fuse.

The slow relaxation time is now divided up into two distinct regimes, the slow relaxation time due to monomer exchange is denoted as τ_{s1}, and the time constant from the micelle coalescence is τ_{s2}. The inverse of the observed slow relaxation time τ_s is then the sum of the two processes

$$\frac{1}{\tau_s} = \frac{1}{\tau_{s1}} + \frac{1}{\tau_{s2}}. \tag{2.24}$$

The extension based on the Aniasson-Wall model can now be used to calculate relaxation times for τ_{s1} and τ_{s2} in terms of the total concentration of surfactant, added ionic strength and the distribution of the micellar sizes for large concentrations (and large aggreagates) [25, 27]

$$\frac{1}{\tau_{s1}} = M\frac{(1+\mu)x^p}{1+(1+\mu)(\sigma^2/\overline{m})x}(\overline{N}_g/\overline{N}_1)^{-q}, \tag{2.25}$$

where x is a dimensionless concentration variable, $\overline{m}$ is mean aggregation size, $\overline{N}_g$ is the number of free counterions and $\overline{N}_1$ the equilibrium number of surfactants in solution. M, p and q are fit parameters, where p and q depend on $\overline{m}$ and the degree of dissociation of the aggregates.

The time constant for growth by coalescence is given by [27]

$$\frac{1}{\tau_{s2}} = \frac{\beta_0\overline{m}X}{1+(\sigma^2/\overline{m})X}\left(\frac{\overline{N}_g}{\overline{N}_{g0}}\right)^s \tag{2.26}$$

where β_0 is depends on the potential barrier for fusion, $\overline{N}_{g0}$ refers to the flocculation concentration (i.e. concentration at which the micelles would coalesce extremely rapidly) and s is a function of the surface potential of the micelles and the charge of the counterions. For τ_{s2} the (1+μ) term has been left out as the correction is only required at low ionic strengths, when $\overline{N}_g/\overline{N}_{tot} \ll 1$, μ is very small compared with one and has a negligible effect on the time constant.

The form of τ_s against the ionic strength of the solution is shown in figure 2.3.

As illustrated in Figure 2.3, at low ionic strengths τ_{s1} dominates due to the high repulsion between the aggregates and the main relaxation pathway is through monomer exchange. This contribution decreases with increasing ionic strength due to the lower solubility of the monomers in the solution. At higher ionic strengths τ_{s2} becomes dominant increasing with ionic strength as the repulsion between the aggregates is further screened. It levels off as the added ionic strength approaches $\overline{N}_{g0}$, the onset of rapid coagulation.

The theory has been verified by p-jump experiments with good agreement [25, 27].

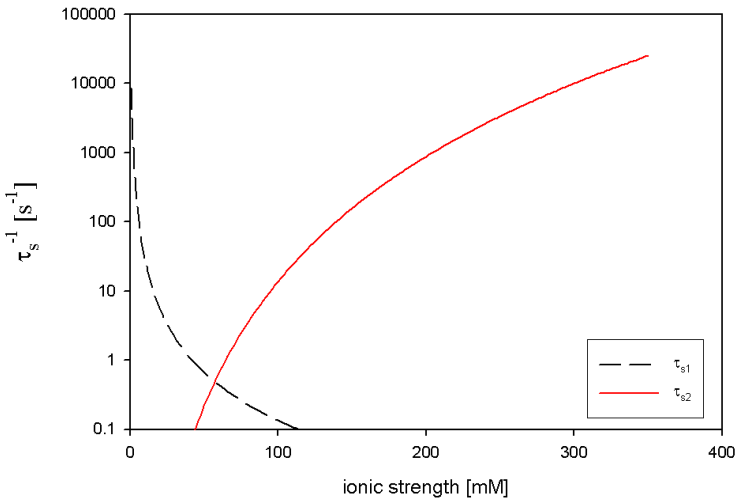

Figure 2.3: Schematic diagram of the ionic strength dependence of τ_s.

2.5.2 Kinetics of worm–like micelles

The kinetics of relaxation after a small perturbation to the equilibrium state of the worm–like micelles was theoretically studied by Turner and Cates [28]. Starting with the equilibrium length distribution (as shown in equation 2.17), they examined a system which could evolve through scission and recombination, both characterised by rate constants k and k' respectively, which are assumed independent of the chain length. This scheme leads to an equation for the time evolution of the length distribution $c(t, L)$ [29]:

$$\begin{aligned} c(t,L) &= -kLc(t,L) + 2k\int_L^\infty c(t,L')dL' + \\ &\quad k'/2\int_0^L c(,L')c(t,L-L')dL' - k'c(t,L)\int_0^\infty c(t,L')dL'. \end{aligned} \tag{2.27}$$

Where the first term describes the break up of chains of length L, the second term describes a longer chain breaking up into a chain of length L, the third term denotes two shorter micelles combining to create a chain of length L and the final term describes a chain of length L combining with another chain to form a micelle longer than L.

It was found that after a small initial perturbation causing a shift in the mean length L of the micelles a single exponential relaxation is expected which can be written in terms of the initial and final lengths of the micelles, L_0 and L_∞ respectively.

$$L(t) = L_\infty + (L_0 - L_\infty)\text{exp}[-t/\tau], \tag{2.28}$$

with a characteristic decay time τ of $1/2kL_\infty$, where k is the reaction rate per unit length for the scission of micelles.

This work was extended by Marques and Cates [29] to take into account larger perturbations in the mean length of the micelles. The evolution of the length of the micelles $L(t)$ differs depending on whether they are growing ($L_\infty > L_0$) or shrinking ($L_\infty < L_0$) as

$$L(t) = L_\infty \text{coth}[\frac{t + t_0}{2\tau}] \quad \text{if } L_0 > L_\infty \tag{2.29}$$

$$L(t) = L_\infty \text{tanh}[\frac{t + t_0}{2\tau}] \quad \text{if } L_0 < L_\infty \tag{2.30}$$

where the constant t_0 is given by

$$t_0 = 2\tau \text{tanh}^{-1}[L_\infty/L_0] \quad \text{if } L_0 > L_\infty \tag{2.31}$$

$$t_0 = 2\tau \text{coth}^{-1}[L_\infty/L_0] \quad \text{if } L_0 < L_\infty \tag{2.32}$$

The resulting time evolution of the length, for both growing and shrinking micelles is illustrated in figure 2.4

This means that the initial size of the micelles bears no influence on the relaxation, and a single time constant τ is expected for the growth (and shrinking) process when the final equilibrium size is the same for the pertubations.

At intermediate times $L(t) \approx \frac{t}{2\tau}$ and for small pertubations the growth can be approximated by exponential decay as found previously [28].

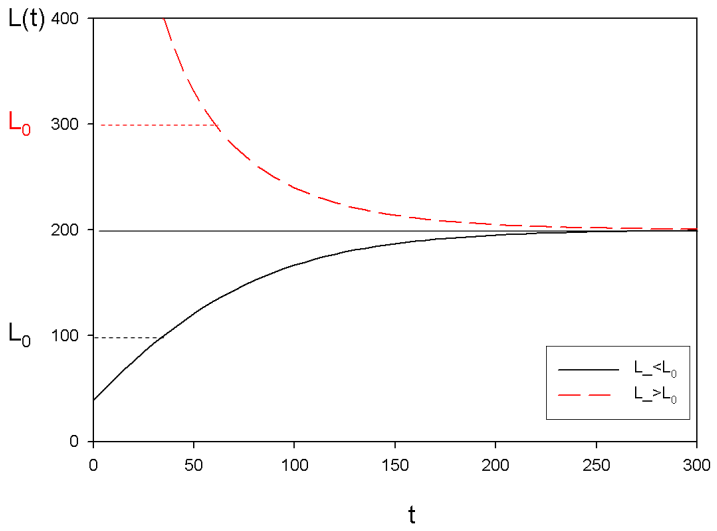

Figure 2.4: Expected growth or shrinkage of micelles starting with micelles of 300Å or 100Å long and jumping to micelles of 200Å in length. The time constant τ is 50s.

Chapter 3

Lipid-surfactant systems

In the previous section only micelles formed from a single species of amphiphile were considered. This section discusses the behaviour of mixed amphiphile systems, more specifically mixtures of lipids and detergents (mainly bile salt).

It is found that any mixtures of amphiphiles (without repulsive headgroup interactions) readily form mixed micelles [1]. The exact forms of the mixed micelles depend on the particular properties of the amphiphiles used.

In this section the mixed micelles discussed in detail are composed of lecithin and bile salt, but much of the theory will apply to other lipid-detergent systems.

3.1 Lecithin and bile salt: a biological system

The early work on lecithin-bile salt systems was done by Small and Carey [30, 31, 32]. They concentrated on the behaviour of lecithin-bile salt systems with and without added cholesterol, in order to understand gallstone formation. Lecithin, bile salt and cholesterol are the major components of bile. It is these mixed micelles that transport lipids (including lecithin and cholesterol) around the digestive system. The origins of gallstone formation are explained through the supersaturation of cholesterol in the gallbladder and hepatic biles of patients [31].

The normal human gallbladder bile has between 80-279g of solids per litre, composed mostly of bile acids (53-71%) and lipids (23-29%) with the rest made up of electrolytes, bile pigments and proteins [33]. The lipids found are phospholipids (lecithin) and cholesterol.

3.1.1 Lecithin

Lecithin is a whole family of phospholipids (lipids which have one or more phosphate groups) and they differ in the fatty acid chains that are attached to them. Lipids are amphiphiles with small headgroups and two hydrocarbon tails, and can be very insoluble in water if the tails are long.

In the experiments presented in this thesis egg yolk lecithin was used, the exact composition varies slightly depending on the eggs. However it is mainly phosphatidylcholine (PC) with some phosphatidylethanolamine (a few percent) [34]. There are different types of PC with different numbers of hydrocarbons attached to them, most of the PCs in egg yolk lecithin have two tails of 16 or 18 hydrocarbons [35]. Lecithin is zwitterionic at the pH used for the experiments, hence overall neutral.

A picture of a PC with 18 and 16 long hydrocarbon chains is shown in figure 3.1.

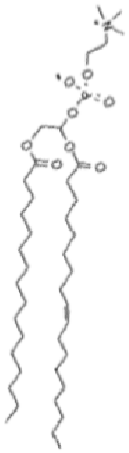

Figure 3.1: A phosphatidylcholine molecule (POPC) (16:0-18:1) which makes up about 38.2% of egg yolk lecithin.

Lecithin [1] is highly insoluble in water (monomeric solubility 10^{-10} M) due to it having two long hydrocarbon chains. The two tails combined with the small hydrophilic headgroup ($a_0 \approx$ 72Å [36]) result in lecithin having small spontaneous curvature. Hence the addition of lipids into water results in the formation of flat bilayers or (as these close up on themselves in order to avoid the unfavourable edges with water contact) vesicles. Lecithin is fully saturated with water/buffer at about 35-45 $\%$ w/w [37] after which it separates into two phases, water and a lamellar phase.

3.1.2 Bile salt

The primary forms of bile acid are made in the liver from cholesterol and these are converted into secondary forms by gut bacteria. The bile acids are normally secreted conjugated with glycine or taurine, which usually exist as salts of various cations. The discussion that follows is applicable for all the different bile salts, but most of the examples are with taurine conjugated bile salts (as used in our experiments, see chapter 5.) In figure 3.2 an unconjugated bile acid is shown.

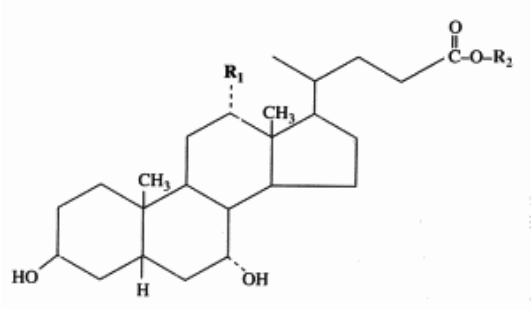

Figure 3.2: Cholic Acid.

Bile salt is a rather unusual amphiphile as it has the hydrophilic and hydrophobic parts on the two sides of the backbone instead of two distinct parts, it ionises in water so these bile salts also carry a negative charge. This means that the optimal headgroup area (a_0) for bile salts tends to be large, measured values ranging from 150Å to 250Å [30, 38, 39]. The bile salts only

[1] Lecithin is now used to refer specifically to egg yolk lecithin unless otherwise specified

have a small hydrophobic part, which results in much higher monomeric solubility than lecithin (typical CMCs are a few mM [30].)

These properties mean that beyond the CMC bile salts pack into spherical or elliptical micelles (i.e. it has high spontaneous curvature).

3.2 Equilibrium behaviour of the lecithin-bile salt system

As lecithin and bile salt form mixed aggregates and have different spontaneous curvature, changing the relative amounts of lipid and surfactant in the aggregates can be used to control their average curvature.

The equilibrium behaviour of the lecithin-bile salt systems is well understood, and has been studied using egg lecithin or a single lipid component as well as various different bile salts [40, 41, 42, 43]. The ternary phase diagram of the lecithin-bile salt-water (egg lecithin-sodium cholate) system is shown in figure 3.3 from [44].

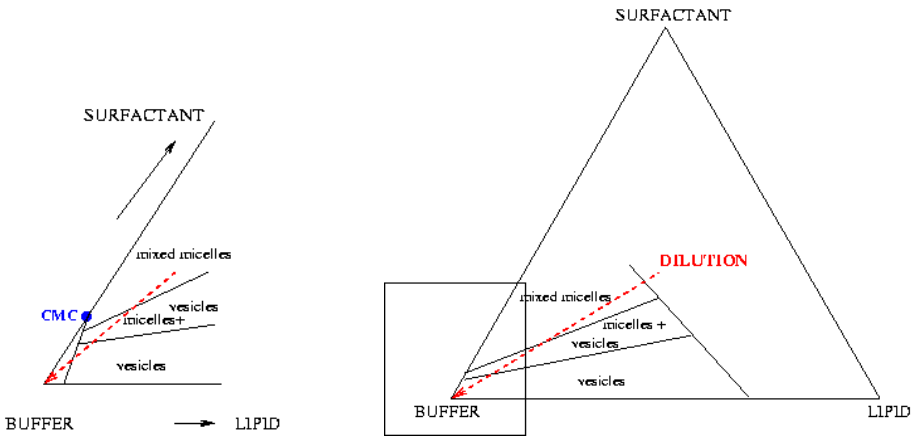

Figure 3.3: A schematic phase diagram of the lecithin-bile salt-water system.

The base of the triangle shows the binary buffer-lecithin phases. As explained previously lecithin is highly insoluble in water and forms lamellar phases on its own.

The left side of the triangle shows the bile salt behaviour with only buffer. In the inset the CMC of the bile salt can be noticed, up to this concentration the bile salt exists as monomers

in solution. Beyond the CMC simple and mixed micelles are formed.

The behaviour of the mixed system is very complicated with a plethora of phases, however these will not be discussed in more detail (for one of the first phase diagrams see [40]).

The inset shows the behaviour at high water content, which is where the experiments described in the thesis were carried out (see chapter 5). This happens to be the area of interest from the physiological point, (including the typical total lipid concentrations in hepatic ($\approx$ 30mg/ml) and gallbladder bile ($\approx$ 100mg/ml) [31]).

A lot of the previous work on lecithin-bile salt systems has been explored through a dilution series [45, 43, 46]. The effect of dilution will be discussed further in section 3.2.2, it is only noted that a dilution of a sample (with given lecithin to bile salt ratio) is shown by the dashed line in figure 3.3. Starting from a region with mixed micelles, upon dilution the coexistence region of mixed micelles and vesicles is met and even further dilution crosses into the phase with only vesicles.

3.2.1 Thermodynamic model for the phase behaviour

The lipid–detergent phase diagram can be shown in terms of the total concentrations of lipid and detergent as shown in figure 3.4 from [47].

The phase behaviour is explored in terms of the detergent to lipid molar ratio in the aggregates (whether mixed micelles or vesicles) denoted as R_e, which is found to be the controlling parameter for the phase behaviour. The bile salt to lecithin molar ratio R_e^{-1} will be denoted as Q_e i.e. R_e = LEC/BS and Q_e = BS/LEC.

This can be explained in terms of the average spontaneous curvature of the aggregates (as explained in section 2.3.2), where now there are two competing curvatures within the aggregate. The spontaneous curvature of the mix is estimated, taking into account the surface occupied by each species (area a times number density ρ) and the spontaneous curvature of lecithin and bile salt on their own [48],

$$C_0 = \frac{a_S \rho_S C_B + a_L \rho_L C_L}{a_S \rho_S + a_L \rho_L}. \tag{3.1}$$

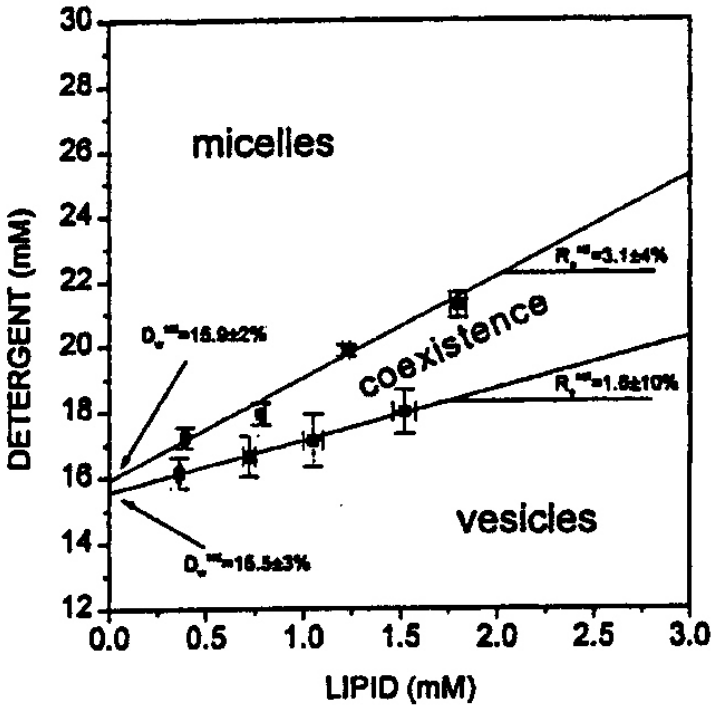

Figure 3.4: A phase diagram of a lipid–detergent system.

The spontaneous curvature of lecithin C_L is taken as 0 (bilayer forming) and that of bile salt C_B as $1/R$, where R is the radius of the micelles it would form on its own.

The phase diagram in the high buffer content region, and more specifically the transitions from micelles to the coexistence region and from the coexistence again to pure vesicular region, were found to follow straight lines (as shown in figure 3.4). Focusing on the transition between micelles and the coexistence region, there is a linear dependence on the amount of detergent D required to solubilise vesicles (i.e. to transform all the vesicles to micelles) and the amount of lipid in the system LEC.

This straight line dependence has been interpreted through thermodynamic arguments where the micelles and the detergent in bulk (it is generally assumed that the amount of lipid in bulk

solution is negligible) are described as a separate thermodynamic phases as [49]

$$D = D_w^{SOL} + Q_e^{SOL} LEC, \tag{3.2}$$

where D_w^{SOL} represents the aqueous concentration of surfactant monomers, corresponding to Q_e^{SOL}, which is the critical detergent to lipid ratio in the aggregates required to solubilise all the vesicles. It was found that D_w^{SOL} corresponds very closely to the CMC of the detergent (in figure 3.4 where the line meets the detergent axis) and Q_e^{SOL} is given by the slope of the phase boundary.

Similarly for the lower line (between the micelle-vesicle coexistence and the vesicular phase) the transformation is discussed in terms of the saturation concentration of detergent in the vesicles and given by

$$D = D_w^{SAT} + Q_e^{SAT} LEC, \tag{3.3}$$

where D_w^{SAT} now corresponds to the aqueous concentration of detergent corresponding to Q_e^{SAT}.

This results in there existing an experimentally easily accessible value for the detergent to lipid ratio in the micelles Q_e^{SOL}, which tells how much detergent is required to transform all the vesicles into micelles, and conversely for Q_e^{SAT} what is the maximum amount of detergent that can be accommodated in the vesicles before any micelles are formed.

This interpretation gives rise to an inconsistency at very low lipid concentrations, where experimentally it was found [50] that the linear dependencies of the bile salt concentration on lecithin, for both solubilisation and saturation (transition from vesicles to micelle-vesicle coexistence), did not cross the lipid axis at the same point. This disagrees with the thermodynamic formulation used, and led to an improvement to the model taking into account the dependence on absolute concentrations of lipid and detergent [47] by removing the assumption that the mixed micelles are a separate thermodynamic phase, but instead taking into account the finite size of the micelles. One of their conclusions is that the composition of the cylindrical part of the micelles does not depend on the size of the micelles.

For a more detailed overview on the models for the phase behaviour of lipid-detergent systems see [51].

3.2.2 Effect of Dilution

Several light and neutron scattering studies have been carried out to understand the exact behaviour of the lecithin-bile salt system. In many of these the lecithin to bile salt molar ratio has been kept constant [43, 52, 46, 53] (i.e. along the line of dilution as shown by the dashed line in figure 3.3).

A pictorial phase diagram along the axis of dilution at constant lecithin to bile salt molar ratio is shown in figure 3.5. The phase behaviour is very similar for most bile salts, the only difference arises from the difference in the CMCs. For a given concentration a higher CMC means increased R_e as more of the bile salt is in solution, which means lower average curvature of the aggregate. Hence bile salts, such as taurocholic acid compared with taurochenodeoxycholic acid, that have higher CMCs shift the changes in the morphologies to lower dilutions.

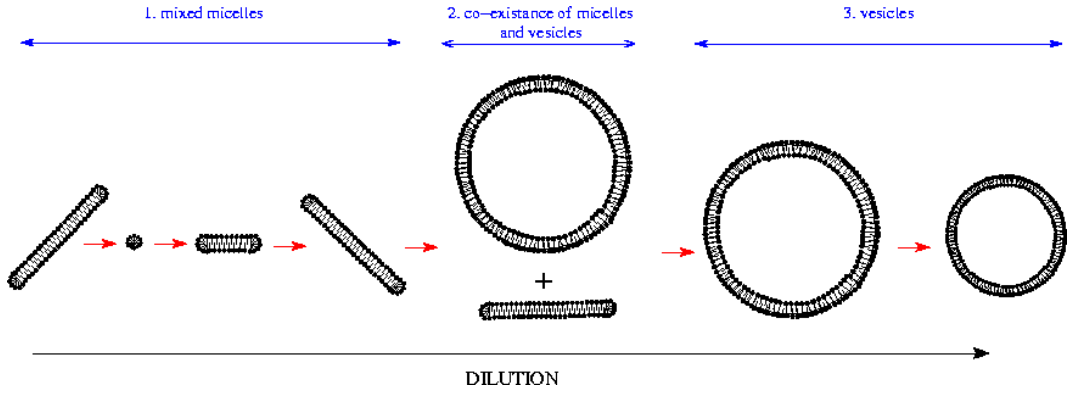

Figure 3.5: A schematic phase diagram of the lecithin bile salt system at increasing concentrations of water (i.e. higher dilutions)

In the mixed micellar region (1.), at high total lipid concentrations long cylindrical micelles form, which upon dilution become shorter. There exists a minimum length for the micelles and upon further dilution the micelles start growing again. These cylindrical (or worm–like) micelles can grow to several persistence lengths, where the persistence length is $\approx$ 200Å and the total length can be greater than 1000Å. Upon further dilution there exists a definite concen-

tration below which mixed micelles and vesicles coexist (region 2.). At even higher dilutions, again after a definite transition point, the only aggregates in solution are vesicles (region 3.).

The three regimes will be discussed in more detail in the following sections. It is noted that the concentrations at which the morphology changes are also affected by the solvent. Using D_2O instead of H_2O as the solvent (as done for neutron scattering experiments), shifts the transistions to higher dilutions, whilst keeping all the features of the transitions [52].

The reason for the behaviour upon dilution arises from the different solubilities and spontaneous curvatures of lecithin and bile salt. Because lecithin is almost insoluble (10^{-10}M), but bile salt has an appreciable CMC, dilution of the sample results in more of the bile salt leaving the aggregates than lecithin. This leads to an increase in the lecithin to bile salt molar ratio in the aggregates, i.e. increased R_e.

Lecithin has very small spontaneous curvature compared to that of bile salt, hence changing R_e also changes the average spontaneous curvature of the micelles.

Regime 1 Mixed micelles

As explained in Section 2.4 for simple cylindrical micelles a concentration dependent growth law of Φ^{α} has been found theoretically with α = 0.5. There exists no such theory for mixed micelles, and due to the two regimes in the mixed micellar system a simple exponential could not explain the features.

At increasing concentrations of lecithin and bile salt the growth of the micelles is assumed to be caused by simple concentration dependent growth [46], whilst the origin of the growth at lower dilutions is caused by the increase in the average spontaneous curvature of the micelles (with decreasing bile salt contents) in order to avoid the highly curved end–caps.

A simple growth law assuming the end–caps of the micelles are made purely of bile salt with a constant number of bile salt molecules required to make an end–cap and where along the cylinder axis the lecithin to bile salt ratio is fixed has been investigated [46]. However, it was found that this was not sufficient to explain the observed growth.

An empirical growth law was found to model the growth reasonably well [46]. The growth law has a double power law form with length L

$$L(\Phi) = B_1\Phi^{\alpha} + B_3\Phi^{\gamma}. \tag{3.4}$$

Here Φ is the total volume fraction of lipid in the system (lecithin + bile salt). If B_1, α and B_3 are all positive and γ is negative, the first term will be dominant at higher concentrations and the second term will become dominant at lower concentrations.

For a lecithin-glycochenodeoxycholate system the above law was found to give good agreement with data using α = 0.5 (typical concentration dependent growth) and γ = -2. The constants B_1 and B_3 were fitted to 2.16$\times 10^3$ Å and 7.14 $\times 10^{-3}$ Å respectively [46].

Regime 2 Micelle-vesicle coexistence

The existence of the micelle-vesicle coexistence region was found using light scattering methods [43] and was further explored using small angle neutron scattering [52]. In particular, for a TCDC-lecithin system at dilution[2] 40, most of the lipid is in worm–like micelles which coexist with a small population of vesicles (the mass fraction of lipid in vesicles is about 0.1 [52].)

The size of the micelle-vesicle coexistence region is known, and for TCDC ranges from dilution 20-44 in H_2O. Light scattering studies on the coexistence region were able to show, assuming the size of the micelles does not change (fixed to the size found for micelles found at points within the micellar region and closest to the coexistence) that the size of the vesicles in the coexistence region is almost constant (radius $\approx$ 540Å), and it is only the size of the population that grows with dilution [43].

Regime 3 Vesicles

Light and neutron scattering experiments have probed the vesicular region of the phase diagram [43, 52, 44], where it was found that the size of the vesicles decreases with dilution [43, 44].

[2] Dilution 1 refers to 50mg/ml lecithin+bile salt and R_{tot} of 0.9

This is in contrast with theoretical predictions of the equilibrium size of mixed vesicles [54,55], where it is predicted that the size of the vesicles should increase upon increased dilution.

This discrepancy has been explained as arising from the fact that the vesicles produced through dilution are not equilibrium structures, but their size is governed by the kinetic pathway of relaxation [56, 57] (this will be explained in more detail in the section on the kinetics of mixed amphiphile mixtures 3.3). The resulting vesicles are not in equilibrium, but are trapped by the kinetics of the transformation and during observable timescales they do not relax to their thermodynamic equilibrium.

This is in agreement with experiments done on the temperature dependence of the micelle-vesicle transition as studied by time-resolved X-ray scattering [58]. Where the final size and/or polydispersity of the formed vesicles changed dramatically with the rate of change of temperature i.e. path to vesiculation.

3.2.3 Organisation of lecithin and bile salt in cylindrical micelles

It is accepted that the equilibrium micelles formed by lecithin and bile salt are cylindrical in shape [43]. However, the arrangement of the lecithin and bile salt within the micelles was only clarified by small angle neutron scattering experiments [53]. It was found that the lecithin is arranged with its tails radially inward and the headgroups on the surface of the cylindrical micelles with the bile salt molecules slotted in between on the surface to protect any open hydrophobic tails. This is in agreement with the radial shell model proposed by Ulmius and Lindblom [59] and by Nichols and Ozarowski [60].

By deuterating the headgroups of the lecithin molecules (DPPC in the study) their scattering length is matched with that of the solvent and information on the organisation of the lecithin within the micelles could be obtained by comparisons with non-deuterated DPPC.

The neutron scattering experiments found that the number of lecithin molecules per length of cylindrical micelle varies only slightly with the length of the micelles, being always close to 0.9 molecules $Å^{-1}$. This value is close to 0.7 molecules $Å^{-1}$ as found from experiments using higher lecithin to bile salt molar ratios [43].

The lecithin to bile salt number ratio along the cylindrical micelles has also been calculated from the amount of lecithin along the axis using a specific geometrical packing model [53]. It was found to be 3-4 lecithin molecules per one bile salt.

The cross-sectional radius of the micelles has been found to stay relatively constant at around 27-29Å for different bile salts and concentrations [52, 46].

3.2.4 Effect of ionic strength

It is known that increasing the ionic strength of the solution has an effect on the CMC of ionic surfactants [1, 61]. The partitioning of amphiphilic molecules between aggregates and solution depends on the difference in the chemical potentials in the two states. The electrostatic repulsion between ionic surfactants makes a strong contribution to the chemical potential in the aggregates. The addition of electrolyte into solution decreases this repulsion, resulting in a lower chemical potential for the surfactants in aggregates and thus reducing the amount in solution.

The same effect is applicable to the ionic bile salts in mixed micellar systems [62]. The transition from micelles to the coexistence region and from the coexistence to pure vesicular region shifts with added electrolyte. For a sample in the vesicular region a sufficient increase in the ionic strength of the solution will drive a transformation from vesicles to micelle-vesicle coexistence region (e.g. for lecithin-TCDC, starting with dilution 50 at 150mM added salt there are only vesicles and monomeric bile salt, with more than 200mM added salt the sample is in the coexistence region [57].)

However, the increase in ionic strength did not have an influence on R_e^{SAT} or R_e^{SOL} (the lecithin to bile salt ratios in the micelles at the saturation and solubilisation of lipid bilayers i.e. transformations to and from coexistence region) [62]. This means that the transitions are driven mainly by the spontaneous curvature of the aggregates, where the electrostatic interactions have only weak effect on the spontaneous curvature itself. This means that the main effect of the ionic strength is to change the monomer concentration in solution, whilst not affecting the packing in the aggregates themselves (i.e. through decreased optimal surface area as the ionic interactions are screened).

The size of the vesicles is found to depend strongly on the amount of added electrolyte with a marked increase in radius upon increased ionic strength. This is explained by the kinetics controlling the formation of vesicles, where the rates of coalescence of intermediate micelles before closure are much faster with increased ionic strength, whilst the rate of closure is almost unaffected [57].

3.2.5 Effect of temperature

The CMC of bile salts increases with increased temperature [61, 30]. This leads to a change in the transition concentrations analogous to decreasing ionic strengths [45, 58]. Hence at increasing temperatures the micelle to vesicle transition (and coexistence) occur at lower dilutions.

3.3 Kinetics of micellar growth

The kinetics of mixed micelle systems have not been studied in great detail, the current state of understanding in the kinetics of morphological changes has been reviewed by Gradzielski [63].

A theory, developed for the coalescence controlled growth of mixed lecithin-bile salt disc–like micelles (which are the intermediate structures found during the formation process of vesicles) [64, 56, 57] will be explained briefly.

Upon dilution of a micellar sample, the cylindrical micelles form disc-like micelles very fast [64], which grow through coalescence until a certain size at which they can bend to close up into vesicles (depending on the rigidity of the bilayer). Due to the very low solubility of lecithin, it is energetically unfavourable for the discs to break up or indeed for the lecithin to leave the micelles (for growth through monomer exchange). The growth of the disc-like micelles is explained in detail in Leng *et al*. [56, 57]. A similar sequence of vesicle formation has been also found within mixtures of cationic and anionic surfactants, followed by time-resolved small-angle X-ray scattering [65].

3.3.1 Growth of disc-like micelles

The description of the growth of disc–like micelles starts with a model for the disc–like micelle. It can be assumed that all the lecithin is in the flat part (where the amount of bile salt is sufficiently small that it can be disregarded). This means that knowing the amount of lecithin in the system and the size of the initial discs, the number of discs (for a given disc size) can be calculated.

Estimates of the diffusion limited growth for such aggregates show that it would be much faster than the observed time-scales. This means that the growth is coalescence limited, with an activation barrier arising from the interactions between the micelles.

Interactions between the micelles

The adsorption of bile salt molecules onto the rim is very fast compared with the growth process [19, 2], and Davies' isotherm can be used to describe the equilibrium between the bile salt molecules in bulk and those on the rim (see equation 2.1). Where ϕ_r now refers to the area fraction of the edges of disc–like micelles occupied by bile salt molecules.

At the pH used for the experiments the lecithin is zwitterionic and hence overall neutral. However, the bile salt is fully dissociated and carries a negative charge [30], it is also assumed to be fully dissociated in the micelles. The charge on the bile salt leads to a surface charge density on the micelles $\sigma = e\phi_r/a_B$, where a_B is the surface area of the bile salt headgroup on the surface and e the charge on one bile salt. This in turn gives rise to an electrostatic potential ψ_0 at the interface.

The Gouy-Chapman Theory describes the surface charge distribution for a given potential [66]. The potential for a given surface fraction covered by bile salt in a 1:1 electrolyte (such as NaCl) is given by

$$\phi_r = -4c_s a_B N_A \kappa_D^{-1} \sinh(\frac{1}{2} e\psi_0/kT). \tag{3.5}$$

Where $\kappa_D^{-1} = (2c_s N_A e^2/\epsilon kT)^{-1/2}$ is the Debye length, and the number density of salt

molecules is given by $c_s N_A$, where c_s is the total ionic strength (added NaCl plus ionic strength of the buffer).

It is assumed that the Gouy-Chapman theory is valid for curved surfaces, as the smallest radius of curvature is larger than the smallest Debye length [57].

As well as the electrostatic interactions arising from the charge on the bile salt, there are topological contributions.

The topological barrier is modelled starting with a fusing bilayer (as if the two discs would fuse face-to-face) and then it is assumed that the topological barrier would be smaller if the area of amphiphile that needs to bend is smaller as would be the case for edge-to-edge configuration.

The calculations for the exact value of the topological barrier are very complicated [4, 67], but arguments based on the area of amphiphile that needs to bend, result in values of $\approx 25kT$ for face-to-face fusion, $\approx 17kT$ for edge-to-face fusion, and $\approx 8kT$ for edge-to-edge fusion. As these values are larger than the electrostatic contributions it is assumed that the micelles will only fuse edge-to-edge.

The DLVO interactions combine the Van der Waals attraction and the electrostatic repulsion. The Van der Waals attraction between two surfaces per unit area is taken as [4]

$$V_a(h) = -\frac{H}{12\pi h^2}, \tag{3.6}$$

where h is the distance between the two interacting monolayers and H is the Hamaker constant (for the lipid-water-lipid system H $\approx$ 3-10 $\times 10^{-21}$ J [4]).

Calculating the electrostatic interaction between micelles is extremely difficult due to the mobility of the charges. When the bile salt molecules on one micelle start feeling the potential from another micelle, they could either move along the micelle or simply leave into the bulk solution. The actual behaviour is bracketed by the two extreme cases of constant charge V^σ and constant potential V^ψ

$$V_e^\sigma(h) = \frac{\sigma^2}{\epsilon\kappa_D}\frac{1+\exp(-\kappa_D h)}{\sinh(\kappa_D h}, \tag{3.7}$$

$$V_e^{\psi}(h) = \frac{4c_s N_A e^2 \psi_0^2}{\kappa_D kT} \frac{1 + \exp(-\kappa_D h)}{\exp(\kappa_D h}. \tag{3.8}$$

The two equations describe the DLVO interactions between two flat monolayers at a distance. We can now use the Deryaguin approximation to take into account the curvature of the two monolayers. It is based on the total potential; Van der Waals and electrostatic (either constant potential or constant charge). The interaction energy E_d(h) of two approaching monolayers of arbitrary curvature and orientation can be found using [68]

$$E_d(h, \phi) = L(\phi) \int_h^{\infty} V(h^{'}) dh^{'}, \tag{3.9}$$

where

$$L(\phi) = 2\pi[(\frac{1}{R_1} + \frac{1}{R_1^{'}})(\frac{1}{R_2} + \frac{1}{R_2^{'}}) + sin^2\phi(\frac{1}{R_1} - \frac{1}{R_2})(\frac{1}{R_1^{'}} - \frac{1}{R_2^{'}}), \tag{3.10}$$

and R_1, R_2, $R_1^{'}$, $R_2^{'}$ are the principal radii of the two approaching monolayers. Here they are the radus of the edge ($\approx$ 25Å) and the radius of the disc ($\approx$ 80Å).

The argument of edge-to-edge fusion through estimates of the topological barriers are supported by the experimental evidence. The ionic strength of the solution was shown to have a strong impact on the rates of growth, hence implying an electrostatic barrier, which is only found at the edges [57].

A statistical approach can be used to estimate the reaction surface as well as the effect of the fusion barrier. The growth is modelled using a set of Smoluchovski rate equations [69], which allow for the calculation of the rate of initial growth τ_g (where the topological contribution is left as an adjustable parameter for fitting.)

The model gives the upper and lower boundaries (constant potential and constant charge respectively) for the rate of growth and is found to agree well with the obtained data [57].

Closure

After a period of coalescence the discs close upon themselves to form vesicles. This is driven by the line tension of the edges of the discs and opposed by the bending modulus and Gaussian

bending modulus of the lecithin bilayer in the middle part of the disc.

The balance between the line tension and rigidity depends on the size of the discs; with increasing disc size the line tension increases and hence closure will become more favourable. There exists a characteristic closure time τ_c, which decreases with increasing disc size. A comparison between the coalescence time and the closure time allows for the determination of a radius r^* for which closure is faster than growth. This critical radius will then result in vesicles of size $R = r^*/2$.

Comparisons between the calculated vesicle size and the experimental one are in good agreement [57]. This means that the formation of vesicles is driven by kinetic arguments and is not an equilibrium process.

Chapter 4

Scattering Techniques

Scattering methods are widely used in soft condensed matter. Light, X-ray and neutron scattering are powerful tools for the exploration of structure, interactions and dynamics at length-scales involved in soft condensed matter. Here all the experiments are of static scattering, where the dynamics are not probed.

The basic principles of scattering will be introduced and the specifics of neutron scattering will be discussed in further detail, including data correction methods. This will be followed by a presentation of the models and exact procedures used for the fitting of the data with a worm–like micelle model.

4.1 Introduction to Scattering

The theory and experimental applications of scattering in soft condensed matter have been extensively written about. For a thorough introduction into scattering in soft condensed matter see, for instance: Neutrons, X-rays and Light: Scattering Methods Applied to Soft Condensed Matter [70] or Polymers and Neutron Scattering [71].

When radiation is incident on a sample, as shown in figure 4.1 some of it passes through and some is scattered. There is only a measurable scattering pattern when there are fluctuations in the scattering medium. In light scattering it is changes in the index of refraction, for X-rays

it is changes in the electron density of the material and in neutron scattering it is changes in scattering length density of the isotope. The angular dependence of the resulting scattering can be used to reveal information on the structure (shape and spatial arrangement) of the scattering medium.

A simple diagram of the scattering process is shown in figure 4.1. The scattering is characterised by the wavelength of the incoming radiation λ and the angle of scattering θ. It is convention that the scattering is described in terms of the scattering wavevector $\mathbf{q}$, which has units of inverse length.

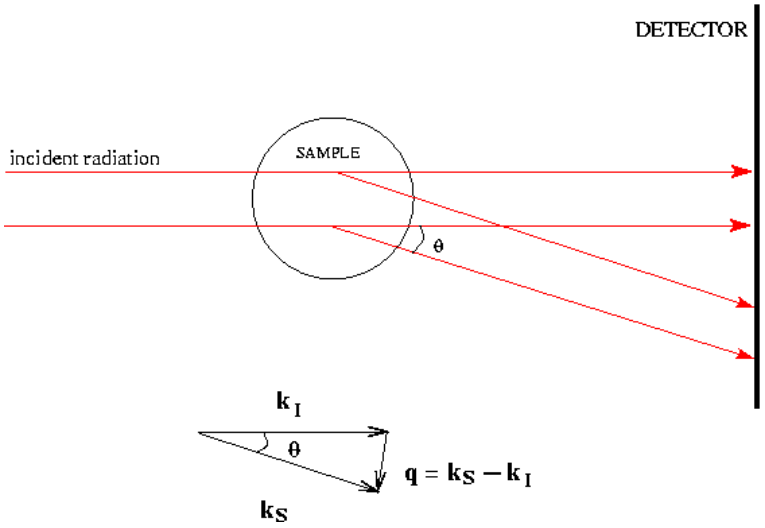

Figure 4.1: A simple diagram of the scattering process

In figure 4.1 the change in the direction of the scattered neutrons is shown as $\mathbf{q}$, which is defined as the difference between the scattered and incident wave vectors ($\mathbf{k}_S$ and $\mathbf{k}_I$). The magnitude of $\mathbf{q}$ is given as

$$\mid \mathbf{q} \mid = \frac{4\pi}{\lambda}\sin(\theta/2), \tag{4.1}$$

where λ is the wavelength of the radiation in the medium and θ the angle at which the scatter is measured. Hence structural information in the scattering medium can be explored by varying $\mathbf{q}$, as this in effect changes the length-scales explored. The ability to 'see' different length-scales using a different q-range arises simply from the fact that the waves of radiation combine

in or out of phase, hence producing a scattering pattern. The larger the distances between the scattering surfaces, the smaller the **q** at which the waves will combine in phase for the structure to be able to be studied.

The scattered amplitude of the radiation can then be written in terms of the scattering length b, the scattering vector **q**, the separation between the scatterers **r** and ω the angular frequency of the radiation as

$$E(q,t) \equiv be^{i(\mathbf{q}\cdot\mathbf{r}-\omega t)}, \tag{4.2}$$

where ω will only change if the wavelength of the incoming radiation changes.

The intensity (the quantity that can actually be measured) is the square of the amplitude

$$I(q,t) =\mid E(q,t) \mid^2, \tag{4.3}$$

which for a discrete collection of homogeneous spheres can be shown to be equivalent to

$$I(q,t) = N\rho^2(0)P(q)S(q). \tag{4.4}$$

Where N is the number of scatterers per unit volume, $\rho(0)$ the scattering length density of scatterers at **q** = 0 (see section 4.1.1), $P(q)$ the form factor and $S(q)$ the structure factor of the scattering particles.

$S(q)$ gives information on the arrangement of the particles in space (and hence the interactions), whereas $P(q)$ depends on the structure of the particles themselves.

There is constructive interference (and hence difference in the scattering pattern) only when there are fluctuations in the scattering length density. This means that the shape of the aggregates can be followed if they are suspended in a solution with a different scattering length density to that of the aggregates.

4.1.1 Neutron scattering length density

In neutron scattering it is the interaction of the neutrons with the nucleus of the isotope (which has a spin) under study that results in the scatter.

There is a particularly large difference between the coherent scattering lengths of hydrogen and deuterium at a_H = -3.74$\times 10^{-12}$cm and a_D = 6.646$\times 10^{-12}$cm respectively. This can be exploited in neutron scattering, where the choice of solvent and/or deuteration of the sample can be used to mask out or look at particular details. The scattering length of a molecule is simply the sum of the scattering lengths of the isotopes it is composed of.

sample	a 10^{-12} (cm)	M (g/mol)	V (Å^3)	ρ 10^{10} (cm^{-2})
D_2O	1.915	20	30	6.38
D_2O Tris buffer				7.32
lecithin	3.350	770	1266	2.65
lecithin, head group		336	377	1.57
lecithin, tail		434	889	-0.29
TCDC	5.880	521.7	660	0.89
TC	6.460	537.7	680	0.95

Table 4.1: Neutron scattering lengths a, molecular mass M, molecular volume V and scattering length densities of sample constituents.

In the scattering experiment it is the differences in the scattering length densities between the solvent and the scatterers that are of interest. The scattering length density of the scatterer is expressed as the following:

$$\rho = \frac{aDN_A}{M} \tag{4.5}$$

where D is the molecular density (g/cm^3), M the molecular mass (g/mol) and N_A Avogardro's number. The scattering lengths and scattering length densities of the sample constituents used in the present work are shown in table 4.1. For all the SANS experiments a Tris-based D_2O buffer was used for enhanced scattering contrast with the hydrogen containing samples.

4.2 Data Correction and Reduction

Here the generic process for data correction and reduction is briefly explained, further details can be found in [70, 71].

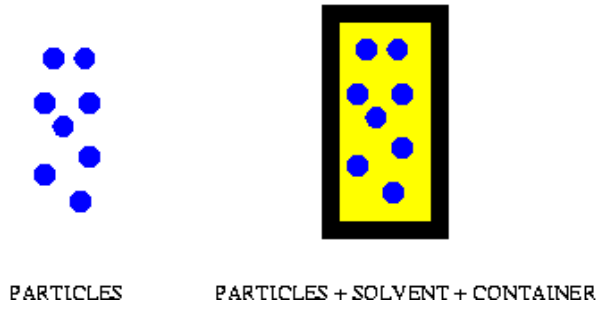

Figure 4.2: Scattering from sample and background contributions.

The scattering experiment is carried out to probe the structure and interactions of the particles under study. As illustrated in figure 4.2 what is of interest is the scattering by the particles themselves. However, the experimentally measured intensity includes contributions from sources other than the particles themselves, and these background sources must be subtracted before proceeding with data analysis.

The background can be broadly divided into two parts: external and internal background.

The external background consists of contributions from the sample container and the buffer, as well as, general background. The general background (B_g) arises from natural radiation and noise from the instrument electronics. The samples are usually measured suspended in buffer in a closed container (in these experiments quartz cells). There is scattering both from the buffer and the sample cell.

The internal background arises from the incoherent scattering of the sample, which can be considerable with hydrogenated samples.

The measured intensity $I_X(q, \lambda)$ can be written in general terms as [71]:

$$I_X(q, \lambda) = C(\lambda)T_X e_X \sigma_X + B_g + T_X B(\theta)C(\lambda) \tag{4.6}$$

where T_X is the attenuation of the beam through the sample, called the transmission of the sample), e_X is the path length of the radiation in the sample, σ_X is the differential scattering cross-section per unit volume, $B(\theta)$ is the scattering by the walls of the scattering cell. $C(\lambda)$ is an instrument dependent parameter defined as $C(\lambda) = \phi(\lambda)A\Delta\Omega E(\lambda)$, where $\phi(\lambda)$ is the incident flux of neutrons (neutrons/cm^{2}s), A is the effective area of the incoming beam (cm^2), $\Delta\Omega$ is the solid angle of sample seen by the detector and $E(\lambda)$ is the detector efficiency.

It is the differential scattering cross-section σ_X which is of interest in the experiment and the other contributions must be removed.

Measurement of B$_g$

The general external background can be measured by placing a highly absorbent sample at the sample position and measuring for a known time the collected radiation on the detector. For these experiments a piece of cadmium was used and hence the intensity is denoted as I_{Cd}. The cadmium intensity measured is equal to the general background and can be directly subtracted from all sample and other background measurements, i.e. $I_X(q,\lambda) - I_{Cd}$.

Normalisation by transmission and sample thickness

The measured intensity has to be normalised by the sample transmission and the scattering path length.

$$I'_X(q,\lambda) = \frac{I_X(q,\lambda) - I_{Cd}}{T_X e_X} = C(\lambda)\sigma_X + \frac{B(\theta)C(\lambda)}{e_X}, \tag{4.7}$$

where $'$ refers to the transmission and external background corrected intensity.

Background from cell and buffer

The subtraction of the background contributions from the sample container and the buffer require measurements of the intensity and transmission of the buffer in an identical cell (i.e.

$e_X = e_B$) as used for the sample measurements (I_b and T_b). The buffer intensity has to be corrected to the transmission and the thickness of the sample cell as shown in equation 4.7.

This leads to

$$I'_X(q,\lambda) - I'_b(q,\lambda) = C(\lambda)(\sigma_X - \sigma_b), \tag{4.8}$$

where $B(\theta)$ has been eliminated through the use of identical cells for the two measurements.

Incoherent background normalisation

Normalisation by an incoherent scatterer, i.e. one where there is no q-dependence in the scattering, allows for the correction of the instrument detector variation. Usually, as in these experiments, a light water sample in a 1mm path length quartz cell is used.

The measured intensity by the water I_w is again corrected by the transmission and thickness of the cell according to equation 4.7 to give I'_w. The corrected intensity has also to be corrected for the background contributions from the cell (similarly as the sample the correction was for the cell and buffer), this means that the scattered intensity and transmission of the empty cell need to be measured, I_{ec} and T_{ec}.

This leads, in similarity with equation 4.8, to the following

$$I'_w(q,\lambda) - I'_{ec}(q,\lambda) = C(\lambda)\sigma_w \tag{4.9}$$

where the subscript w refers to the incoherent background sample, in this case water.

Now, equation 4.8 can be normalised by $C(\lambda)\sigma_w$ (given by equation 4.9), which results in:

$$\frac{\sigma_X - \sigma_b}{\sigma_w} = \frac{e_w}{e_X} \frac{\frac{I_X(q,\lambda)-I_{Cd}}{T_X} - \frac{I_b(q,\lambda)-I_{Cd}}{T_b}}{\frac{I_w(q,\lambda)-I_{Cd}}{T_w} - \frac{I_{ec}(q,\lambda)-I_{Cd}}{T_{ec}}} \tag{4.10}$$

There is also some residual scattering from the edges of the aperture and beamstop, resulting from the finite collimation of the beam. This unwanted contribution is usually removed by creating an appropriate mask to remove the contribution around the beamstop and then neglecting these regions in the data analysis.

4.2.1 Radial Averaging

For samples which have no preferential orientation, which includes micelles in solution, the data from the two-dimensional detector can be radially averaged about the middle of the sample. This results in increased efficiency in the data gathering.

4.3 Instrumentation

There are two main types of neutron sources: steady-state reactors and spallation sources. At Institute Laue-Langevin (ILL, France) they have a steady-state reactor source where the neutrons are produced continuously in a nuclear reactor. The neutrons at the Paul Scherrer Institute (PSI, Switzerland), are produced using a spallation source which creates neutrons by firing highly accelerated protons into targets. This means that the source is not continuous but has a frequency of 50Hz. Both small angle neutron scattering instruments used in this work (D22 at the ILL and SANS-I at the PSI) use cold neutrons, i.e. low energy neutrons with λ from 4.5 to 40 Å.

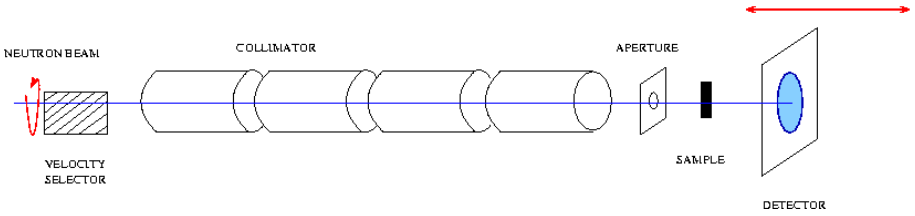

Figure 4.3: A schematic picture of a neutron scattering setup.

The schematic setup shown in figure 4.3 is applicable for both D22 and SANS-I. The neutron beam passes through a rotating velocity selector where the neutrons with the desired wavelengths (λ) are selected, for both instruments the spread in the wavelengths is about 10%. Depending on the source there is also a wavelength dependence on the intensity of the neutrons.

The selected neutrons pass through the neutron guide, which has a movable collimator. The neutron guides are 40x55cm^{-2} and 50x50cm^{-2} at D22 and SANS-I respectively. The colli-

mation distance in effect gives the apparent source-sample distance, and hence controls the divergence of the incoming neutron beam. This means that the longer the collimation distance the less intense the neutron beam.

The aperture is matched with the sample shape and size so that, whilst using the largest aperture size possible (for increased flux), there will only be scattering from the middle of the sample and not the edges of the container or sample holder.

The scattered neutrons are counted as they hit the detector. The detector can be moved along the axis of the neutrons as well as offset horizontally and vertically in the plane of the neutrons or tilted along the axis. The detector has finite spatial resolution and time response.

4.3.1 Experimental Setup

Through control of the sample to detector distance and the collimation distance the q-range probed can be varied. The wavelengths and different sample-detector and collimation distances used at the PSI and ILL are shown in table 4.2 along with the resulting q-range.

	λ [Å]	S-D [m]	coll. [m]	q_{min} [Å^{-1}]	q_{max} [Å^{-1}]
ILL	7	18	17.6	0.002	0.033
	7	14.4	14.4	0.002	0.061
	7	8	8	0.006	0.118
	7	2	8	0.028	0.404
PSI	5	8	18	0.039	0.046
	5	4.5	4.5	0.016	0.255

Table 4.2: Detector configurations used for the SANS experiments.

Cell

For all the equilibrium experiments cells made of quartz glass (Hellma) were used with 2mm path length and the water measurement was done in a quartz cell (Hellma) with 1mm path length.

The time resolved experiments using the stopped flow, were done in a cell with aluminium or steel sides and quartz glass windows again with a path length of 2mm.

4.3.2 Time Resolved Experiments

At D22 and SANS-I it is possible to do time-resolved experiments, which are required for use with the stopped flow setup in order to follow the kinetics of the system. The sample setup is as described in the previous section, but instead of one continuous measurement for each equilibrated sample there are many shorter measurements following one another. At D22 400 time-frames can be collected in one experiment with varying time resolution (from ms-s). At SANS-I the number of time-frames can be changed and the time resolution of individual measurements ranges from ms-s.

Typical data (after data correction as outlined in section 4.2) is shown in figure 4.4. Where the scattered intensity as a function of q and time is shown.

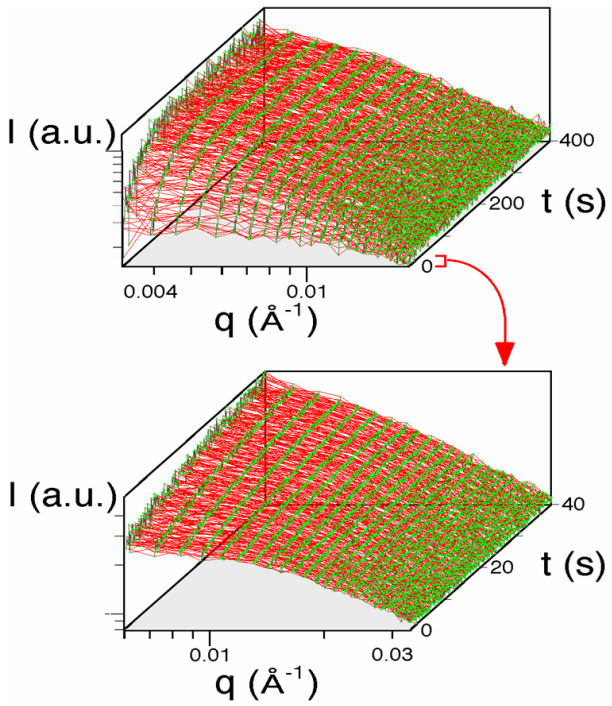

Figure 4.4: Time resolved neutron scattering data above with 400 time frames of 1000ms each and below 400 time frames of 100ms each.

The typical measurement times for lecithin-bile salt samples in the concentration range studied are many minutes for the equilibrium samples. For the kinetic measurements the measuring time for each individual measurement (as used for the experiments in this study) varies from 50ms to 1000ms. This means that one time–resolved measurement does not result in statistics good enough for data fitting and analysis, and many repeats of the same experiment are carried out and averaged before data fitting.

At the ILL the averaging of the time resolved runs happens after the collection and saving of the individual runs whilst at the PSI the runs are averaged before saving and any data treatment.

4.4 Shape Determination

The data is fitted using expressions for polydisperse worm–like chains with elliptical cross-section. The intermicellar interactions are taken into account using the Polymer Reference Interaction Site Model (PRISM), which has been found to perform well for lecithin-bile salt micelles [46].

The SANS data is fitted for polydispersity of the micelles as well as the interactions. It has been shown [42] that the effect of the length distribution is small compared with the effect of the intermicellar interactions in concentrated solutions. However, as the experiments with TCDC are at relatively low concentrations (where the interaction effects are small) and ones with the TC are at higher concentrations, the data is fitted taking into account interactions and the length distribution, so as to be able to use the same model for both sets of data.

4.4.1 Structure

The micelles are modelled as semi-flexible cylinders with an elliptical cross-section. The total volume of a single micelle is given by $V_{mic} = \pi\epsilon R^2 L$ where R is the minor axis radius and ϵ is the axis ratio of the cross-section of the micelle and L is the length of the micelle.

The scattering by the micelles includes the contributions of the individual micelles as well as the interactions. Firstly, the scattering by non-interacting single micelles will be explained and the interactions will be taken into account later.

If the micelles are long enough ($L > 10R$) the form factor can be separated into the cross-sectional ($P_{CS}(q)$) and longitudinal contributions ($P_{WC}(q)$)

$$P(q) = \Phi V_{mic} P_{CS}(q) P_{WC}(q) \tag{4.11}$$

where Φ is the volume fraction of the micelles and V_{mic} the volume of an individual micelle.

The cross-sectional term depends on the different scattering lengths of the hydrophobic tails and the hydrophilic head groups, but the difference between these is not significant enough to be noticed compared with the difference with the buffer of D_2O [52]. The average scattering length of the micelle is denoted as (ρ_{mic}) and hence $P_{CS}(q)$ can be given by

$$P_{CS}(q) = \frac{2}{\pi} \int_0^{\pi/2} (\rho_{mic} - \rho_{buffer}) \frac{2J_1(qR(\epsilon,\theta))}{qR(\epsilon,\theta)} d\theta \tag{4.12}$$

where $R(\epsilon,\theta) = \sqrt{R^2 sin(\theta)^2 + \epsilon^2 R^2 cos(\theta)^2}$, ρ_{buffer} is the scattering length density of the buffer and R is the radius of the minor axis of the cross-section. J_1 is the first order Bessel function of the first kind.

The longitudinal contribution to the scattering is given by Pedersen and Schurtenberger [72]. The expression is based on Monte Carlo simulations on semi-flexible chains with excluded volume effects. These results were then parametrised numerically using the procedure of Yoshizaki and Yamakawa [73], which leads to an expression

$$P_{WC} = [(1 - \chi(q,L,b)) P_{chain}(q,L,b) + \chi(q,L,b) P_{rod}(q,L)] \Gamma(q,L,b) \tag{4.13}$$

where L is the length of the chains and b is the Kuhn length (twice the persistence length l_c). P_{chain}(q) is the scattering function for a flexible chain with excluded volume interactions (as given by equation 13 in ref [72]). $P_{rod}(q)$ is the scattering function of an infinitely thin rod (as given by equation 6 and 7 in [72]). At small q $P_{rod}(q)$ dominates and at larger q $P_{chain}(q)$ dominates. $\chi(q,L,b)$ is a cross over function which links the two q regimes (given by equation 8 and 9 in [72]). $\Gamma(q,L,b)$ is a correction function for the crossover region (given by equation 10 in [72]).

4.4.2 Interactions

Following Arleth *et al* [42, 46] the interactions were taken into account using the Polymer Reference Interaction Site Model (PRISM) which when calculated for worm–like chains gives for the scattered intensity $I_{cyl}(q)$

$$I_{cyl}(q) = \frac{P(q)}{1+\nu(X)c(q)P_{WC}(q)}\text{, where} \tag{4.14}$$

$$\nu(X) = \frac{1}{8}(9X-2+\frac{2\ln(1+X)}{X}\exp\left\{\frac{1}{2.565}\left[\frac{1}{X}+\left(1-\frac{1}{X^2}\right)\ln(1+X)\right]\right\} \tag{4.15}$$

where $P(q)$ is the scattering function of an individual chain, given by equation 4.11, and $\nu(X)$ is related to the concentration of the micelles as shown in equation 4.15 through X, as X depends on the micellar volume and the volume fraction of lipids (See [74] for further information). $c(q)$ is the normalised Fourier transform of the direct correlation function corresponding to the correlation hole arising along the chain if the chain has a finite radius. It has been empirically found to resemble the form factor of an infinitely thin rod [75].

Hence the expression becomes

$$I_{cyl}(q) = \frac{\phi V_{mic} P_{CS}(q) P_{WC}(q)}{1+\nu(X)P_{rod}(q, L_{c(q)})P_{WC}(q)}, \tag{4.16}$$

where $L_{c(q)}$ denotes a characteristic length which is related to the correlation length of c(q).

Polydispersity of the Lengths of the Micelles

As explained before (section 3), even at equilibrium, the length distribution of the micelles is expected to be broad. The polydispersity in the length of the micelles is taken into account in the fitting by following the example of Arleth *et al* [42], and assuming a Schulz number distribution. The Schulz number distribution has been shown to be in agreement with the multiple equilibrium predictions for simple micelles, but it is assumed to be valid for mixed micelles as well.

The resulting volume distribution is incorporated into the PRISM expression as

$$I_{cyl}(q) = \frac{\phi\langle V_{mic} P_{WC}(q)\rangle_{\phi} P_{CS}(q)}{1 + \nu P_{rod}(q, L_{c(q)})\langle P_{WC}(q)\rangle_{\phi}}. \tag{4.17}$$

All the results defined as having been fitted using a polydisperse worm–like micelle model were fitted using the above expression. Where the fitting parameters were $S(0)$, b, L, R, ϵ and a background term.

4.4.3 Fitting Routines

The fitting routines use the Marquart-Levenberg fitting method, where the original programs were written by Jan Skov Pedersen. The programs have been modified for use with time–resolved data and the interactions have been included.

Chapter 5

Sample Preparation

5.1 Materials

There are several different bile salts, for these experiments two different bile salts were used: taurochenodeoxycholic acid sodium salt (TCDC) and taurocholic acid sodium salt (TC).

The bile salts, TCDC, with molecular weight 521.7gmol^{-1}, and TC, molecular weight 537.7gmol^{-1} were obtained from Sigma-Aldrich. The bile salt arrives as powder and it can be dissolved into ethanol or methanol. Stock solution of 20mg/ml of bile salt in ethanol was used for all the experiments. The bile salt in ethanol mixture was left on a tumbler overnight, which resulted in a clear solution.

Egg yolk lecithin, with molecular weight 770gmol^{-1} was obtained from Lipid Products (South Nuffield, Surrey, UK (grade I)). The lipid arrives in 500mg pellets, where it is already dissolved in a chloroform-methanol mixture. To this ethanol is added to obtain a 20mg/ml lecithin stock solution.

Both lecithin and bile salt in the ethanol solutions are tightly sealed with laboratory film and wrapped in foil to avoid sunlight. The solutions are stored at -5C^{o} to avoid evaporation. The stock solutions last for months, but for the experiments presented were used within a few weeks of preparation.

5.2 Stock Solution

A TRIS based D_2O buffer (for reasons of scattering contrast as explained in section 4.1.1) at pH 8.0 is used in the experiments. The pH is achived through using fixed amounts of Tris-HCl ($NH_2C(CH_2OH)_3 \cdot HCl$) and Tris-Base ($NH_2C(CH_2OH)_3$). The buffer has a total concentration of 50mM, with 21.8mM Tris-Base and 28.2mM Tris-HCl. The correct amount of D_2O is measured by weight.

The mixed lecithin and bile salt stock solution was prepared in the same way as has been described previously [43, 76]. The stock solution has 50mg/ml total concentration of amphiphile (lecithin + surfactant) with varying lecithin to bile salt molar ratios R_{tot} i.e. even when the R_{tot} changes, the stock solution will have a total amphiphile concentration of 50mg/ml. For example, the resulting stock solution for lecithin-TCDC system with R_{tot} = 0.9 has 41.1mM TCDC and 37.1mM lecithin, whereas when R_{tot} = 0.3 it has 66.4mM TCDC and 19.9 mM lecithin.

The volume fraction of lipid (lecithin+bile salt) in the stock solution can be calculated using the volumes of lecithin 1266Å^3 [77, 37], TCDC 660Å^3 [78] and TC 680Å^3. This results in stock solutions (at R_{tot} = 0.9) for the TCDC–lecithin system of volume fractions of lecithin ϕ_L=0.0282 and ϕ_{TCDC} =0.0164, and for the TC stock ϕ_L=0.0289 and ϕ_{TC}=0.0166.

The preparation of the stock solution is as follows: the required amounts of lecithin and bile salt solution in ethanol are mixed together. This is set on a rotavaporator, to evaporate the ethanol and leave a thin film consisting of mixed lecithin and bile salt. As the name suggests the rotavaporator is used to evaporate the ethanol, whilst rotating the sample continuously tilted at an angle to wet a larger surface of the flask and hence create a large surface for the film. The samples were set on a rotavaporator driven by a water pump to a pressure of about 50 mbar. The film dried over a period of 3-4 hours, or was set overnight, where the film produced was clear with sometimes visible cracks on the surface.

Upon removal of the film from the rotavaporator it is flushed with nitrogen. Buffer is added to make the 50mg/ml concentrated stock solution, which is referred to as dilution 1. The sample is shaken to ensure that all of the film has dissolved into the buffer and left for a few hours to

make sure that all the lecithin and bile salt are in solution.

The stock solution is moved into a smaller storage vial (with a narrower neck - to minimise the loss from evaporation), topped with N_2, sealed with laboratory film and covered with foil to protect the components from sunlight and left in a darkened place at room temperature (T≈ 23°C) for 1-3 days for equilibration before further use. After equilibration the stock solution can be diluted with varying amounts of buffer to produce the required sample concentrations, and again after dilution they will be flushed with nitrogen before sealing.

For the neutron scattering experiments at higher ionic strengths i.e. ≈ 100mM, the stock solution was diluted 1-2 hours before the start of the kinetic experiments, which is sufficient for the equilibration of the micellar samples (see section 8). For experiments at lower ionic strengths care was made to ensure that the micelles had sufficient time to relax, before the start of the experiments. The 'start' dilution solution was then used during the next few days.

5.3 Ionic Strength

The ionic strength of the buffer is comprised of a contribution from the buffer (HCl) and the added salt. The ionic strength contribution from the buffer is 28.2mM. The amount of added sodium chloride (NaCl) varies for different samples. Hence the ionic strength of the buffer will be 28.2mM + [NaCl].

As the bile salt ionises, the counterions of bile salt (Na^+) have to be included in the total salt concentration, where this contribution is especially significant for samples at low added NaCl and/or low dilution. The ionic strength arising from TCDC with R_{tot} = 0.9 at dilution 1 is 41.1mM and for TC at R_{tot} = 0.9 and dilution 1 is 40.6mM. The total ionic strength of the sample, denoted as c_s is the sum of the contributions from the buffer, NaCl and the bile salt.

The experiments into the effect of R_{tot} and dilution were all done with 75mM or 100mM added NaCl, where the salt content will be clearly indicated in the results sections. The kinetic experiments into the effect of the ionic strength (section 8.3) used different initial and final c_s, details of which will be explained along with the results.

Chapter 6

Construction and Commissioning of The Stopped Flow Apparatus

In this section the construction and commissioning of the stopped flow setup is explained. It describes the basic idea of a stopped flow and progresses to the specific requirements of a stopped flow designed for neutron scattering experiments. This is followed by an explanation of the workings of the final design, with details for the electrical wiring shown in appendix A.

6.1 Concept of Stopped Flow for SANS

Stopped flow setups are used to study evolving mixtures of liquids at very small time resolution. The basic idea of a stopped flow is to mix two liquids thoroughly and as fast as possible; then arresting the flow, to allow for the study of the evolving mixture.

Most commercially available designs of stopped flow are optimised for very small volumes (μl range or below), which are ideal for the highest speed of mixing and used widely in fluorescence spectroscopy, HPLC and with many other techniques. However, for our samples in neutron scattering experiments such small volumes are not possible (due to the low scattered intensity of the types of samples studied) and samples of hundreds of μl are usually required. The design of a fast stopped flow for larger volumes has many complications, which is why the

few commercially available stopped flow systems designed for such systems were not deemed of suitable reliability for the experiments.

The most important considerations in the design of a stopped flow for neutron scattering experiments are:

- time resolution obtained,
- repeatability of mixing,
- time between the measurements.

6.1.1 Time Resolution

The idea of the stopped flow is to study the kinetics of the system, so the best possible time resolution is the main focus of the design. Time resolution in SANS experiments is not limited by the dead time of the detector, as this is much smaller than experimentally possible mixing times for such large volumes.

The main factors for the start time of measurement from initial contact are the speed of filling the scattering cell (i.e. how fast you can get Xml into the cell) and the time taken by the mixture to stabilise. For the measurements the mixture itself has to be still to make sure that what is measured are changes in the structure of the sample constituents and not artefacts of the mixing process.

The main goal is to have the fastest possible mixing and stabilisation of the two solutions, so that the earliest possible times after the solutions come into contact can be followed.

6.1.2 Repeatability of Mixing

As well as requiring fast filling and prompt stabilising the fluids need to be well mixed. This is a basic requirement for a meaningful study on a system, and important for the repeatability of measurements.

As mentioned in section 4 it is typical for an equilibrium SANS measurement for systems considered in this study to take hundreds of seconds. This means that for time-resolved experiments (where the time resolution is 50-1000ms) many experiments have to be repeated and averaged for meaningful data analysis. The mixing has to be thorough, and as such the same for each measurement.

6.1.3 Time between Measurements

The requirement for many repeat measurements for each experiment, and the need for exact starting conditions means that the cell needs to be cleaned between measurements. Not only does the cleaning have to be thorough, it also has to be fast. Neutron beam time is expensive and not readily available, so as much as possible must be used for measuring.

6.2 Design and Construction of the Stopped Flow

6.2.1 Overview of Working Principle

The most important part of the stopped flow set up is the measuring cell, this is designed with two parts: a mixing chamber, and above this the measuring chamber. The mixing chamber (as seen in figure 6.1) has seven inlets, six of which are for the stock and buffer (three each A1-A3, B1-B3) [1] and one at the base of the chamber is for emptying and cleaning the cell (C).

After the stock and buffer have entered into the mixing chamber at high speed, they mix vigorously, eventually slowing down and moving up (as more fluid is injected) to fill the upper (measuring) chamber.

There is an overflow outlet at the top of the measuring cell (D), which is open to air, so that as the cell is filled the air within can escape, and the cell can be slightly overfilled if so desired, which can become useful when working at the limits of the filling process.

[1] The two liquids for the stopped flow will be referred to as stock and buffer as this is what is used in this work, however it could be any two liquids for mixing.

At the other end of the fluid circuit are two disposable syringes. These are controlled by linear motors which can be moved to fill the syringes (from the refill), and then to shoot the contents into the cell. The flow from each syringe is divided into three for increased efficiency in the mixing.

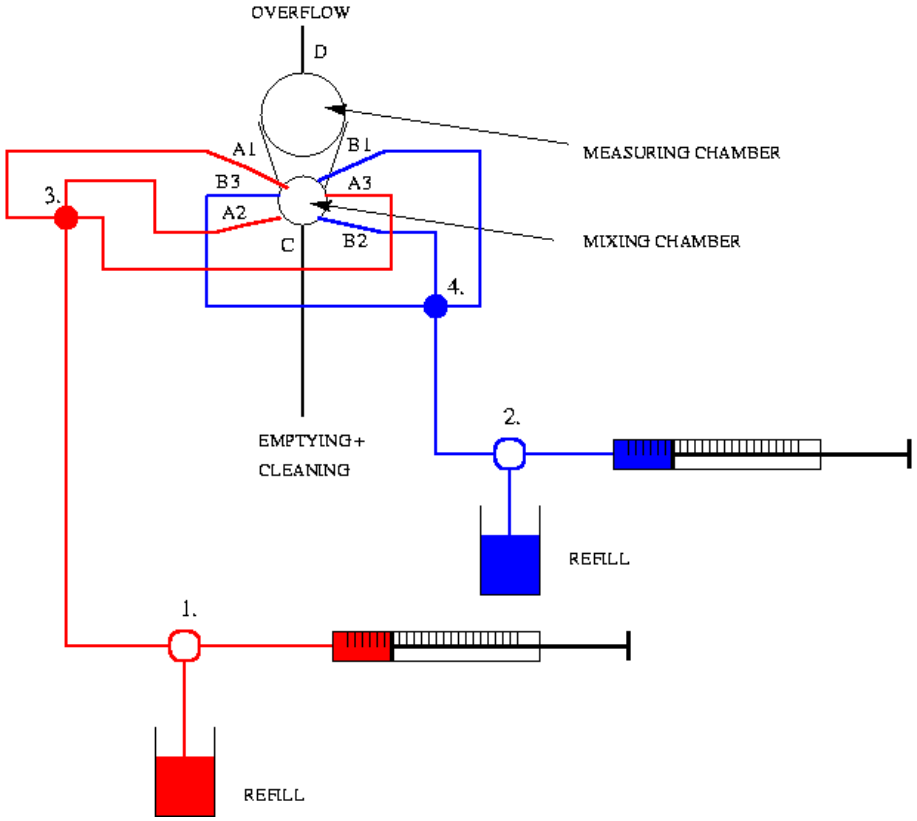

Figure 6.1: Schematic diagram of the stopped flow setup.

After the measurement is over, the cell is emptied and cleaned before the start of the next measurement.

The emptying and cleaning as well as details of the component parts will be further explained in three sections: the stopped flow cell; the fluid circuit; the motors and controllers.

6.2.2 The Cell

The cell consists of two chambers: mixing chamber and measuring chamber. A photograph of the cell is shown in figure 6.2.

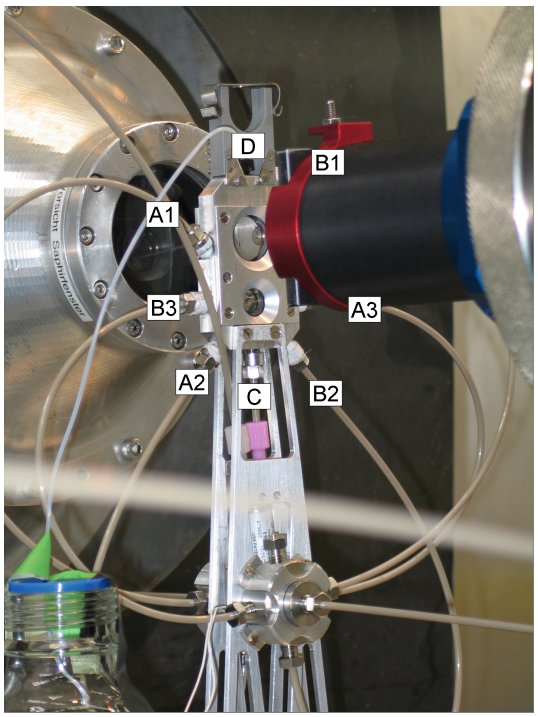

Figure 6.2: A photograph of the stopped flow cell in the neutron beam at PSI, with the different inlets marked.

The cell is designed to have no sharp corners where the fluid could possibly get trapped during emptying and cleaning. Sharp corners, were also noticed to lead to problems, if between the mixing and measuring chambers, as the fluid travels at such speed as to trap air in any corners.

The six small diameter inlets for the stock and buffer ensure the high speed of the incoming fluid, resulting in thorough mixing. The mixing chamber is relatively small (10 mm diameter) which ensures that speed at contact is very high for the incoming fluids. As more fluid enters into the cell the fluid rises through the thick neck, designed to slow down the turbulence and fill the measuring chamber in a uniform fashion. The measuring chamber is designed to be used with a 15mm diameter circular aperture for the neutron scattering. As soon as the measuring chamber has filled the measurement can start.

As seen in figure 6.2 the mixing chamber has seven inlets, six of which are for the incoming stock and buffer (three each). The main body of the cell is made of aluminium (or steel), for minimum reaction and oxidation with used solvents. The main body of the cell is machined as one unit, allowing for the connections to the tubing and the bulk of the fluid circuit (see section 6.2.3). On both sides Teflon seals are fitted with 1mm quartz glass slides, another set of latex seals and to hold everything in place an aluminium cover which is attached with 6 M2 screws on either side.

Due to machining the main body of the cell from one piece of metal the inlets and outlets have a diameter of 1mm inside the metal unit. These have steel fittings attached to 1/8" PEEK™tubing (as used for the rest of the fluid circuit.)

At the top of the cell there is a semicircular section, where any air bubbles that have remained in the solution can rise up to, so as not to interfere with the measurements. At the top of this section, there is an outlet designed for the air to leave through as well as for any overflow. This outlet has a polypropylene fitting (Bola, Germany) with UNF 1/4" 28 G thread, attached to PTFE (PolyTetraFluoroEthylene) tubing (Bola, Germany) with a 1/16" inner diameter. The tube runs into a glass beaker.

Sitting above the cell, on the mounting, there is a place for a 2mm path-length (Hellma) cell, which can be used for equilibrium measurements without unmounting the stopped flow setup.

6.2.3 Fluid Circuit

The fluid circuit is divided into two separate parts: a section for the filling of the cell with stock and buffer; and a section for the emptying and cleaning of the cell. These are both shown schematically in figure 6.3. Only one of the filling circuits is shown, as they are identical for the stock and the buffer.

All the tubing (apart from over-flow part as mentioned in section 6.2.2) is 1/8" PEEK™tubing (Vici AG, Switzerland) the large diameter of the tubing is required due to the speed and volume of the flow.

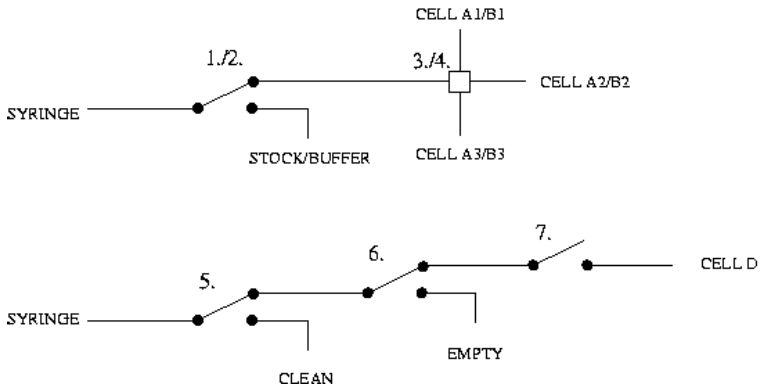

Figure 6.3: Circuit diagram for the fluid flow around the filling circuit (above) and the cleaning circuit (below).

Connection to syringes

The liquids are dispensed using 1ml disposable syringes with a luer lock fitting (BD, US) attached to linear motors. The luer lock fitting on the syringes is attached to the tubing using a luer adapter and standard fittings (Vici, Switzerland).

The choice of disposable syringes was to allow for the easy change of the samples. The syringe can be changed along with the filling solution and with refilling the tubing from the new solution the setup is ready to continue.

Valves

All the valves used can be switched using a 24V DC signal.

As can be seen from figure 6.3 there are in total five valves used in the setup, three in the cleaning circuit and two in the filling part. In the filling part two high pressure, two-position switching valves (to connect syringe-cell or syringe-refill) with microelectronic control are used (VICI Valco, Switzerland. Part no. 3TL3UW). The valves have PVDF (PolyVinyliDene Fluoride) as the wetted surface. They can take pressures upto 5000 psi liq which is beyond the limits of the system.

In the cleaning circuit there are two low pressure 3/2 valves (Fluid Automation Systems,Switzerland. Part no. 9-333E-03-51) with 1.6mm inner diameter and PVDF as the wetted surface. Un-

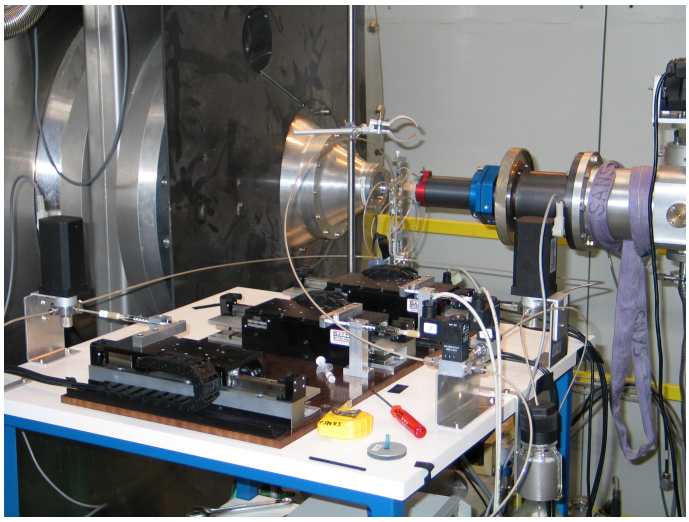

Figure 6.4: Motors and switches for the fluid circuit.

der the cell a simple open/closed valve is used (LEE, UK. Part no. LFVA24301134) with FCR/PEEK™as the wetted surfaces. Both types of valve require 24V power supplies.

6.2.4 Motors and Controls

The motors used for the setup have to be accurate in their positioning, as well as very fast and powerful. The syringes used are standard one ml disposable syringes (BD, US), which have a plunger of 80mm for dispensation of the total volume. The aim of the stopped flow is to be able to fill the cell in less than 100ms. This means that the motors have to be able to move, starting from stationary, 80mm in less than 100ms. Assuming a triangular velocity profile (i.e. continuous acceleration, followed by continuous deceleration with no constant speed section) the motors would have to get to 1.6ms^{-1} in 50ms, which requires an acceleration of 32ms^{-2}.

There are not many motors capable of such acceleration, especially as the accuracy (with no overshoot) should be less than 10μl per movement, which leads to positional accuracy of 8μm. The specifications were filled by Baldor's linear motors, which are seen in figure 6.5.

Three linear cog-free motors are used (Baldor Motors, US. Part no. LSS1TECF06006). They have optical linear encoders (Renishaw, UK. Part no. RGH22) with 5μm resolution. The

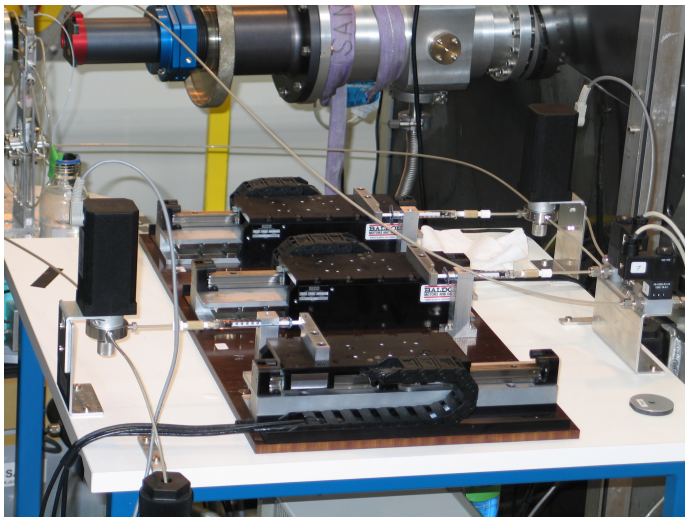

Figure 6.5: Linear motors used for the filling of the cell and the emptying and cleaning.

motors have a stroke length of 15.2mm and have a peak force of 58N (continuous force 19N).

They are driven using FlexDrive ^{II} ™(Baldor, US) controllers which in turn can be linked to a NextMove™(Baldor, US) PCI-card and expansion box which means that the control of the motors can be done from a laptop computer, see section 6.3.

6.2.5 Setup Table

Due to the complexity of the setup and the numbers of components a sample table with place for all the motors and controllers (for motors and valves) is required. A photograph of the setup at the PSI is shown in figure 6.6. Having a well defined way of setting it up also helps if the setup needs to be dismantled and reconstructed (for example for use at another institution).

The motors and switches are on the top tier as part of the fluid circuit. The table is 1500mm tall, designed to have the height of the syringes and the fluid circuit close to the beam height (1570mm at the PSI). This also allows for the shortest possible tubing lengths to be used, to minimise the dead volume in the system.

The middle tier has the controllers and power supplies for the valves (to transform signal from the PCI outputs, at 5V to 24V).

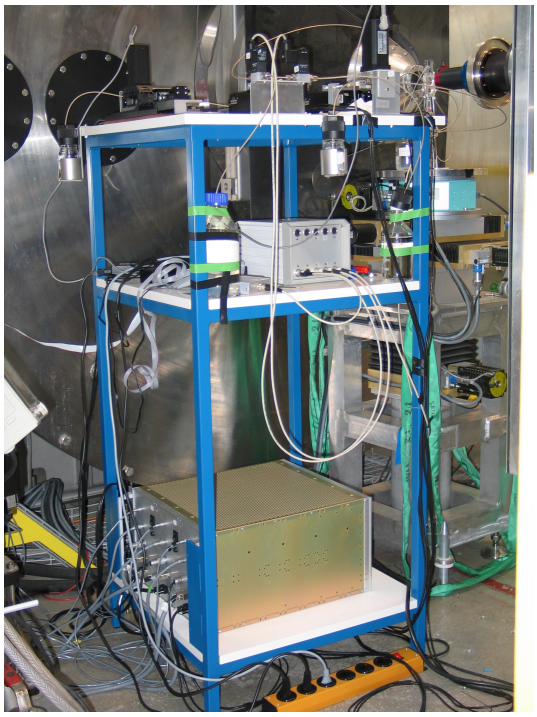

Figure 6.6: Stopped flow stand with (starting from the top level) motors, connections and power supply for switches and controllers for motors.

On the bottom level are the FlexDrive^{II} controllers for the motors with the connections to mains power, to drive the three motors from the same supply a three-phase supply is required.

On the side there are places where the storage bottles for stock and buffer can be attached (refill), these are 250ml Pyrex bottles. There is also space for 500ml Pyrex bottle for cleaning fluid and 1000ml for fluid emptied from the cell.

6.3 Control and Running of the Stopped Flow

The switching of the valves as well as the movement of the motors is controlled using a laptop computer with a docking station (for the PCI card). This is designed keeping in mind the distance between the neutron area and the control room. At the PSI the control can be set up in the SANS-I control room, which requires all the connecting wiring to be 10m long. A photograph of the laptop and the PCI expansion box (to allow for connection to the PCI card)

is shown in figure 6.7.

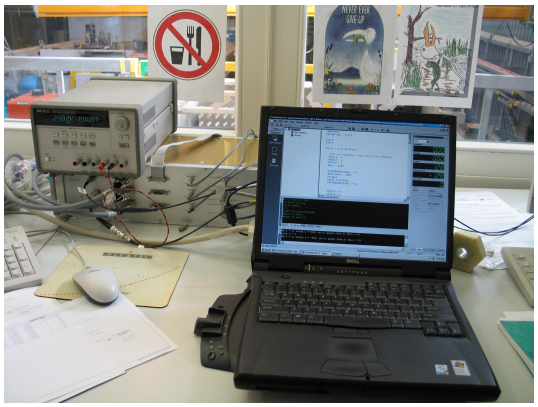

Figure 6.7: Control of the stopped flow setup using a laptop and pci expansion box.

As mentioned before the use of the PCI-card and with it Mint Motion software (Baldor, US), allows for the complete control of the whole setup from one program. This means that the whole sequence from filling the cell to emptying and cleaning the cell and contact with the PSI electronics can be programmed into one program, which is included in appendix B.

A flow diagram of the control sequence is shown in figure 6.8, where the dialogue with the PSI electronics is included. The input parameters required are: 1. speed of filling the cell (in ms), 2. volume for each syringe (in ml) and 3. number of repeats of the cycle (i.e number of measurements). This allows for a fully automated setup linked to the PSI instrument electronics.

As mentioned before (section 6.2.4) the velocity profile used for the motors is triangular, so all the program does is to calculate appropriate acceleration given the time it has to perform the movement in and the distance moved, which is specified by the volume for each syringe.

The total volume used should be 1200μl, and different ratios of mixing can be obtained by changing the volumes shot by each syringe i.e. mixing ratio of 1:3, requires 400μl of stock and 800μl of buffer. The movement of the syringes is also such, that both syringes move for the same length of time so that the mixing process is the same during the whole time of mixing.

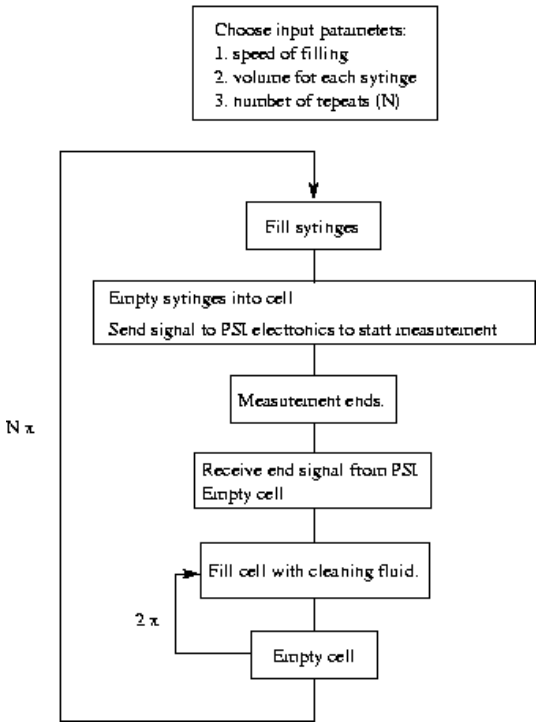

Figure 6.8: Simplified flow diagram of the stopped flow control program.

6.4 Testing of Stopped Flow

The testing of the stopped flow was carried out using a high speed camera 10ms per frame to allow for the direct visualisation of the mixing and filling of the stopped flow cell.

Various different cell designs were experimented with and the fastest reliable mixing and filling were found for the cell presented in section 6.2.2. For the current cell and setup the fastest reliable filling time for the cell is 200ms.

6.5 Manual Stopped Flow Setup

The stopped flow as presented in this chapter was not ready for the experiments at the ILL and they were done using a manual stopped flow setup which is explained briefly.

The basic working principle is exactly the same as explained in the previous sections, the only

differences are that all the switches used were manually controlled 3-way switches (Hamilton, UK) and that the driving of the syringes was not done using the motors. Instead of the motors, a special frame was built for 2-3 syringes attached to a handle that could be pushed down with speed. All the data collected using this setup was checked for the consistency of the filling before data averaging or data treatment. It was found that the minimum time for filling was about 200ms.

Chapter 7

Equilibrium Results

The equilibrium results will be presented in three sections: the SANS experiments on the different L-BS systems studied; description of the model for the composition of the micelles; the comparison of the model with the experimental results, both as obtained by SANS experiments here, and with other data from the literature.

7.1 SANS experiments on lecithin-bile salt systems

The SANS experiments on the system are divided into four sections: the TCDC-lecithin system as studied at the ILL (at constant lecithin to bile salt molar ratio = R_{tot} and varying dilution) section 7.1.1; on the TCDC-lecithin data obtained by S. U. Egelhaaf at the ILL (at varying R_{tot} and varying dilution) section 7.1.2; TC-lecithin data obtained at the PSI (at varying dilution and R_{tot}) section 7.1.3; and TC-lecithin data from the PSI at constant R_{tot} and varying dilution, where the effect of ionic strength is explored section 7.1.4.

After background reduction and corrections, the intensity as a function of q is fitted using the excluded volume worm–like micelle model with included interactions (polymer reference interaction site model (PRISM) [79]). The fitting procedure is explained in detail in section 4.4.

7.1.1 TCDC - Lecithin System

The SANS experiments were carried out on samples with R_{tot} = 0.9, 75mM added NaCl and at dilutions 6.6, 10, 13.3 and 20. These are also the 'start' and 'end' dilutions for the kinetic experiments on the TCDC-lecithin system as will be discussed in chapter 8.

The background corrected scattering intensity as a function of q, as well as the resulting fits are shown in figure 7.1. Three different settings were used to gather information over a large range of length-scales, the exact settings used for these experiments are found in chapter 4. The intensity across the full q-range can be fitted simultaneously to obtain all the structure parameters of the micelles.

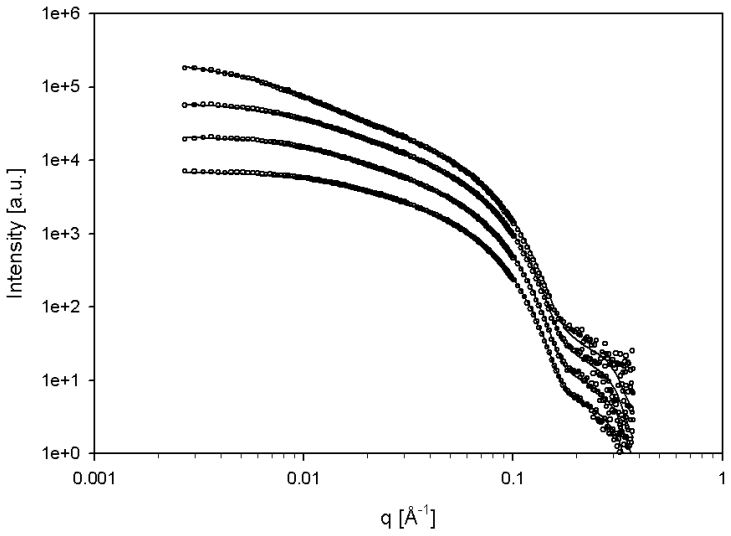

Figure 7.1: Scattered intensity and resulting fits on the TCDC-lecithin system, with R_{tot} = 0.9 and [NaCl] = 75mM, where each data set is multiplied by 2^n, where n ranges from 0 to 3 with increasing dilution. Starting from the bottom with dilution 6.6, 10, 13.3 and dilution 20 at the top.

The resulting fit parameters for each sample (defined by the dilution and equivalently the volume fraction of lecithin and bile salt Φ) are shown in table 7.1. The fitted parameters are the contour length of the micelle (L), polydispersity in length ($\frac{\sigma_L}{L}$), minor axis of the cross-section (R), axial ratio of the cross-section (ϵ) and Kuhn length (b).

The fit results are in good agreement with those found in experiments on similar systems [46,

dilution	Φ	L $\pm$ 2%[Å]	$\frac{\sigma_L}{L}$	R [Å] $\pm$ 0.1	$\epsilon\pm$ 0.01
6.6	0.00657	102	1.0	17.9	1.54
10	0.00446	157	1.0	18.0	1.55
13.3	0.00335	220	1.0	17.8	1.55
20	0.00222	494	1.0	18.4	1.59

Table 7.1: Fitted parameters for the equilibrium data with R^{tot} = 0.9, where the Kuhn length has been fixed to 400 Å.

52]. The contour length of the micelles increases from 102Å to 494Å with increased dilution, this length dependence will be discussed further in the following section. With the shortest micelles the Kuhn length does not really have much meaning as the micelles are essentially stiff rods, the Kuhn length is twice the persistence length i.e. the length after which the micelle forgets previous orientation. Hence it was fixed to 400Å, which is similar to values found for L-BS systems in previous studies [46, 52]. Worm–like micelles are very polydisperse (as discussed in section 2.4), this polydispersity was found not to vary significantly between the dilutions and so was fixed to 1.0 for consistency with the kinetic results. In fitting scattering data there exists a relationship between L and σ_L/L due to the change in the average mass of the micelles (at q=0 the scattering can be normalised to give the total mass of the micelles) and hence having differing polydispersities would complicate the following discussion.

Length of micelles

The dependence of the length of the micelles on the volume fraction of lipid and bile salt Φ is complicated for a mixed micellar system, as explained in section 3.2.2, with two distinct regimes at high and low volume fractions Φ. The experiments presented in this section are all in the low concentration regime, where growth of the micelles is observed with decreasing Φ (increasing dilution).

For a mixed micelle system there exists only an empirical growth law for the concentration dependence of the length [46]. The length of the micelles is found to follow a double power law dependence of the form $L = B_1\Phi^{0.5} + B_3\Phi^{-2}$. Where $\Phi^{0.5}$ term dominates at high volume

fractions and corresponds to a mean-field-theory type of growth law, and Φ^{-2} takes over at low volume fractions.

The results presented here are all in the low volume fraction limit hence the data can be fitted with a simpler power law of $L = B_3\Phi^{-2} + C$ where C is a constant. The resulting fit is shown in figure 7.2.

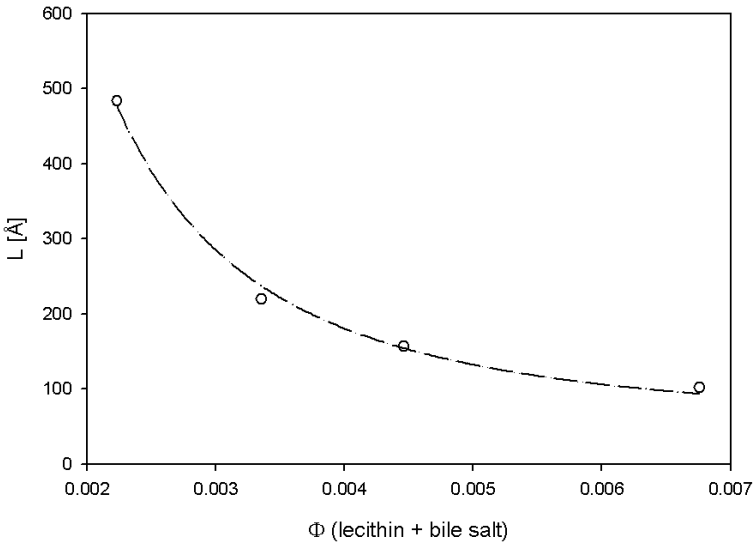

Figure 7.2: Length as a function of volume fraction with B_3 = 2.1$\times 10^{-3}$Å and C = 46Å.

The growth of the micelles with decreasing concentration follows a Φ^{-2} dependence reasonably well. Comparing the results for the GCDC-lecithin system [46], where the data was fitted over a larger concentration range, and hence the full form of the power law was used, B_3 was found to be 7.14$\times 10^{-3}$Å, which is of the same order of magnitude as the value found here of 2.1$\times 10^{-3}$Å. They are not expected to be exactly the same as different bile salts were used for the experiments.

This is mainly useful for predicting the length of the micelles for a given dilution. As explained in section 8.2, it is used to estimate the final dilution as obtained from the stopped flow setup, when this was found to vary slightly from the expected value from the equilibrium measurements.

Cross-section of micelles

There is very little change in the cross-section of the micelles with dilution, it could be imagined that the micelles would want to be slightly flatter with decreasing amounts of bile salt. At dilution 20 the cross-sectional area of the micelles is slightly larger than at the other dilutions studied. However, it has been observed [53, 43] that the number of lecithin molecules per length of cylindrical part of the micelle is constant, independent of the length of the micelles. This would be in agreement with the result of constant cross-section of the micelles. In other experiments with GCDC-lecithin system [46] across a wider concentration range only a very weak decrease in the cross-section of the micelles has been observed with increasing dilution.

7.1.2 TCDC-lecithin: Effect of R_{tot}

Four different L/BS ratios (R_{tot}) were examined (SANS experiments by S. U. Egelhaaf at the ILL) 0.3, 0.6, 0.9 and 1.2 all at various dilutions, and all with 100mM added NaCl. As explained in section 5, dilution 1 refers to 50mg/ml total lipid (i.e. lecithin + bile salt) for all the different R_{tot} series.

All the experiments shown in this section are in the high dilution regime, where a high dilution (in terms of concentration) changes for different R_{tot}, but here is used to refer to dilutions where the sample is close to the micelle to micelle-vesicle coexistence phase boundary. It is known that R_{tot} changes the onset of the micelle-vesicle coexistence region, with higher R_{tot} the transition occurs at lower total amphiphile concentrations.

The position of the phase boundary between mixed micelles and mixed micelle–vesicle coexistence in terms of the total amount of lecithin and bile salt is shown in table 7.2. These values were found from SANS experiments as the q–dependence of scattered intensity for micelles and for the mixed micelle–vesicle samples are very different. The errors in the table on the position of the phase boundary arise from the limited number of SANS measurements carried out.

The data from table 7.2 is shown graphically in figure 7.3. The data is fitted with a straight line crossing the BS-axis at 0.71mM, which agrees well with the CMC of TCDC ($\approx$ 0.7mM

R_{tot}	dilution	BS [mM]	LEC [mM]
1.2	10	3.6 ±0.2	4.32 ±0.24
0.9	32	1.3 ±0.08	1.17 ±0.07
0.6	41	1.2±0.03	0.72 ±0.02
0.3	77	0.9±0.03	0.27 ±0.01

Table 7.2: The phase boundary between mixed micelles and micelle-vesicle coexistence region in terms of the total amount of bile salt in the system. [NaCl] = 100mM.

[30, 52]) and the bile salt to lecithin ratio required for the solubilisation of the vesicles is found to be 0.67. The data is at sufficiently large lecithin concentrations that a linear fit to the data is appropriate [47].

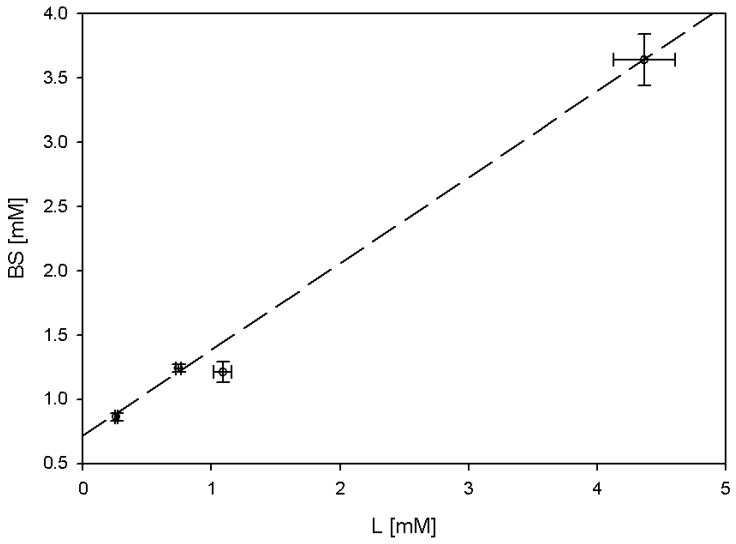

Figure 7.3: Phase boundary between mixed micelles (above) and mixed micelles and vesicles (below) as a function of the lecithin and bile salt concentrations.

It is noted that the results with R_{tot} = 0.9 are quite different from the other results. This might indicate a problem with the samples, and the further data treatment and discussion of this series will be treated with caution.

The SANS data, for the samples in the micellar region, was fitted using the same polydisperse worm–like chain model as previously, and the fits are shown in figure 7.4.

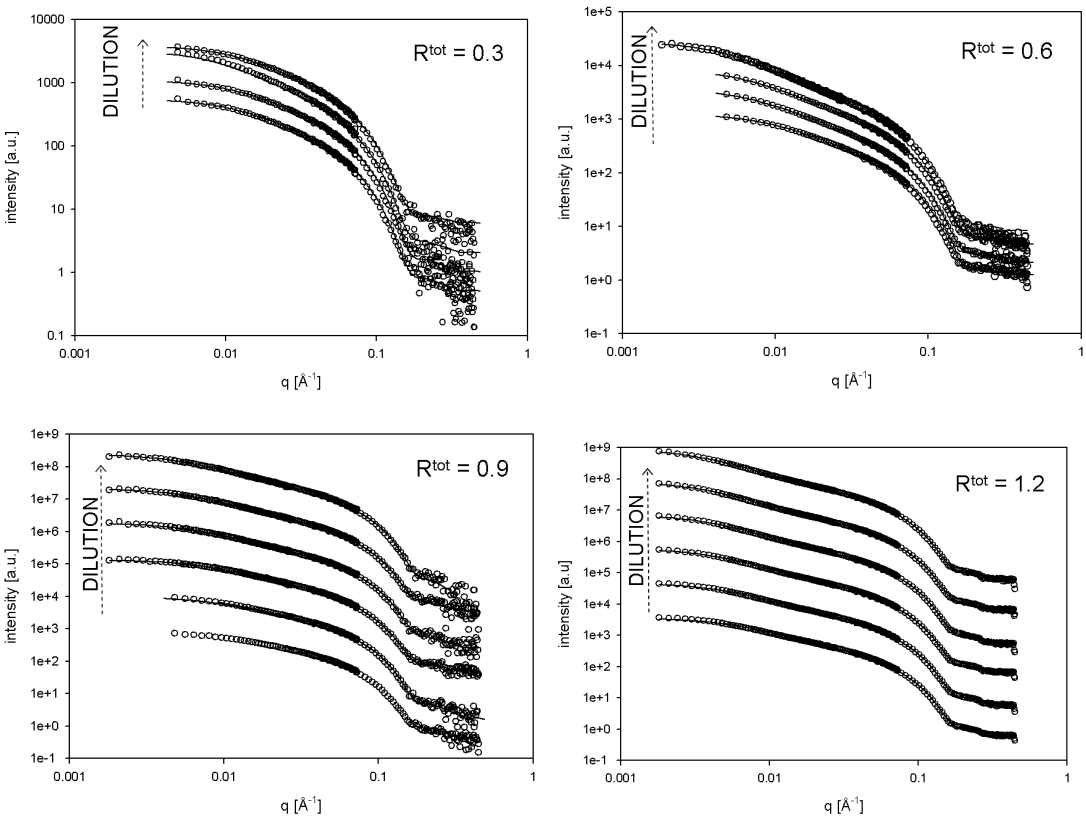

Figure 7.4: Data and fits for TCDC-lecithin system at 100mM NaCl and varying dilution and R_{tot}. Top left R_{tot} = 0.3, from bottom to top dilution 65, 68, 71 and 74. Top right R_{tot} = 0.6, from bottom to top dilution 32, 36, 38 and 40. Bottom left R_{tot} = 0.9, from bottom to top dilution 24, 26, 28, 30, 31 and 31.5. Bottom right R_{tot} = 1.2, from bottom to top dilution 4.3, 5.0, 5.6, 6.0, 6.3 and 6.6.

The fit parameters from the fits shown in figure 7.4 are summarised in table 7.3. For the fits the polydispersity is fixed to 1.0 and the Kuhn length to 400Å.

There is a slight increase in the cross–sectional area of the micelles $\pi(\sqrt{\epsilon R^2})^2$ with increasing R_{tot} and with increasing length of the micelles. The fact that the cross–section of the micelles seems flatter with increasing R_{tot} is not surprising, as with increasing amounts of lecithin in the system there will also be more lecithin (or conversely less bile salt) in the micelles and hence the curvature will be smaller.

However, this is in disagreement with the model for the phase behaviour of lipid–detergent systems: where the ratio of lipid to detergent in the micelles R_e is believed constant at the phase transition [47]. If R_e is constant at the phase transition, either the micelles should have

R_{tot}	0.3			R_{tot}	0.6		
dilution	L ±2 % [Å]	R [Å] ± 0.1	ϵ±0.01	dilution	L ±2 % [Å]	R [Å] ± 0.1	ϵ±0.01
65	138	18.1	1.52	32	203	18.1	1.52
68	137	18.0	1.51	36	297	18.2	1.54
71	223	18.2	1.53	38	341	18.1	1.53
74	141	18.2	1.53	40	595	18.1	1.54
R_{tot}	0.9			R_{tot}	1.2		
dilution	L ±2 % [Å]	R [Å] ± 0.1	ϵ±0.01	dilution	L ±2 % [Å]	R [Å] ± 0.1	ϵ±0.01
24	160	18.3	1.50	4.3	477	18.2	1.53
26	223	18.1	1.52	5.0	621	18.3	1.53
28	285	18.1	1.52	5.6	785	18.3	1.54
30	382	18.2	1.55	6.0	914	18.4	1.55
31	448	18.2	1.55	6.3	1070	18.4	1.55
31.5	523	18.1	1.54	6.6	1160	18.5	1.53

Table 7.3: Fit parameters for the TCDC micelles at varying R_{tot} and dilutions

the same length at the phase boundary regardless of R_{tot} (and the same composition), or the amount of bile salt in the cylindrical parts of the micelles should increase for longer micelles, assuming that the endcaps have a higher concentration of bile salt than the middle, as there is more middle part to endcaps for these longer micelles.

The length of the micelles can again be fitted with the Φ^{-2} dependence as used for the R_{tot}=0.9 data set in section 7.1.1. The length against the volume fraction of lecithin and bile salt is shown in figure 7.5 along with the corresponding fits.

The corresponding parameters are for $R_{tot} = 1.2$: B_3 = 5.7 $\times 10^{-2}$ Å, C = -62 Å. R_{tot} = 0.9: B_3 = 1.6 $\times 10^{-3}$ Å, C = -332 Å. R_{tot} = 0.6: B_3 = 1.5 $\times 10^{-3}$ Å, C = -463 Å. R_{tot} = 0.3: B_3 = 1.8 $\times 10^{-4}$ Å, C = -320 Å. The data for R_{tot} = 0.3 was fitted only using the first three points, where the length of the micelles is increasing with decreasing concentration. The fits are not as good as for the R_{tot} = 0.9 with 75mM added NaCl, possibly because here the concentration range studied is very narrow.

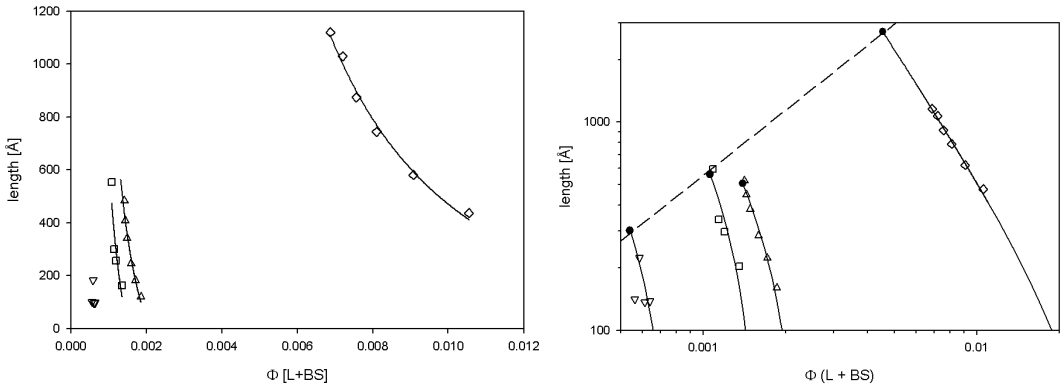

Figure 7.5: The length of the micelles against the volume fraction of lecithin and bile salt with fitted lines using L = $B_3\Phi^{-2}$ + C. R_{tot} = 1.2 diamonds, 0.9 triangles up, 0.6 squares and 0.3 triangles down. On the right the fits are extended to the micelle-vesicle phase boundary, where the points at the boundary are filled circles, dashed line fitted to length at the phase boundary (excluding R_{tot} = 0.9).

At the phase boundary the length of the micelles increases linearly with increasing concentration of lecithin and bile salt. The fact that the size of the micelles is linear with the concentration is suprising, as normally a $\Phi^{0.5}$ behaviour is expected for concentration induced growth. This might suggest that all the added amphiphile goes into the micelles, whilst the packing in the micelles does not change. This would be in agreement with the models for the phase behaviour, where at the phase transition a constant bulk concentration of bile salt is assumed with everything else in the micelles.

However there is a problem with fitting using L = $B_3\Phi^{-2}$ + C, as all C are negative. This would imply a minimum length of the system which is negative. Only the R_{tot} = 1.2 can be reasonably fitted using Φ^{-2} dependence and with a positive C. This would suggest that the growth of the micelles is different depending on R_{tot}, with lower R_{tot} the micelles grow faster than Φ^{-2} close to the phase boundary. Hence the empirical result of Φ^{-2} is only applicable for the specific case of the GCDC-lecithin system at R_{tot} = 1.1. A very simple model for the length of the micelles will be described in section 7.2.

7.1.3 TC - Lecithin System

Two different data series were measured for the TC-lecithin system, both with 100mM NaCl and one at R_{tot} 0.8, and another at R_{tot} at 0.9. Two different settings were used for the SANS experiments (as detailed in section 4.3.1) to explore the cross-section and the overall size of the micelles.

At R_{tot} = 0.9, two different dilutions 2.5 and 5 (only low q) were studied, the resulting intensities, as well as the resulting fits are shown in figure 7.6 on the left.

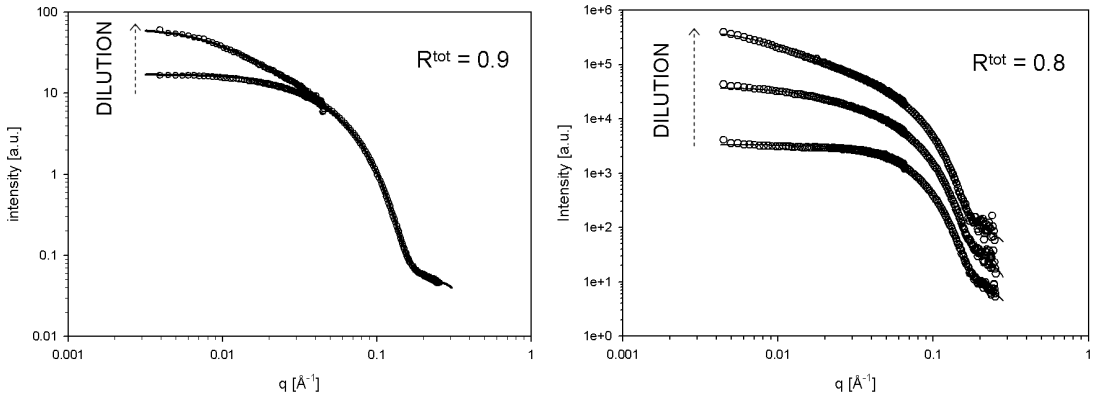

Figure 7.6: Lecithin-TC system variance of intensity. On the left R_{tot} = 0.9 and 100mM added NaCl, dilution 2.5 in below (covering the whole q-range) and dilution 5 above. On the right R_{tot}=0.8 and NaCl = 100mM, variance of intensity with q. Starting from the bottom with dilution 2, 4 and dilution 6 at the top.

At R_{tot} = 0.8, three different dilutions were measured 2, 4 and 6. The resulting intensities and fits are shown in figure 7.6 on the right.

The data was fitted for the length of the micelles L, the polydispersity σ_L/L, the radius of the cross-section R and the ellipticity of the cross-section ϵ. The resulting parameters are shown in Table 7.4.

Again there is not much variation in the size of the cross–section for the different samples, although there is an observable increase in the cross–sectional area for samples at higher dilution or increased R_{tot}. For the fits the Kuhn length was fixed at 400Å. The polydispersity was fixed to 1.0 for the longer micelles, but for the very short micelles this was not possible and the polydispersity was fitted and found to be much smaller. This is probably because the micelles

R_{tot}	dilution	L/BS	Φ	L ± 2 % [Å]	$\frac{\sigma L}{L}$	R [Å]	ϵ
0.8	2	0.8	0.022	50	0.35	17.6	1.55
0.8	4	0.8	0.011	84	1.0	18.2	1.54
0.8	6	0.8	0.007	295	1.0	18.4	1.60
0.9	2.5	0.9	0.018	80	0.5	18.1	1.60
0.9	5	0.9	0.009	216	1.0	18.0*	1.60*

Table 7.4: Lecithin-TC system with 100mM NaCl. Fitted parameters for the equilibrium data Kuhn length fixed to 400 Å.

are more ellipsoidal than worm–like and hence there is a large energy penalty of growing much beyond the optimum size.

7.1.4 TC-Lecithin: Effect of Added Salt

TC-lecithin SANS experiments were carried out to study the effect of added salt on the kinetics of micellar growth, and hence some equilibrium characterisation of the samples was also required. The dilution is 5 and two different amounts of added NaCl were studied, one with 150mM and the other with 600mM NaCl and R_{tot} was kept constant at 0.9. Only the low q behaviour is shown in figure 7.7.

The fits resulted in a length of 216 $\pm$ 3.2 Å for 150mM added NaCl and 143 $\pm$ 2.5 Å for 600mM NaCl. The other parameters in this q-range, b and σ_L/L were kept constant at 400Å and 1.0 in accordance with previous results (cross-section i.e. R, ϵ are not accessible at this q-range).

Although the data shown in figure 7.7 covers only the small q range, kinetic experiments have been carried out where the whole q-range has been explored (see section 8.3). It was found that the cross-section of the micelles does not change with the addition of salt. However, the length of the micelles decreases strongly with increased ionic strength. This is explained in section 3.2.4: the added salt screens the electrostatic repulsion between the bile salt molecules and more bile salt enters into the micelles. As the bile salt has higher spontaneous curvature than lecithin, the overall curvature of the micelles increases, leading to smaller micelles. However

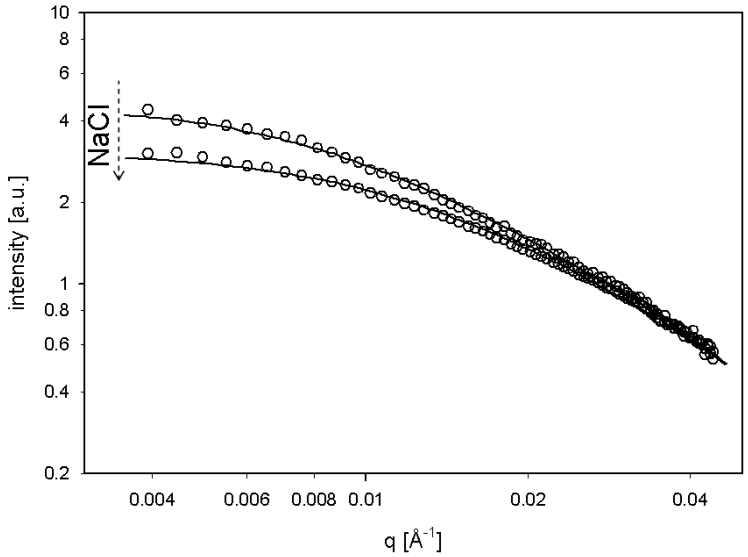

Figure 7.7: Effect of added salt lecithin-TC at dilution 5 and R_{tot}=0.9. Below 600mM added NaCl and above 150mM added NaCl.

there is also a competing term as the headgroup area per bile salt molecule decreases (as it is largely governed by the charge on the bile salt), which leads to a decrease in the spontaneous curvature of the bile salt molecules and hence 'flatter' i.e. longer micelles. This effect is too small to be noticed in comparison with the increased numbers of bile salt in the micelles [62].

7.1.5 GCDC-lecithin system

For the calculation of the composition of the micelles we will also use data from Arleth et al [46]. The system under study was lecithin–GCDC[1]. Their results are from SANS experiments and extend through a larger concentration range. The experiments were also carried out using a TRIS–based buffer and with 100mM added NaCl. The L/BS ratio, R_{tot} is 1.1, and again dilution 1 refers to 50mg/ml total lipid concentration (i.e. lecithin + bile salt)[2]. They fitted the resulting intensities to the worm–like chain model for the micelles, where this time the difference in the scattering densities of the lecithin and bile salt was taken into account.

[1]GCDC or glucochenodeoxycholate acid sodium salt is a bile salt similar to TCDC, instead of a taurine base it has a glycine group. The CMC of GCDC is 0.8mM, compared with 0.7mM for TCDC [30].

[2]In the paper the experiments were carried out referring to dilution one as 50mg/ml of lecithin only. However, the dilutions have been rescaled for simplicity to refer to a 50mg/ml lecithin+bile salt solution as dilution one.

The equilibrium length dependence on concentration for the lecithin–GCDC system is shown in table 7.5.

dilution	Φ	L [Å]	dilution	Φ	L [Å]
1.4	0.033	395	5.1	0.0090	294
1.9	0.024	342	6.9	0.0067	344
2.9	0.016	300	10.2	0.0045	531
3.8	0.012	284	13.4	0.0034	851

Table 7.5: Length of GCDC–lecithin micelles with dilution.

The length dependence on the volume fraction of lecithin and bile salt in the system Φ is shown in figure 7.8, where the two different growth regimes can be seen.

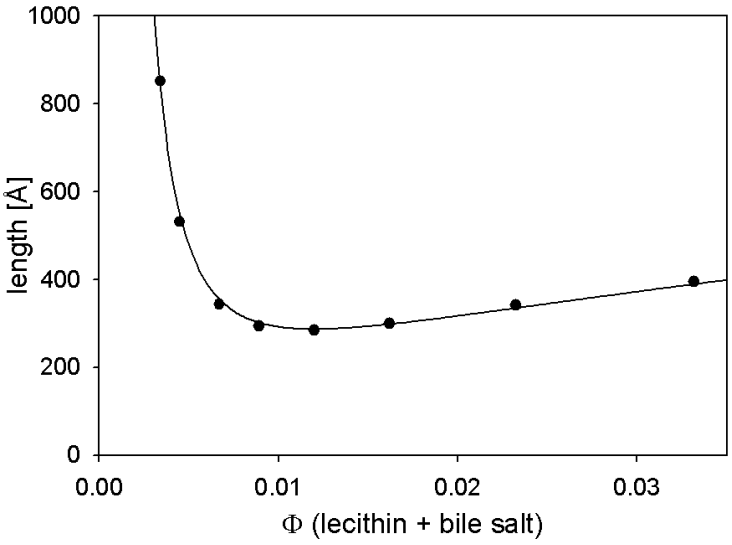

Figure 7.8: Length of the micelles as a function of the volume fraction of lecithin and bile salt for GCDC-lecithin micelles with 100mM NaCl and at R_{tot} = 1.1. Fitted line shows $\Phi = B_1\Phi^{0.5} + B_3\Phi^{-2}$.

At high concentrations the concentration induced growth can be seen, whilst reducing the concentration the micelles initially get shorter and afterwards they start to grow again through dilution induced growth (as explained in section 3.2.2).

7.2 Length of Micelles

We can make a very simple model for the composition of the micelles in the dilute regime, by assuming that close to the phase boundary (and in the dilute regime) the bile salt bulk concentration is constant at the CMC (0.71mM for TCDC), then one could expect that the length of the micelles would depend simply on the lecithin to bile salt molar ratio in the micelles R_e^m, given as [LEC]/([BS]-CMC), where [LEC] and [BS] refer to the total lecithin and bile salt molar concentrations. This is shown in figure 7.9 with GCDC-lecithin data from [46].

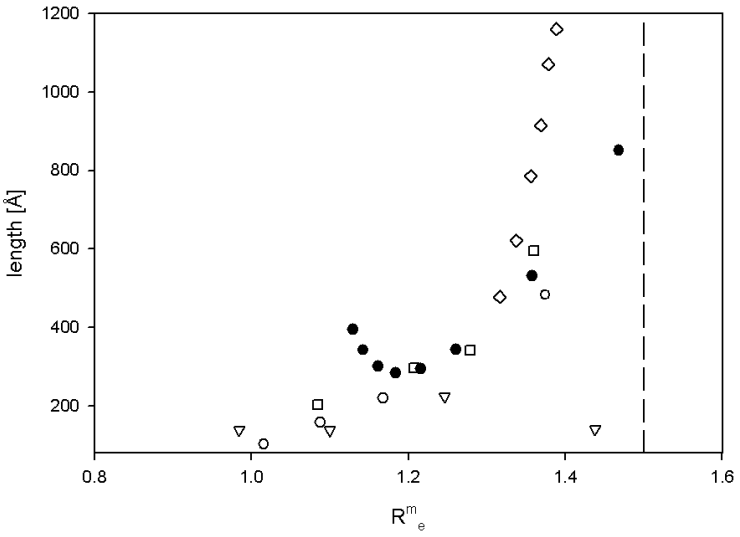

Figure 7.9: Length of the micelles as a function of R_e^{mic} for the different R_{tot} for TCDC with 100mM added NaCl R_{tot} = 1.2 - diamonds, 0.6 - square, 0.3 - down triangle, TCDC with 75mM added NaCl with R_{tot} = 0.9 - empty circles and GCDC-lecithin with 100mM NaCl and R_{tot} = 1.1 - filled circles. A dashed line indicates the position of minimum R_e^m at 1.5 indicating the phase boundary.

The data almost collapses onto one line (see figure 7.9), and we must remember that here any concentration effects on the size of the micelles have been ignored. Even the GCDC-lecithin series in the high dilution is close to the others. At the higher concentrations of amphiphile, R_e^m continues to decrease with increasing length, as the micelles start to grow through concentration induced growth.

Continuing with this simple model for the dilution induced growth of the micelles, we can calculate the partitioning of the bile salt into the bulk solution, endcaps and middle parts by using

a simple description for the mixed micelles. We assume that the bile salt bulk concentration is constant at the CMC (0.71mM) and the micelles consist of two endcaps and a cylindrical middle part. We assume furthermore that the composition of the micelles is constant throughout, i.e. that the bile salt surface cover of the endcaps and middle will be constant, and that the number of lecithin molecules per length of the middle λ will be constant as has been found experimentally [53, 43] (with no lecithin in bulk solution or in the endcaps).

This means that we can calculate the number of micelles n_{mic} in the system from the total amount of lecithin [LEC] and the length of the middle part of a single micelle L_{mid}:

$$n_{mic} = \frac{[LEC]N_A}{\lambda L_{mid}} \tag{7.1}$$

from the number of micelles and the length of the middle parts, taking λ = 0.7 $Å^{-1}$ (here we only use 0.7 $Å^{-1}$ [43] for the calculation and not 0.9 $Å^{-1}$ [53] as it is only a constant in the calculation and hence does not influence the trends observed), and assuming a constant bile salt surface cover of the middle parts ϕ_m of 0.7, we can calculate the amount of bile salt in the middle parts of the micelles. The amount of bile salt in the endcaps is then simply [BS] - $[BS]_{mid}$ - CMC. Plotting the number of endcaps in the system as a function of the amount of bile salt in the endcaps we get a linear dependence figure 7.10.

A linear fit to the data indicates that indeed the number of micelles depends only on the amount of bile salt in the endcaps, this would imply that the length of the micelles is chosen to be the minimum length for which there is enough bile salt available for the creation of the endcaps. The inverse of the slope gives the amount of bile salt required to create one endcap, this results in 11 bile salt molecules. If we now calculate the surface cover of the endcaps, assuming that an endcap is a semi-sphere with a radius of 22 Å and the surface area of one bile salt molecule in the endcap is 200 $Å^2$ the surface cover is 0.74.

However, these results are quite different from simple bile salt micelles, where it is found that the number of bile salt molecules (TDC) per micelle is about 12 and the radius of the simple micelle is around 10Å [38]. This might indicate that the endcaps of the mixed micelles are not pure bile salt, but in fact there is some lecithin in there as well, or then the fact that the endcaps

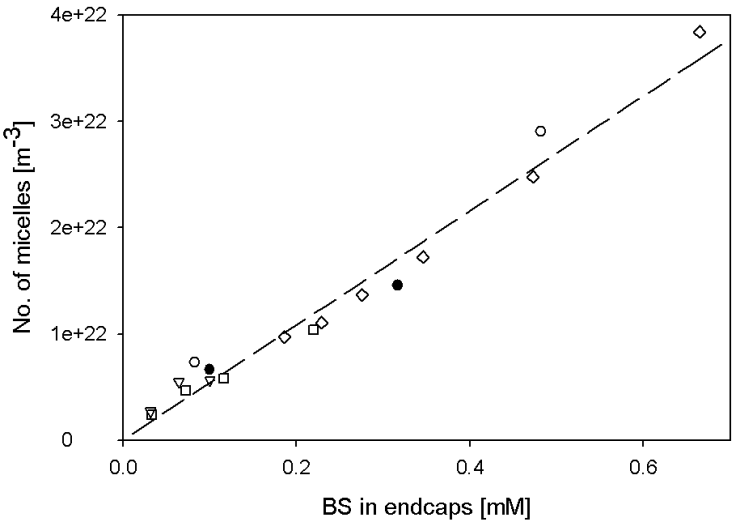

Figure 7.10: Number of endcaps in the system as a function of the amount of bile salt in the endcaps. TCDC with 100mM added NaCl R_{tot} = 1.2 - diamonds, 0.6 - square, 0.3 - down triangle, TCDC with 75mM added NaCl with R_{tot} = 0.9 - empty circles and GCDC-lecithin with 100mM NaCl and R_{tot} = 1.1 - filled circles. A dashed line shows a linear fit to the data at 75mM added NaCl.

are attached to the cylindrical part with a cross-sectional radius of 22 Å means that more bile salt is required to cover the endcap than to form a simple micelle.

The result of a linear relationship between the number of endcaps and the amount of bile salt in the endcaps is in agreement with the understanding that it is indeed the creation of these highly curved ends that results in the growth of the micelles at low concentrations. In the section 7.3 we will explore a slightly more sophisticated model for the composition of the micelles, where the partitioning of bile salt into bulk solution, the middle parts and endcaps is achieved through adsorption isotherms.

7.2.1 Spontaneous Curvature Model

The simple model is reminiscent of the spontaneous curvature model for the mixed micelles [48], where the curvature of a mixed micelle (i.e. fixing the length of the worm–like micelle) is given solely by the surface concentration of lipid and detergent (i.e. lecithin and bile salt).

The transitions between the different phases (mixed micelles to micelle-vesicle coexistence

etc.), as well as the curvature of the micelles has also been explained in terms of the average curvature of lecithin and bile salt [48] (as mentioned in section 3.2.1). It is assumed that the curvature of the aggregate is only defined by the different surface concentrations of lecithin and bile salt with their different spontaneous curvatures. If it is assumed, as previously, that lecithin only exists in the aggregates, the partitioning of bile salt and lecithin between the bulk solution and the micelles can be calculated. The model effectively assumes that the lecithin to bile salt ratio in the middle parts will be constant and likewise the endcap coverage.

In the dilute regime, this seems like a reasonable assumption, as the growth of the micelles is related to the extra lecithin in the aggregates. Calculating the spontaneous curvature of the micelle C_m, in terms of the surface fraction of cylindrical middle part and curved endcaps.

$$C_m = \frac{L_m + 4R}{RL_m + 2R^2}, \tag{7.2}$$

where L_m is the length of the cylindrical part (given by $L - 2R$) and R is the average radius of the cross–section, as well as the radius of the spherical endcap.

The spontaneous curvature of a mix of lecithin and bile salt C_0 can be calculated as follows [48]

$$C_0 = \frac{a_B \rho_B C_B + a_L \rho_L C_L}{a_B \rho_B + a_L \rho_L}, \tag{7.3}$$

where a_B is the area of a bile salt molecule on the surface of a micelle, ρ_B is the number density of bile salt molecules on the surface, C_B is the spontaneous curvature of bile salt, taken as $1/R$. a_L is the area of a lecithin molecule on the surface of a micelle, ρ_L is the number density of lecithin molecules in the micelles (taken as total number density of bile salt in the system) and C_L is the spontaneous curvature of lecithin, which as it is bilayer forming, is taken as 0. We take a_B = 200 Å^2 as used for the compositional model and a_L as 72 Å as found for the surface area of lecithin molecules in a bilayer [36]. The result of R_e^m with length of the micelles is shown in figure 7.11. Where the amount of bile salt in the bulk solution has been left as a free parameter fitted such that the correct R_e^m is achieved for a given length of micelle i.e. C_0 is fixed by the size of the micelle and we can use this to calculate required C_B and C_L to achieve this curvature, where C_L is fixed by the total concentration in the sample and C_B is the result

of total amount of bile salt in the sample minus the bulk concentration (which can vary from sample to sample).

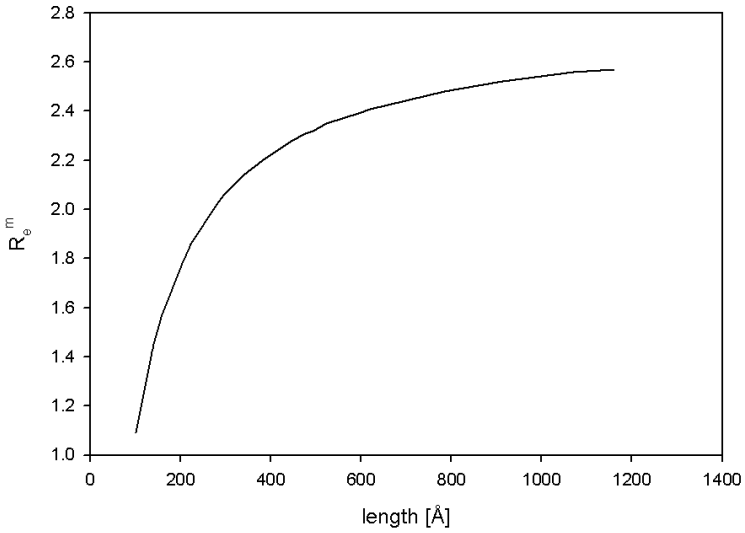

Figure 7.11: R_e^m as a function of the length of the micelles as calculated using the spontaneous curvature model, where the bile salt bulk concentration was left as a free parameter.

This means that for a given total concentration of lecithin and length of the micelles, we can calculate the amount of bile salt that is required in the micelles to satisfy the spontaneous curvature arguments, and hence the amount of bile salt that is in the micelles. It is obviously not possible to differentiate the amount of bile salt in the cylindrical parts of the micelles and the endcaps.

It is not possible to achieve consistent R_e^m values for the system using this model with a constant bile salt concentration in solution (as described in the previous section). However, we will return to the spontaneous curvature model in section 7.4.1 where the bile salt bulk concentration is allowed to vary throughout the dilute regime and indeed it is possible to model the growth as arising from the spontaneous curvature of the aggregates.

7.3 Model for the Composition of Micelles

A model that can be used to calculate the composition of the micelles is described. The basis lies in the equations for the conservation of bile salt and and lecithin, and on the partitioning of the bile salt between the bulk and the micelles, where the amount of bile salt in the endcaps and in the cylindrical parts of the micelles are treated separately. It is also assumed that the lecithin recides solely in the cylindrical part of the micelles.

Starting with a model for the worm–like micelle: it is modelled as consisting of a cylindrical central part with an elliptical cross-section and two ellipsoidal endcaps. Thus, the average curvature of the cylindrical part can be approximated as $1/R_{av}$, where R_{av} is the average radius of cross-section, and the curvature of the endcaps is approximately $2/R_{av}$. The length of the middle part for each micelle L_{mid} is taken as the contour length L, from which the length taken by the two endcaps is removed i.e. L_{mid} = L - $2R_{av}$.

It is assumed that the lecithin resides solely in the middle part of the micelle. Lecithin in bulk is neglected, because of its extremely low solubility (10^{-10}M). Lecithin in the endcaps is also ignored due to the lower spontaneous curvature of lecithin, it is assumed to prefer the lower curvature of the middle part to the highly curved ends. This means that the entropy of mixing within the micelles is assumed negligible.

Neutron scattering experiments by Hjelm [53] and Egelhaaf [43] indicate that the amount of lecithin in the cylindrical part is almost independent of the length of the micelles. It was found to be constant at λ = 0.9 Å^{-1} lecithin molecules per length of cylindrical part in the experiments where R_{tot} = 0.22 [53] and λ = 0.7 Å^{-1} when R_{tot} = 0.7 to 1.1 [43]. This means that the volume fraction of lecithin Φ_L can be used to express the length density of the cylindrical part of the micelles (length of the middle part of one micelle L_{mid} times number density of micelles n_{mic}) through conservation of lecithin as

$$\Phi_L = n_{mic} L_{mid} \lambda v_L, \tag{7.4}$$

where v_L is the volume of a lecithin molecule.

However, the bile salt is divided between the bulk solution, the curved endcaps of the micelles and the cylindrical parts. This means that the bile salt resides in three different environments, freely in bulk solution, in highly curved endcaps (with no lecithin) and in the cylindrical parts. This means that the entropy of mixing for the endcaps is effectively ignored, however as it is believed that the bile salt concentration is higher in the endcaps than the middle parts by taking an 'effective' area for the endcaps that is smaller than what is used here could be used to include some lecithin in the endcaps as well. Alternatively a increase in λ will result in smaller n_{mic} which leads to the bile salt having a smaller surface area of endcaps, resulting in a similar effect as incorporation of lecithin molecules into the endcaps. This can be expressed through mass conservation of bile salt Φ_{tot} as:

$$\Phi_{tot} = \Phi_{mid} + \Phi_e + \Phi_b, \tag{7.5}$$

where Φ_{mid} denotes the volume fraction of bile salt in the cylindrical part of the micelle, Φ_e is the volume fraction of bile salt in the endcaps and Φ_b is the volume fraction of bile salt in bulk solution.

It is assumed that the bile salt is free to move around between the three environments as shown in figure 7.12, where the bile salt can enter and leave the micelles. The movement of the bile salt is also assumed to be fast so that there is a local equilibrium. It is assumed that the bile salt in bulk solution exists only as monomers.

The partitioning of the bile salt between the encaps, cylindrical part and bulk is modelled using the Davies' isotherm (see section 2.1), where the surface coverage by surfactant molecules ϕ_r[3] can be expressed in terms of the bulk volume fraction of surfactant Φ_b and the energy gain of adding a surfactant molecule onto the surface α as

$$\phi_r = \frac{\Phi_b}{\Phi_b + \mathrm{e}^{-(\alpha+\psi_0)/kT}}, \tag{7.6}$$

where ψ_0 is the electrostatic potential on the surface arising from the charge of the bile salt. The potential on the surface is related to the surface fraction covered by bile salt molecules by

[3]The convention will be to refer to volume fractions as capital Φ and to surface fractions as small ϕ

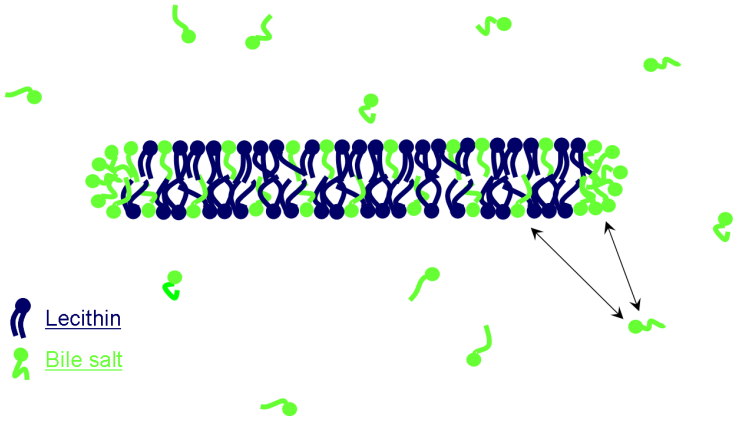

Figure 7.12: Exchange of bile salt between endcaps and cylindrical parts of the micelle and bulk solution.

the Gouy-Chapman theory [66] in a 1:1 electrolyte (such as NaCl) as:

$$\phi_r = -4c_s \mathrm{N}_A a_B \kappa_D^{-1} \sinh(e\psi_0/2kT), \tag{7.7}$$

where c_s is the ionic strength of the solution, N_A Avogadro's number, a_D the surface area of a bile salt molecule on the surface of a micelle and $\kappa_D^{-1} = (2c_S \mathrm{N}_A e^2/\epsilon kT)^{-1/2}$ is the Debye length and ϵ the dielectric constant of water.

As the surfaces of the endcaps and the middle part of the micelle are quite different, each of them has its own equilibrium distribution through the shared bile salt concentration in bulk. This leads to the assumption that the energies of adding a bile salt molecule onto the endcaps or onto the cylindrical part of the micelles are different. Using equation 7.6 the surface cover of the endcaps and the middle part lead to:

$$\Phi_b = \frac{\phi_e \mathrm{e}^{-(\alpha_e+\psi_{0e})/kT}}{1-\phi_e} = \frac{\phi_m \mathrm{e}^{-(\alpha_m+\psi_{0m})/kT}}{1-\phi_m}, \tag{7.8}$$

where the subscripts e and m refer to the endcaps and the cylindrical parts respectively.

Furthermore, it is assumed that the energy gain of adding a bile salt molecule to the endcaps is higher than adding one to the cylindrical part. This is because at the ends, not only is the curvature higher (more like the spontaneous curvature of bile salt), but adding a bile salt molecule to the end will also help shield the hydrophobic tails of lecithin.

We also assume that the volume fractions and the surface fractions of the bile salt in the end and middle parts can be related through the number density of endcaps n_{ec} ($= 2n_{mic}$) and the total length density of the middle parts of the micelles $n_{mic}L_{mid}$ as:

$$\Phi_e = \frac{2\pi R^2 v_B}{a_B} n_{ec}\phi_e, \tag{7.9}$$

$$\Phi_m = \frac{2\pi R v_B}{a_B} n_{mic}L_{mid}\phi_m, \tag{7.10}$$

where R is the average cross–sectional radius of the micelles and v_B is the volume of a bile salt molecule.

Using the total concentration of bile salt and lecithin, the length of the micelles, the amount of added electrolyte and the area of a bile salt molecule on a surface as input parameters, the above equations can be solved simultaneously to give the partitioning of the bile salt in the micelles. The composition is given in terms of surface cover (and surface potential) of endcaps and cylindrical parts and the amount of bile salt in bulk.

7.4 Calculation of the Composition of Micelles

As explained in section 7.3 the model described can be used to calculate the composition of the worm–like micelles, through the calculation of the partitioning of the bile salt into bulk solution, middle parts and the endcaps of the micelles. However, there remain several uknown parameters in the model: λ, α_m and α_e. For λ there are two values found in literature, where the values have been calculated from neutron scattering experiments. For R_{tot} = 0.2 λ was found to be 0.9 molecules Å^{-1} [53] and for R_{tot} = 0.7-1.1 λ was found as 0.7 molecules Å^{-1} [43]. Both sets of experiments found that λ does not change significantly with changes in the length of the micelles.

For both λ = 0.7 and 0.9 Å^{-1}, we will fix α_e and α_m by comparison with other results in the literature. There are no experiments where the bile salt bulk concentration Φ_b has been measured for the overall concentrations studied here, but there are two distinct ways of fixing α_e and α_m with the available data. Either we can assume that Φ_b is constant for a given total

bile salt concentration, i.e. that the value of Φ_b must be satisfied before the bile salt enters into the micelles. This means that the results can be compared to dialysis measurements, where the bulk concentration of bile salt (monomers and simple micelles) was measured for the TCDC-lecithin system with R_{tot} = 0.2 [80].

Alternatively, it can be assumed that at the phase boundary of mixed micelles and micelle-vesicle coexistence Φ_b should be equal to the CMC (as the experiments are in the low concentration regime [47]) and hence that the bile salt to lecithin molar ratio in the micelles should remain above Q_e^m, which for TCDC-lecithin is equal to 0.67.

The results will be presented in two sections, firstly fitting α_e and α_e with the dialysis data at R_{tot} = 0.2 (section 7.4.1) and secondly fitting with Q_e^m (section 7.4.2). In both sections the TCDC-lecithin experiments at varying R_{tot} are discussed along with results on the GCDC-lecithin system, where the data is from [46], and the length of the micelles was studied across a wider concentration range.

The results for the TC–lecithin system are not presented as there is not sufficient data to draw clear conclusions, and the very shortness of the micelles renders the model less reliable. The assumption of the micelle being constructed of a separate cylindrical part and endcaps is not a reasonable assumption when the micelles are less or around 100Å long.

There are eight input parameters to the model, three of which are known from sample preparation: amount of bile salt Φ_{tot}, amount of lecithin Φ_L and ionic strength of the solution c_S (which includes added NaCl, contribution from the buffer and the bile salt, see section 5.3). The length L is fitted from the SANS data, and the length of the cylindrical part L_{mid} is taken as L - 2R_{av}, where $R_{av} = \sqrt{\epsilon R^2}$ i.e. for TCDC–lecithin micelles this will be L-45Å.

The surface area of a bile salt molecule is taken as 200Å^2 as used in [57] for the area taken by a TCDC molecule on the rim of a disc-like micelle. The volume of a lecithin molecule v_L = 1266 Å^3 [37], the volume of a TCDC molecule = 660 Å^3 [78] and the volume of a GCDC molecule = 600Å^3 [46].

The two values for the number of lecithin molecules per length of micelle found in literature are used i.e. λ = 0.9 Å^{-1} [53] and λ = 0.7 Å^{-1} [43].

The energy gain of adding a bile salt molecule to the endcap α_e and to the middle part α_m are fixed to find agreement with parameters from the literature data, either fixing the bile salt bulk concentration with dialysis results [80] or fixing R_e^m with the phase boundaries [47]. The value of 10kT for the energy gain of adding a bile salt molecule to the edge of a disc–like micelle [57] is chosen as a starting value, where it is expected that α_e and α_m will not deviate greatly from this. It is always assumed that α_e is greater than α_m, i.e. it is more favourable to add a molecule to the endcaps than the middle of the micelle. Several values for α_e and α_m are used, where the details will be in the following sections.

The input parameters are summarised in table 7.6.

Φ_{tot}	exp	λ [Å^{-1}]	0.7/0.9
Φ_L	exp.	a_B [Å^2]	200
c_S [M]	exp.	α_e [kT]	fix
L [Å]	fit	α_m [kT]	fix

Table 7.6: Summary of input parameters for composition of the micelles, exp. = known from experimental detail, fit = fitted from SANS data and fix = fixed for agreement with literature data.

There is no available data for the bulk concentration of GCDC-lecithin, hence α_e and α_m are fixed for the TCDC data and the same input parameters are used to calculate the composition of the GCDC-lecithin micelles.

7.4.1 Comparison with bile salt bulk concentration

Duane [80] has measured the amount of bile salt in bulk solution (TCDC and TC) in the mixed micelle system by dialysis experiments. The dialysis experiments were done through a dilution series with R_{tot} = 0.2 (for TCDC). The experiments were also carried out with 100mM added NaCl in a buffer adjusted to pH 7.3.

The total amounts of bile salt in the system, the amount of bile salt in bulk and the bile salt to lecithin molar ratio in the micelles Q_e^m are shown in table 7.7.

We note that the two lowest concentrations have Q_e^m that is less than what was found at the phase boundary, this suggests that either the samples are in the micelle-vesicle coexistence

BS [mM]	BS bulk [mM]	Q_e^m	BS [mM]	BS bulk [mM]	Q_e^m
19.9	4.45	3.6	3.0	1.57	1.9
19.8	3.95	3.6	2.0	1.25	1.1
11.9	2.99	3.3	1.5	1.02	0.9
11.1	2.97	3.3	1.0	0.78	0.4
6.0	2.18	2.7	0.7	0.59	0.2
4.0	1.81	1.9			

Table 7.7: The experimental data from [80].

region or that we have entered the very low concentration regime where the linearity of the phase boundary breaks down [47].

Using the parameters given in table 7.6, the partitioning of the bile salt and hence composition of the micelles can be calculated for each of the samples where the length has been measured using SANS, by simultaneously solving equations 7.4 to 7.10.

For the GCDC-lecithin system the input values for the model are the same as those used for the TCDC system, apart from the lengths which are taken from the data shown above [46]. It is acknowledged that TCDC and GCDC are different molecules, but in the absence of detailed information on their specific behaviour in the micelles it is assumed that they are similar enough for the purposes of the model.

To fix α_e and α_m, the composition of the micelles is calculated for both λ = 0.7 Å^{-1} and 0.9 Å^{-1} using various α until agreement with Φ_b from the dialysis measurements is found. In figure 7.13 the comparison with Duane's dialysis data [80] is shown. The values for α_e and α_m are 11.5kT and 9.5kT for λ 0.9 Å^{-1} and 10.5kT and 8.5kT for λ 0.7 Å^{-1}.

As can be seen by changing α_e and α_m the calculated values for bile salt concentration in bulk can be made to agree with the dialysis data. It is not suprising that α_e and α_m are higher for λ = 0.9Å^{-1} than for λ = 0.7Å^{-1}, as increasing the packing of lecithin leads to fewer micelles in the solution and to achieve constant bulk concentration the bile salt surface cover will have to increase in the micelles. It is noted that the values for Φ_b are not exactly the same for the two different λ but this is because the data was fitted by inspection to achieve reasonable agreement,

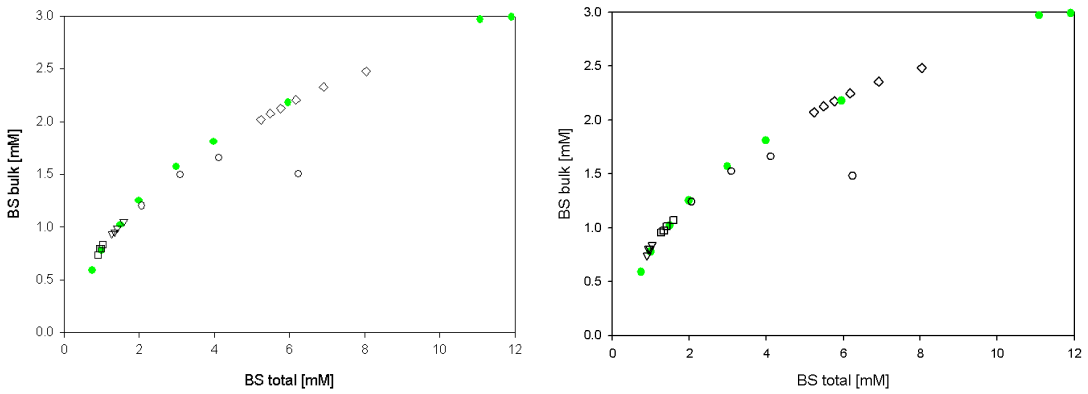

Figure 7.13: Amount of TCDC in bulk against the total amount of TCDC in the system for the dialysis data (filled circles) and for calculated values (black edges). This is shown for different R_{tot} 1.2 diamonds, 0.6 square, 0.3 down-triangle and 0.9 (with 75mM added NaCl instead of 100mM) circle. On the left for λ = 0.9 Å^{-1} with α_e = 11.5 and α_m = 9.5 and on the right for λ = 0.7 Å^{-1} with α_e = 10.5 and α_m = 8.5.

to achieve closer agreement α_e and α_m should be fitted more rigorously.

Now that we have fixed α_e and α_m we can start exploring the resulting composition of the micelles. We start by looking at the surface cover of bile salt and the resulting electrostatic surface potential.

Bile salt surface cover and surface potential

In figure 7.14 the surface cover of bile salt and the electrostatic potential on the endcap and middle surfaces of the micelles are shown for both λ = 0.7 Å^{-1} and 0.9 Å^{-1} as a function of the total amount of bile salt in the solution. The results are shown as a log-linear plot to allow us to see the behaviour at low bile salt concentrations more clearly.

The surface cover of the micelles increases continuously with increasing concentration of bile salt, where especially for the high concentration sample (of GCDC-lecithin highest four points of filled circles) the surface cover of the middle parts increases very fast. In this region the micelles are growing through concentration induced growth and hence the bile salt cover could be expected to grow at a faster rate.

The series with a lower salt concentration (empty circles) has a slightly lower surface cover

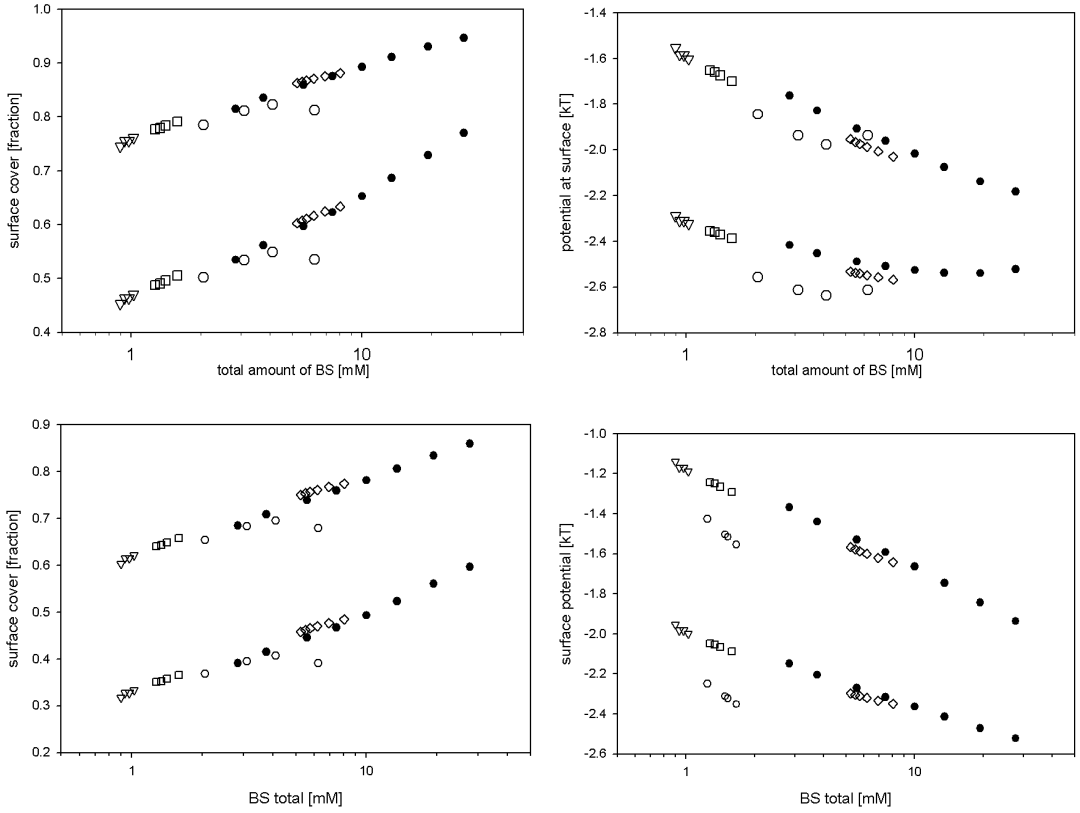

Figure 7.14: On the left the percentage of the surface covered by bile salt for middle part (lower values) and for endcaps (higher values) and on the right the surface potential on the middle part (lower values) and endcaps (higher values). This is shown for different R_{tot} 1.2 diamonds, 0.6 square, 0.3 down-triangle and 0.9 (with 75mM added NaCl instead of 100mM) circle, GCDC-lecithin with R_{tot} = 1.1 and 100mM NaCl filled circles. Above λ = 0.9 Å^{-1} and below λ = 0.7Å^{-1}.

than the others, but the surface potential is considerably more negative. This is not surprising given that there is less screening due to the lower ionic strength of the solution (75mM instead of 100mM NaCl).

We only want to mention that plotting the surface cover (or potential) of the micelles as a function of the length of the micelles results in no discernible trend but the values for the different series are slightly separated with no continuity.

R_e^m with length of the micelles

We will now turn our attention to the lecithin to bile salt ratio in the micelles, which we calculated using the very simple model in section 7.2. R_e^m was found to increase with increasing length of the micelles in the dilute regime and a clear change was seen for the concentration induced growth regime. Plotting R_m^e as a function of the length of the micelles is shown in figure 7.15.

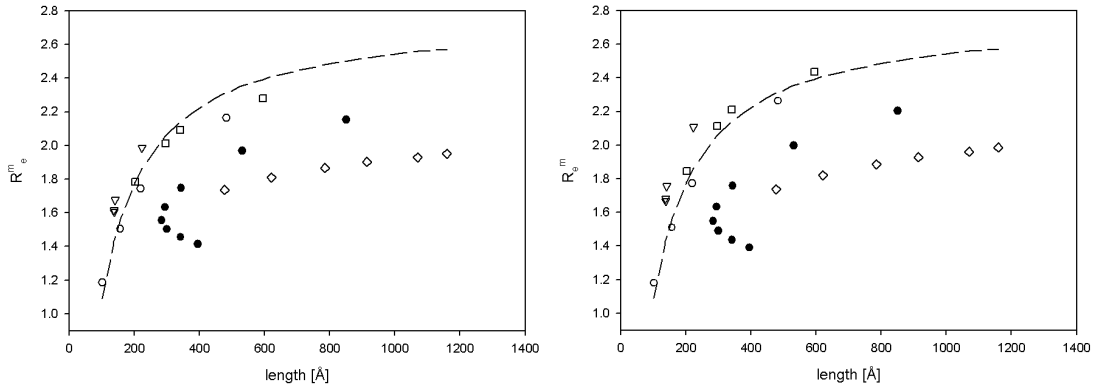

Figure 7.15: R_e^m as a function of the length of the micelles on the left for λ = 0.9 Å^{-1} and right for λ = 0.7 Å^{-1}. for the different R_{tot} symbols see caption in figure 7.14. Dashed line indicates the R_e^m as calculated using the spontaneous curvature model for the given length with Φ_b as a free parameter.

As expected the resulting R_e^m for the two different λ are almost exactly the same, this is not surprising as the two α were chosen so as to find agreement with the bile salt bulk concentration and if this is the same for both λ then R_e^m should be as well.

For all the different data series in the dilute regime R_e^m increases with increasing length and for the lower R_{tot} series it is in reasonable agreement with the calculated R_e^m from the length of the micelles using the spontaneous curvature model (see section 7.2.1). However, the values for R_{tot} = 1.2 are much lower than could be expected for their size. The non-monotonic increase in R_e^m with the length of the micelles is in disagreement with the spontaneous curvature model (where the length is assumed to depend directly on R_e^m). This could mean that the difference between α_e and α_m is too great and if α_m is much smaller then for longer micelles there will be very little bile salt in the middle parts of the micelles.

Where the length of the micelles was measured for a larger concentration range (GCDC-lecithin), there is a clear difference in the results as the micelles begin to grow again through concentration induced growth, where R_e^m starts to decrease with the increasing length (four lowest filled circles in figure 7.15), as more bile salt enters into the micelles.

Bile salt concentration in endcaps and middle parts

We can also look at the total amounts of bile salt in the endcaps and middle parts of the micelles (in mM) as a function of the length of the micelles initially. Firstly presenting the data for both λ = 0.7 Å^{-1} and 0.9 Å^{-1}, without distinguishing the different data series (i.e. different R_{tot}). This is shown in figure 7.16.

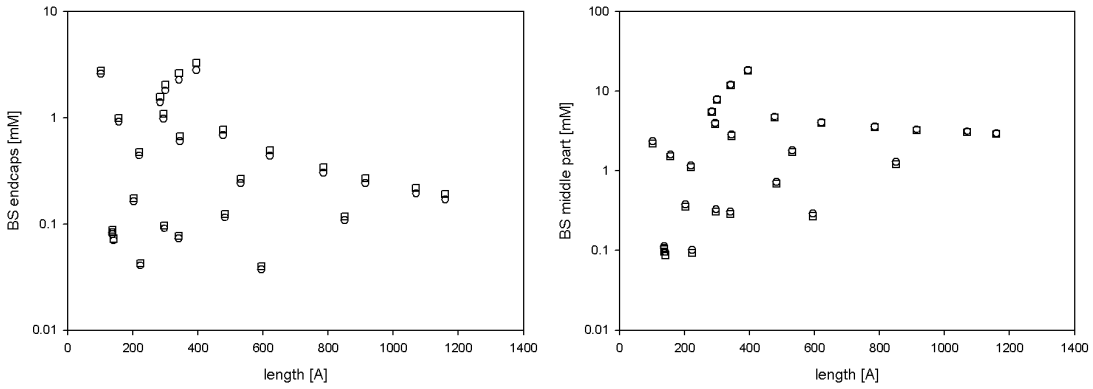

Figure 7.16: On the left the amount of bile salt in the endcaps as calculated with λ = 0.9 Å^{-1} (circles) and 0.7 Å^{-1}(squares) as a function of the length of the micelles.

As can be seen there is no clear trend on the amount of bile salt in the endcaps or in the middle parts of the micelles as a function of the length of the micelles, and in fact looking at the amount of bile salt in the endcaps as a function of the total bile salt concentration results in graphs that are equally chaotic. Between the two different λ the results are the same within the errors of the model, because of this in the following discussion we will only use the results with λ = 0.7 Å^{-1} as those for λ = 0.9 Å^{-1} are exactly the same when looking at the total amounts of bile salt in the endcaps and in the middle parts.

This is already interesting, as it seems that the choice of λ is not very important for the par-

titioning, and by increasing α_e and α_m we can increase the surface cover of the endcaps and middle parts such that the overall amounts in the different parts will remain the same.

To try and understand the partioning of bile salt into the endcaps and the middle parts we will start with a closer look at the amount of bile salt in the endcaps, this is shown now as a function of the length of the micelles divided by the total amount of lecithin in the system $\frac{L}{[\mathrm{LEC}]}$ (which is inversely related to the number of micelles in the system through equation 7.4). This is shown in figure 7.17, as mentioned before here only the results with λ = 0.7 Å^{-1} are shown.

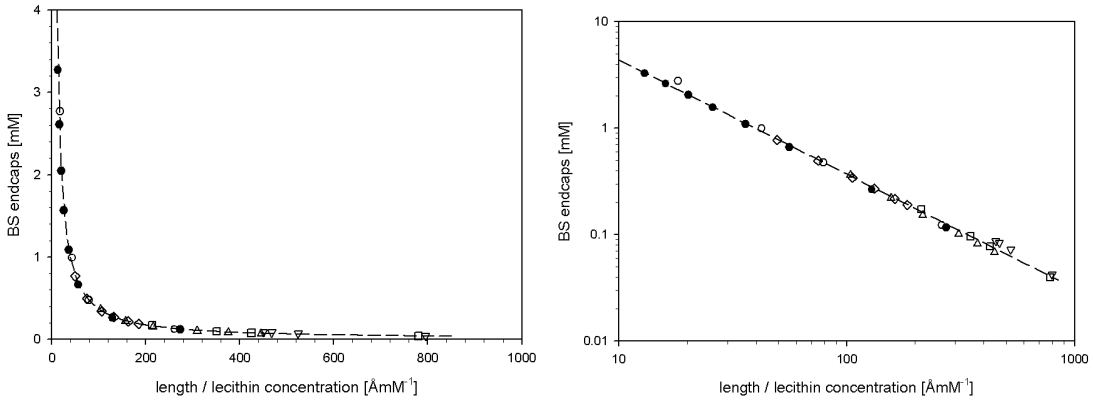

Figure 7.17: Amount of bile salt in the endcaps [mM] as a function of the length of the micelles divided by the lecithin concentration on the left on a linear plot and on the right as log-log representation. The data points for λ = 0.7 Å^{-1} use the standard notation (see label for figure 7.14). Dashed line given by $[\mathrm{BS}]_{ends}$ = 51(L/[LEC])$^{-1.1}$ (for λ = 0.7 Å^{-1}).

The amount of bile salt in the endcaps is almost inversely proportional to L/[LEC] (i.e. linearly dependent on the number of micelles in the system $n_{mic} \propto [\mathrm{LEC}]/L$), resulting in a fit with a power of -1.1. It is surprising that the amount of bile salt in the endcaps continues to follow the observed trend even in the concentration induced growth regime.

Now we can have a look at the amount of bile salt in the middle parts of the micelles, where the amount as a function of L/[LEC] is no longer appropriate. It could be imagined that the amount of bile salt in the endcaps depends strongly on the total amount of lecithin in the system (as this controls the amount of middle parts). The concentration of bile salt in the middle as a function of the lecithin concentration is shown in figure 7.18.

However we can note that the increase in the amount of bile salt in the middle parts of the

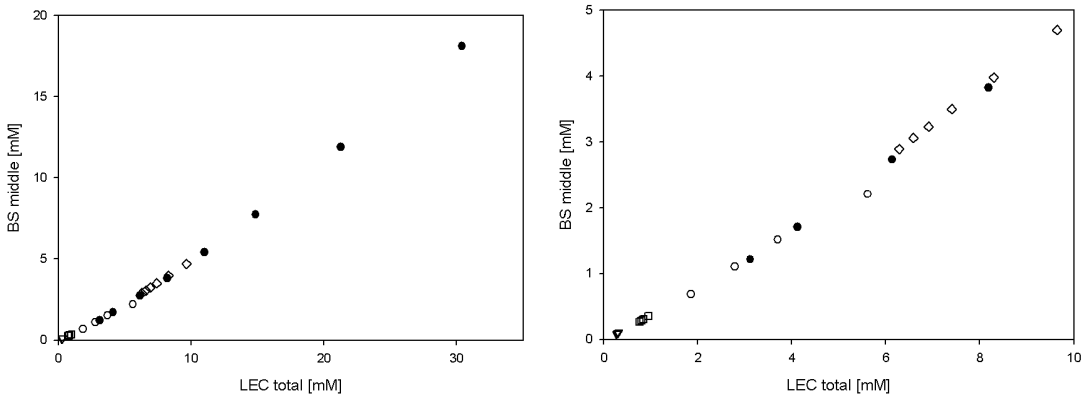

Figure 7.18: Amount of bile salt in the middle parts [mM] as a function of the length of the lecithin concentration, again data for λ = 0.7 Å^{-1} shown with the standard symbols (see figure 7.14). On the left across the whole concentration range and on the left a zoom of the lower concentration range.

micelles is almost linear with the amount of lecithin in the system, however as can be seen it is not completely linear. This is not surprising as the the surface cover by bile salt of the middle parts changes considerably for different concentrations. Especially when the concentration induced growth regime is encountered the amount of bile salt in the middle parts increases faster than previously.

7.4.2 Constant CMC

In this section we will fix α_e and α_m such that the composition of the micelles in the dilute regime will remain roughly constant, with a constant bile salt bulk concentration of 0.71mM. This is in agreement with the maximum R_e^m of 1.5 as found at the phase boundary, i.e. the lecithin to bile salt ratio in the micelles cannot exceed this maximum quantity. The resulting values for α_m and α_e are 11kT and 12kT for λ = 0.7 Å^{-1} and 12.5kT and 13.5kT for λ = 0.9 Å^{-1}. The bulk concentration as a function of the length of the micelles is shown in figure 7.19.

For all sets of data the bile salt bulk concentration remains constant in the dilute regime at around 0.71mM. It is only for the GCDC-lecithin series in the high concentration regime that the bulk concentration starts to deviate strongly from the CMC. It is in the high concentration regime that there are also marked differences in the amount of bile salt in the bulk between λ =

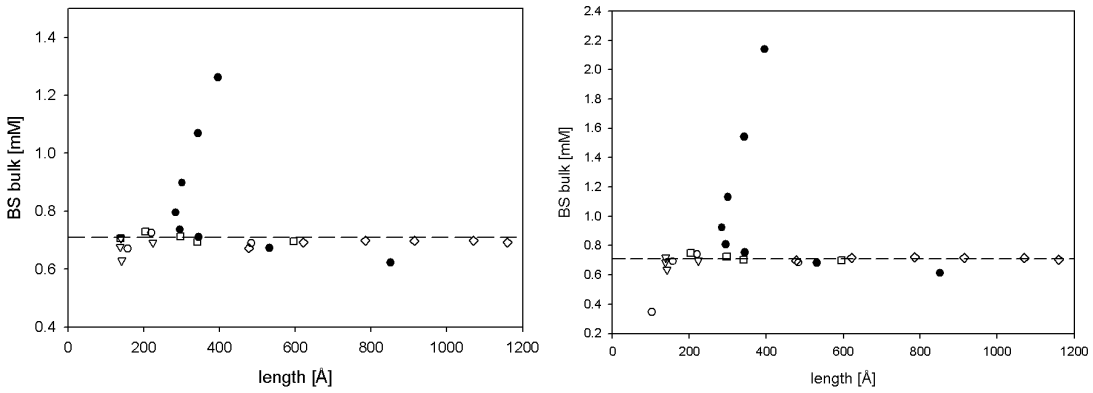

Figure 7.19: Bulk salt bile concentration as a function of the length of the micelles, dashed line indicates the CMC at 0.71mM. On the left for λ = 0.7 Å^{-1} and on the right for λ = 0.9 Å^{-1}. For the symboles see label for figure 7.14.

0.7 Å^{-1} and 0.9 Å^{-1} with the values for λ = 0.9 Å^{-1} being much higher than for λ = 0.7 Å^{-1}.

It is already interesting to note that such different behaviour can be obtained from the model by changing the ratio of α_e and α_m as well as their absolute values. For comparison see the dependence of the bulk concentration on the total amount of bile salt in the system in the previous section figure 7.13. However why this should change so dramatically is not clear, it could show the limitations of the model where the high concentration behaviour is not properly explained. It is known that the bile salt bulk concentration can increase beyond the CMC in the system [80, 81].

It might be that the bulk concentration only starts to increase once the micelles have reached their minimum size (which entropically is favourable) and further increase of the bile salt concentration leads to the growth of the mixed micelles as well as the formation of simple bile salt micelles.

Bile salt surface cover

Making sure that the bile salt bulk concentration remains constant at 0.71mM results in the composition of the micelles being fixed in the dilute regime, i.e. the bile salt surface cover of the endcaps and the middle parts will be constant. The surface cover is shown in figure 7.20.

The resulting surface potentials are almost constant as well (the difference in the ionic strength arising from the bile salt concentration is not easy to observe in the data), apart from R_{tot} = 0.9 with 75mM salt series where the corresponding surface potential is higher due to the lower ionic strength.

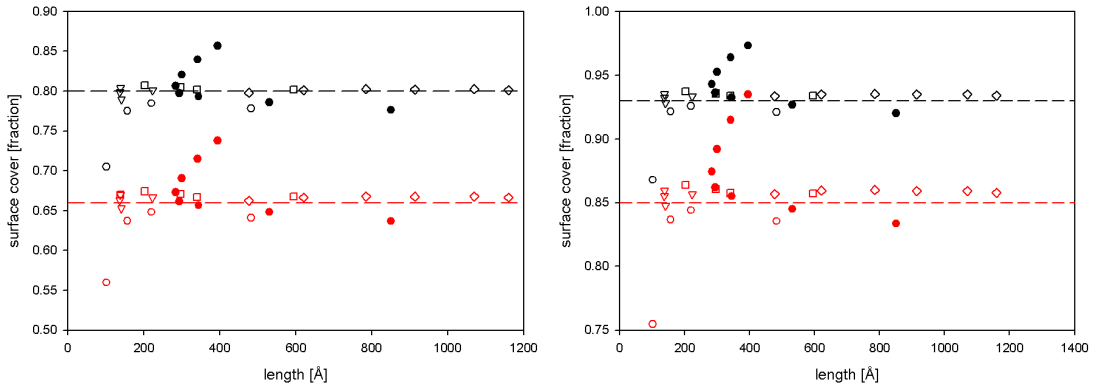

Figure 7.20: Surface cover of the endcaps and middle parts of the micelles as a function of the length of the micelles (higher values are endcap cover and lower values are middle part cover). The dashed lines indicate the average cover.

For both λ = 0.7 Å^{-1} and 0.9 Å^{-1} the surface cover in the dilute regime remains roughly constant. However there is a clear difference in the amount of cover, for λ 0.7 Å^{-1} the surface cover for the middle parts is around 0.66 and for the endcaps at around 0.8, but for λ 0.9 Å^{-1} the surface cover is 0.85 for the middle parts and around 0.93 for the endcaps. The relatively large differences arise from the very different α values used, as with a lower λ there is effectively less middle part and to achieve a constant bulk concentration of bile salt the coverage of the endcaps and middle parts will both be higher. The reason that you cannot only increase the middle cover without the endcap cover arises from the coupling of the surface cover and the endcaps through the bulk concentration.

The different α are required in order to maintain the constant bile salt bulk concentration, with a higher λ the lecithin is more closely packed in the micelles and hence (as there will be less micelles in the system see equation 7.4) there is effectively less surface for the bile salt to attach to and hence the coverage of the smaller surface needs to increase.

Lecithin to bile salt ratio in the micelles

We can calculate R_e^m in the micelles, where the ratio should now be below the 1.5 as fixed by the phase boundaries in this regime. R_e^m as a function of the length of the micelles is shown in figure 7.21.

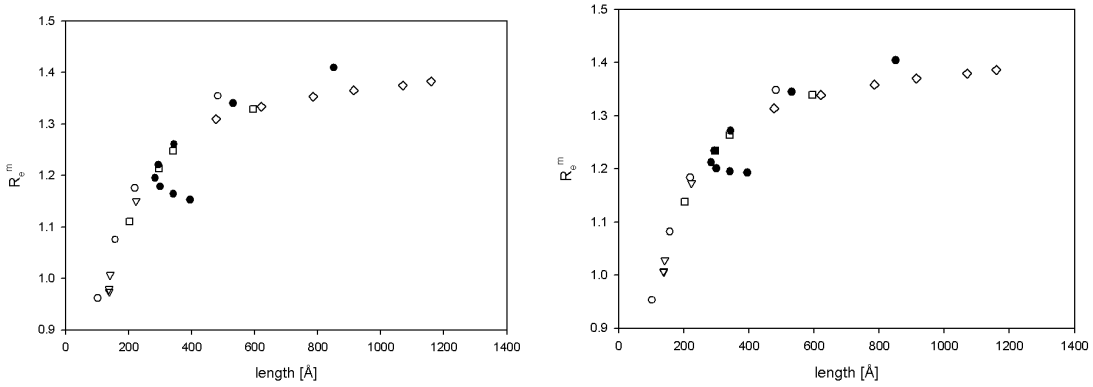

Figure 7.21: The lecithin to bile salt ratio in the micelles R_e^m as a function of the length of the micelles for λ = 0.7 Å^{-1} on the left and for 0.9 Å^{-1} on the right.

As expected R_e^m stays now below 1.5 for all the different sizes, where here the change from the dilution induced regime (increasing R_e^m with increasing length) to the concentration induced growth regime is clear (increasing R_e^m with decreasing length).

It was found earlier that as the micelles start to grow through concentration induced growth the bile salt bulk concentration starts to increase again, this means that there is a minimum R_e^m value which tells about the onset of the concentration induced growth. Making a rough estimate of this for the TCDC-lecithin system i.e. assuming that the micelles cannot be shorter than twice the major axial radius of about 60 Å results in R_e^m of around 0.9. Now we could use this value to predict when the bile salt bulk concentration for the data of Duane [80] should start to increase from the CMC value. This means that once Q_e^m has increased to about 1.1 the bile salt bulk concentration should start to increase in the system. Indeed looking at the results from table 7.7 we find that at Q_e^m = 0.4 the bile salt bulk concentration is about 0.78 very close to the CMC but at Q_e^m = 0.9 the bulk concentration has increased to 1.02mM. This is very approximate, but could explain why the bulk concentrations as measured by Duane are so much

higher than predicted by the model. The R_{tot} is much smaller in Duane's experiments so there is less lecithin in the system to make the mixed micelles, so at lower absolute concentrations of bile salt, the concentration induced regime is encountered.

Bile salt concentration in the endcaps and middle parts

We will now look at the bile salt concentrations in the middle parts and the endcaps, where (as in section 7.4.1) the amounts as calculated with λ = 0.7 Å^{-1} and 0.9 Å^{-1} are so similar that we will only show the results here for λ = 0.7 Å^{-1}. Starting with the bile salt concentration in the endcaps, this will again be plotted as a function of the length of the micelles divided by the lecithin concentration as shown in figure 7.22.

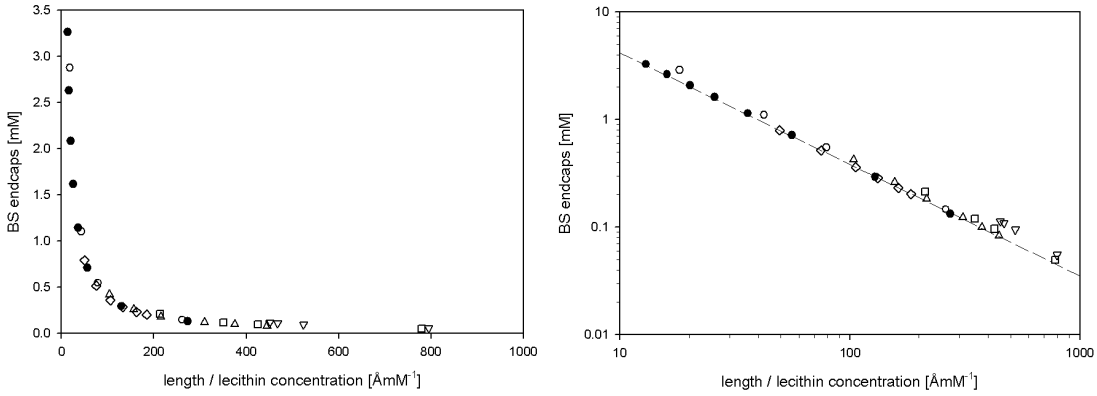

Figure 7.22: The amount of bile salt in the endcaps for λ = 0.7 Å^{-1}. The symbols for the data series are as in figure 7.14. The fitted line corresponds to [BS]$_{end}$ = 45.2(L/[LEC])$^{-1.0}$.

The amount of bile salt in the endcaps and effectively the number of micelles in the system are inversely proportional (power law with -1.0 dependence). This is the same as found for the very simple model section 7.2, which is not surprising as the composition of the micelles is found to be constant with the α used.

We can also look at the amount of bile salt in the middle parts of the micelles, again as a function of the amount of lecithin in the system (i.e. total amount of lecithin in the system as all of it is in the micelles), this is shown in figure 7.23.

The amount of bile salt in the middle parts of the micelles depends linearly on the amount

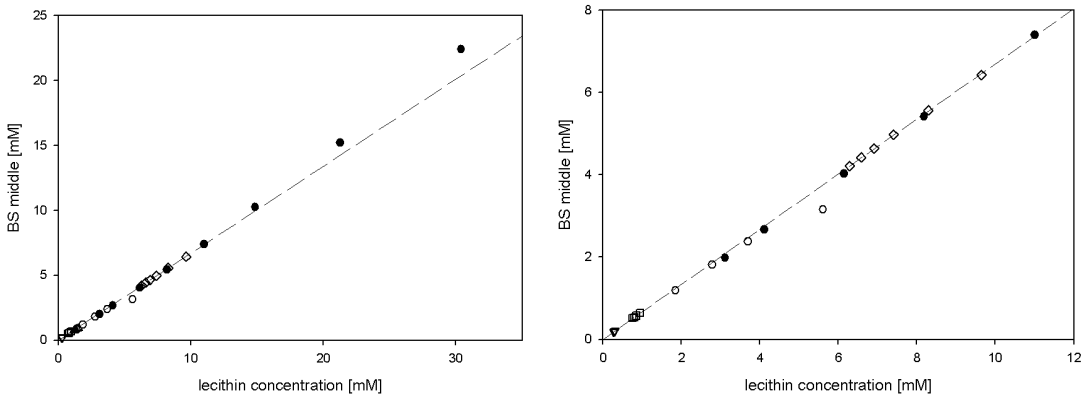

Figure 7.23: The amount of bile salt in the middle parts of the micelles for λ = 0.7 Å^{-1} as a function of the total amount of lecithin in the system. The symbols for the data series are as in figure 7.14. The linear fit corresponds to [BS]$_{mid}$ = 0.67[LEC].

of lecithin in the system, this is not surprising as the surface cover of the middle parts by the bile salt was also found to be constant. It is only at the higher concentrations, where the concentration induced regime is encountered that the relationship is no longer linear as the amount of bile salt in the middle parts of the micelles starts to increase.

The slope gives the number of bile salt molecules per lecithin molecule along the cylindrical axis, which is 0.67 this is equivalent to a lecithin to bile salt ratio R^{mid} of 1.5. This agrees nicely with the phase boundaries where it is found that the maximal R_e^m is 1.5 in the micelles, this would mean that as soon as R_e^m exceeds this value there is only enough bile salt in the micelles to make the cylindrical parts but not the endcaps, and hence some vesicles will be created as well and the phase boundary crossed.

7.4.3 Summary and discussion

Various neutron scattering data for the size of the lecithin-bile salt micelles was presented. The length and cross–sectional information were then used to try and understand the exact composition of the micelles i.e. how is the bile salt divided up between the micelles and the bulk solution.

Starting with a very simple model (7.2) the partitioning of bile salt into the micelles and the

bulk solution was calculated. The model suggested that it is indeed the costly creation of the highly curved endcaps that causes the micelles to grow in the dilute regime.

A further model based on the adsorption of bile salt onto the endcaps and middle parts of the micelles was presented, where the effects of the packing of the lecithin in the middle parts of the micelles through λ; and the energy gain of adding a bile salt molecule to the endcaps and middle parts, α_e and α_m respectively, were studied.

It was found that through changing α_e and α_m the surface coverage of the endparts and the middle can be tuned such that the molar concentrations in the bulk solution, endcaps and middle parts will be in agreement using different values for λ.

It seems that whatever the model used the amount of bile salt in the endcaps is found to be almost inversely proportional to the number of micelles in the system, which is defined by the length of the micelles and the amount of lecithin in the system. It has to be noted that the length of the micelles was an input parameter into all the models, however this suggests that in the dilute regime the length of the micelles is defined by how many endcaps can be created from the available bile salt.

The lecithin to bile salt number ratio in the middle parts of the micelles was found using the different models to vary between 1.5 and 2.8 lecithin molecules per one bile salt molecule (the values are similar for both λ). This has also been estimated by Hjelm [53], from SANS experiments. From their experiments on the arrangement of lecithin in the micelles, they found λ to be 0.9 Å^{-1}, from this the number of bile salt molecules per lecithin molecule along the cylindrical axis of the micelle was calculated according to a specific arrangement of bile salt molecules in the micelle. This resulted in one bile salt molecule per three to four lecithin molecules, which is equivalent to a lecithin to bile salt number ratio of 3-4, which is not very different from the values found from the model calculations.

Two different sets of input parameters for the model were tried, one where agreement with bile salt bulk solution concentration was used to fix the input parameters and another where the input parameters were chosen to agree with the phase boundary models of maximal and constant R_e^m at the phase boundary of 1.5. It seems that the behaviour as found in the latter case is more widely in agreement with the available data and theory, we will now summarise

the main conclusions as found when fitting the model for agreement with R_e^m.

The choice of λ does not change the calculated results from the model if α_e and α_m are changed accordingly. This is very surprising, as changing the packing of lecithin from 0.7 $Å^{-1}$ to 0.9 $Å^{-1}$ decreases the number of micelles in the system by over 20% if the length is constant. This further indicates the importance of the choice of α, and with further experimental data the α could be fixed more certainly.

The length of the micelles in the dilute regime is directly determined by the amount of bile salt available for the creation of the endcaps which have a fixed composition. Once the length of the micelles has reached a minimum, the micelles start to grow again through concentration induced growth, at which point the micelles become more bile salt rich (decreased R_e^m) and the bulk concentration of bile salt also starts to increase with the formation of simple bile salt micelles. It is not clear why the bulk concentration should start increasing at this point as well, although it could be that as the lecithin to bile salt ratio in the middle parts R_{mid} starts to decrease (from the constant composition in the dilute regime) the importance of the electrostatic interactions increases, as minimum bile salt requirement for the curvature stability has been fulfilled. This could also explain the difference in the total bile salt concentration at which the bulk concentration starts to increase between the dialysis data of Duane [80] and the model calculations. His experiments were carried out at R_{tot} = 0.2 (here R_{tot} = 1.1) and hence the 'saturation' of the micelles by bile salt, and the end of the dilute regime occurs at lower concentrations.

The linear relationship between the amount of bile salt in the middle parts and the amount of lecithin in the system in the dilute regime, gives us a measure of lecithin to bile salt number ratio in the middle parts. This is found to be constant at about 1.5, which is interestingly in complete agreement with the maximal R_e^m as found at the phase boundary between micelles and micelle-vesicle coexistence. This supports the theory that the growth of the micelles (which have constant composition of the cylindrical part in the dilute regime) is driven by the amount of bile salt that is available for the creation of the endcaps and as soon as R_e^m passes 1.5 there is effectively no bile salt for the creation of the endcaps and some vesicles start to form.

The model and experiments suggest that the composition of the micelles is constant in the dilute

regime, where the length of the micelles is determined by the amount of bile salt available for endcap creation. Upon increasing concentration, once the length of the micelles has reached a minimum (with constant composition) as the concentration is further increased the bile salt partitions into the micelles (resulting in concentration induced growth), but simultaneously simple micelles start to form in solution, thus leading to an increase in the bulk concentration.

Chapter 8

Growth of Micelles

Two different effects on the rate of growth of the micelles were explored: the influence of the initial and final size/dilution of the samples and the effect of ionic strength. These were studied using two different lecithin-bile salt systems; the experiments on the size/dilution were carried out with TCDC (at the ILL) and the experiments on the effect of the ionic strength were done using TC (at the PSI). Some results on the cross-section of the micelles will also be shown where the dilution dependence is examined using both TCDC and TC.

All the kinetic experiments were carried out using the stopped flow setup as explained in chapter 6. This means that the kinetics were controlled through the dilution of the sample, where the stock solution (initial dilution) and buffer were mixed at different ratios. The SANS data was collected using various time resolutions, details of which are in the individual sections for the different experiments.

The data treatment will be explained initially, as this is common to all the different kinetic experiments. After this, the experimental results on the different systems will be shown in three parts: firstly the size/dilution dependence, followed by the experiments on the effect of the ionic strength and finally data on the cross–section of the micelles during the growth. The chapter will conclude with a discussion on the growth processes for the system.

8.1 Data Treatment

As explained in section 4, time-resolved experiments result in 400 q-dependent scattering intensities (each one of them similar to the individual equilibrium results). Several repeats for each chosen dilution step are averaged (the number of averaged experiments will be detailed in the following sections), and these are corrected for background contributions (as described in section 4.2).

A 3-D view of the transition is shown in figure 4.4, in terms of q, intensity and time, where the increase at low q (i.e. large length-scales) is observed as the growth of the contour length of the micelles. Where each cross-section corresponds to the intensity profile at a given time.

The resulting 400 data series for each pertubation are then individually fitted to gain information on the structure of the micelles at each different time step. In figure 8.1 four different times of the scattering intensities are shown for a dilution step of 6.6 - 20 for the lecithin - TCDC system.

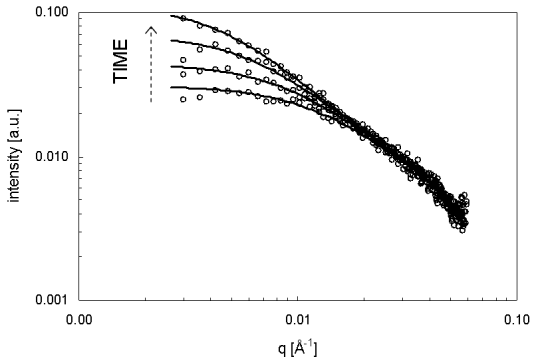

Figure 8.1: Dilution 6.6 to 20 data and fits with R_{tot} = 0.9 and 75mM added NaCl, from bottom to top 6.5s, 20.5s, 50.5s and 150.5s after mixing.

These were fitted using the polydisperse worm–like micelle model with included interactions as described in section 4.4. However, as the kinetic data is much noisier than the equilibrium data due to the significantly shorter acquisition times it was not possible to fit the polydispersity in the length of the micelles σ_L/L whilst they were growing, and this was fixed at 1.0. Several different values of $\frac{\sigma_L}{L}$ were tried and it was found that the χ^2 levels off at $\frac{\sigma_L}{L} \geq 1.0$. An example is shown below.

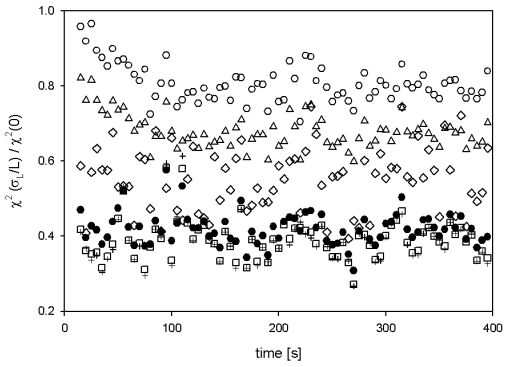

Figure 8.2: $\chi^2(\sigma_L/L)/\chi^2(0)$ values for different polydispersities for the dilution jump 6.6-13.3 with one second time resolution. With σ_L/L = 0.3 circles, 0.4 triangle up, 0.8 diamond, 1.0 filled circle, 1.5 square and 2.0 plus.

Hence the only free parameter in the fitting (apart from the scaling) was the length of the micelles. The corresponding fits for the different time steps are shown in figure 8.1 with the data. Further details of the experiments and analysis on the kinetics of the growth will be presented in the following sections.

8.2 Effect of concentration

The experiments on the size/concentration dependence of the growth of the micelles were done at the ILL, using TCDC as the bile salt. The samples all had R_{tot} = 0.9 and 75mM added NaCl. All the experiments were carried out in the mixed micelle region so the highest dilution was chosen as 20, which is within the mixed micelle phase even within limits of experimental error arising from the stopped flow mixing setup.

Five different dilution steps were investigated (initial dilution d_i to final dilution d_f) using varying time resolution (t_R). The details of the experiments and the number of repeats are shown in table 8.1.

The fitted data presented in this section was taken at relatively small q vectors (large length scales), where the cross-sectional information is not available. The cross-section is also known not to change during the micellar growth, as shown in section 8.4. This means that cross-

d_i	d_f	t_R[ms]	no. averaged	meas. time [ms]
6.6	10	100	11	1100
		250	1	250
6.6	13.3	250	9	1250
		1000	1	1000
6.6	20	100	20	2000
		500	5	2500
		1000	2	2000
10	20	50	9	450
		1000	1	1000
13.3	20	100	16	1600
		500	1	500
		1000	2	2000

Table 8.1: Dilution jumps, time resolution, number of averaged experiments and total acquisition time per time resolution step with the TCDC-lecithin system using the stopped flow setup.

sectional information has very little effect on the fits and these were fixed at the average values found from the equilibrium data i.e. radius = 18.1Å and ϵ = 1.57. The Kuhn length was kept at 400Å and the background was fixed to the value found from the equilibrium fit for the final dilution (0.0003-0.0004). Hence, only a scaling constant and the length are fitted for each sample.

The following results will be discussed in terms of the time-dependence of the length, where the length is fitted from the data. The variation in the length of the micelles between individual time steps varies by about 10% for each consecutive measurement. This arises from the low statistics of the measurements.

In figure 8.3 the length evolution in time is shown for the dilution 6.6 - 20 jump with a total acquisition time of 2 seconds.

The different data sets are averaged from the SANS measurements, but for further data analysis and fitting, the lengths will be binned to minimise the random error further. The data is binned

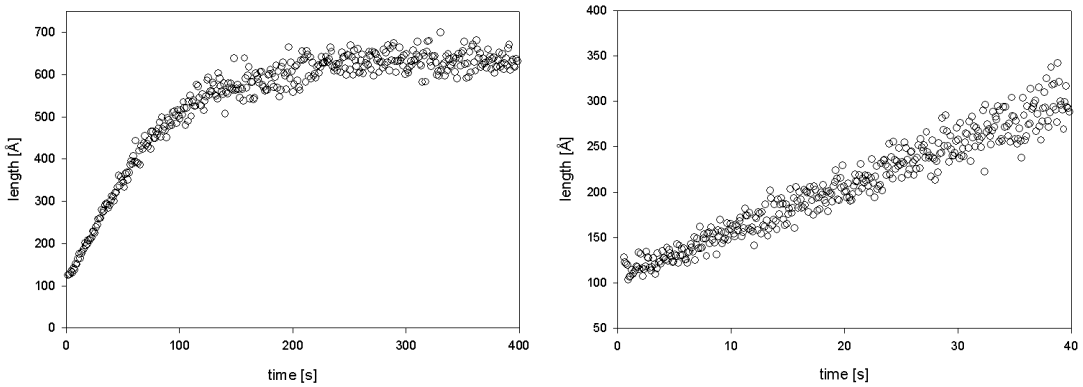

Figure 8.3: Growth of micelles: starting dilution 6.6 and final dilution 20. On the left 400 x 1000ms time frames where the full growth can be followed and on the right 400 x 100ms time frames where the initial growth can be seen in closer detail.

with care so that none of the details of the transformation are lost, but a continuous curve can be plotted for the change of the length in time. This also means that the different time resolutions are averaged to obtain the maximum accuracy. The different data sets (already averaged) are shown in figure 8.4.

Although the aim of the experiments was to carry out dilution jumps starting from 6.6, 10 and 13.3 to a final dilution of 20, the difference in the final length of the micelles found in the kinetic experiments varies considerably from the value found at equilibrium at dilution 20. Equilibrium length at dilution 20 was found to be 494Å, when the values from the kinetic experiments range from 620Å to 660Å. This could arise from the fact that the micelles have not reached their equilibrium size, but this is not believed to be the case. At the ionic strength studied the equilibration should be relatively fast and some of the samples were followed up to a few hours after the transition and no change in the final size of the micelles was observed. This means that the discrepancy arises from errors in the stopped flow filling process.

As explained in section 7.1.1 there exists an empirical model for the concentration dependence of the length. This can be used to calculate the final dilution from the final size of the micelles, and these results are shown in table 8.2 as the final dilutions. The samples with final dilutions 10 and 13.3 the measured final lengths are much closer to the equilibrium values. This is probably because in this concentration region the length varies more slowly with concentration, so a

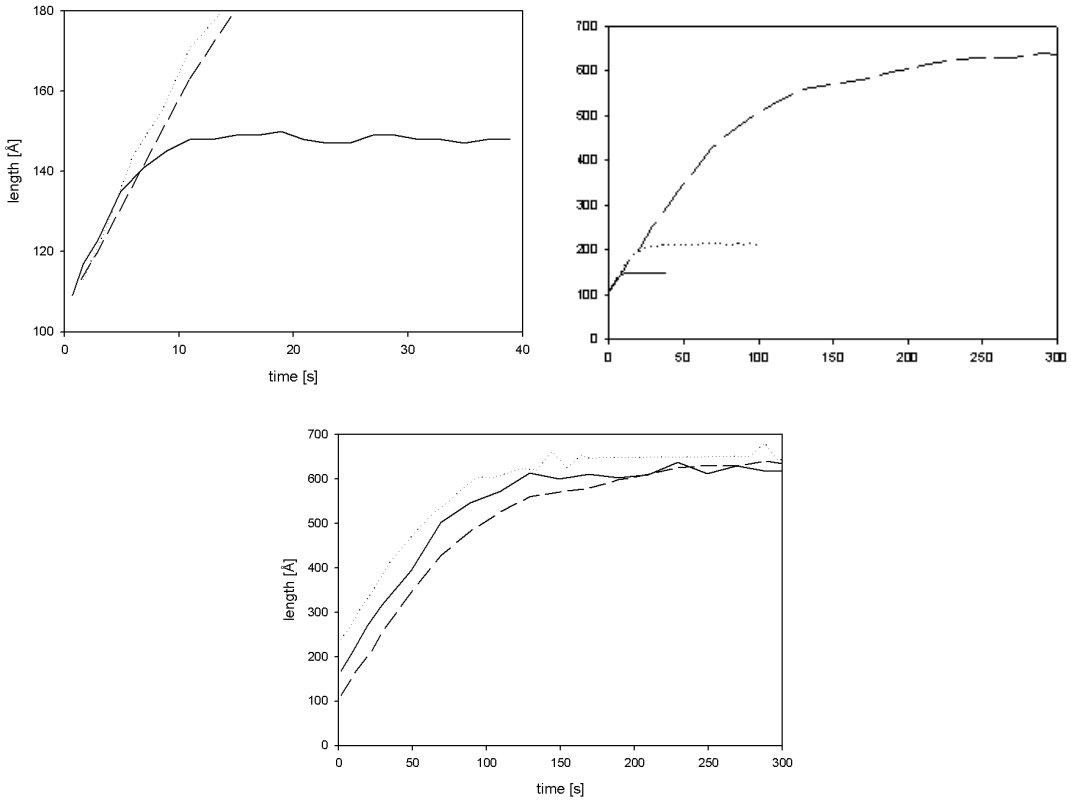

Figure 8.4: Growth of micelles: above starting with dilution 6.6 and ending with dilutions 10 (line), 13.3 (dotted) and 20 (dashed) and below starting with dilutions 6.6 (dashed), 10 (line) and 13.3 (dotted) and ending with dilution 20. The data is an average of the different time resolutions studied.

small error in concentration does not have significant effect on the length of the micelles.

There exists no model describing the kinetics of mixed worm–like micelles, but as explained in section 2.5.2, there exists a theory developed for single component worm–like micelles [29]. This model describes the change in the length of the micelles (for a system where the initial length is shorter than the final length) as:

$$\begin{aligned} L(t) &= L_\infty \tanh\left(\tfrac{t+t_0}{2\tau}\right) \\ t_0 &= 2\tau \coth^{-1}\left(\tfrac{L_\infty}{L_0}\right) \end{aligned} \tag{8.1}$$

where L_∞ is the final length of the micelles, L_0 is the initial length of the micelles and τ is the

relaxation time for the growth. The theory predicts a common time constant for dilution jumps finishing with the same final size of micelles.

The data is fitted using the above relationship, where L_∞ is taken from the final size of the kinetic data and L_0 is taken as the initial size of the micelles. The reason L_∞ is not taken as the size of the micelles at final dilution as found through the equilbrium results, is that there is some discrepancy between these values arising from errors in the mixing process (see section 6.5). However, the initial size is taken from the equilibrium results, as the sample used as initial dilution is the same as that measured in equilibrium. Extrapolation of the length to zero time results in values that are consistent with the lengths as measured at equilibrium.

The data and the fits (using equation 8.1) are shown in figure 8.5, figure 8.6 and figure 8.7. The fit parameters are summarised in table 8.2.

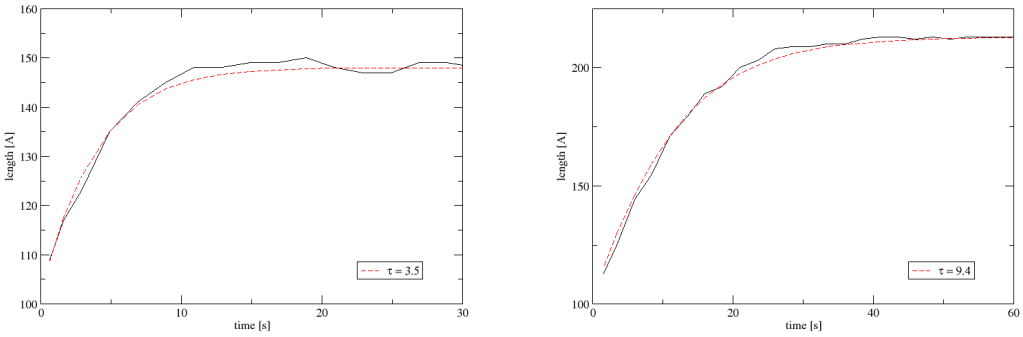

Figure 8.5: Data (continuous line) and fits (dashed) for L(t) on the left dilution 6.6 - 10 and on the right dilution 6.6 - 13.3.

The fits are generally in good agreement with the data, and especially for the larger length changes it is clear from looking at the data that a simple exponential growth is not appropriate, where at early times the growth of the micelles is linear. Only in the case of 6.6 - 10 is there considerable difference around the turning point (getting close to the final size of the micelles), where it almost seems like the size of the micelles overshoots the final equilibrium size. This is the only transition where the final length is less than twice the initial length (even if the samples are highly polydisperse within these values), which could affect the way it grows if the rate of scission is not very fast. However, this could be an artefact arising from the relatively high

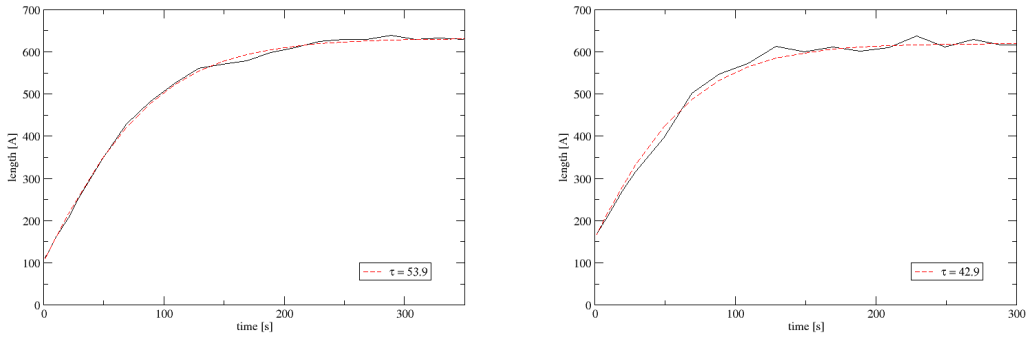

Figure 8.6: Data (continuous) and fits (dashed) for L(t) on the left dilution 6.6 - 20 and on the right dilution 10 - 20.

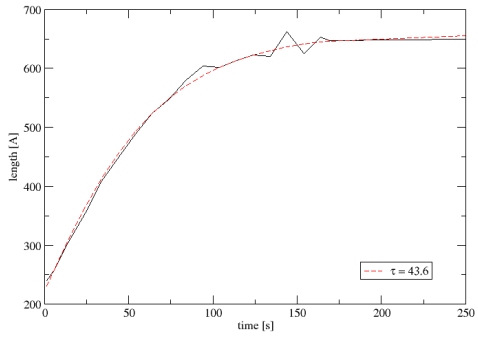

Figure 8.7: Data (continuous) and fits (dashed) for L(t) dilution 13.3 - 20.

amount of noise in the measurement.

As mentioned before the model for the growth of single component worm–like micelles predicts a common τ for the same final size. Basically this implies that it does not matter what the initial size of the micelles is, the growth will be the same providing L_∞ is the same. For the three experiments with mixed micelles where the final size of the micelles is close at 620 Å, 632Å and 660Å, the relaxation times found were 53.9s, 42.9s and 43.6s, respectively. The large variations in the time constants found, espcially for the two smaller final sizes, suggests that the growth of the micelles is not quite the same as for the simple micelles.

d_i	d_f	d'_f	L_0[Å]	L_∞[Å]	τ [s]
6.6	10	10	102	148±0.4	3.5±0.5
6.6	13.3	13.3	102	213±0.6	9.4±1.0
6.6	22.9	20	102	632±10.0	53.9±1.5
10	22.7	20	157	620±5.6	42.9±1.5
13.3	23.4	20	220	660±6.0	43.6±1.5

Table 8.2: Time constant τ, calculated final dilutions d_f, nominal dilutions d'_f and experimentally found lengths for the different dilution jumps.

It is found that the relaxation times τ are proportional to the difference in the initial and final lengths $L_\infty - L_0$; indicating that it is the total amount that the micelles need to grow that is of importance. The relationship between τ and $L_\infty - L_0$ is shown in figure 8.8.

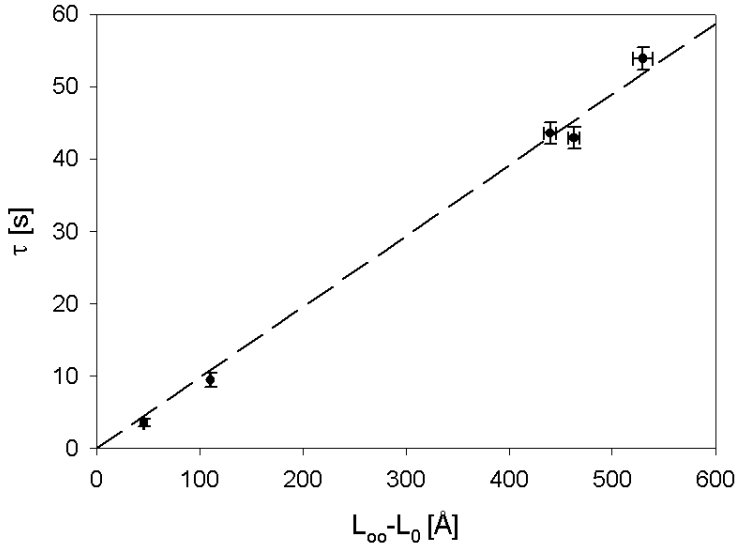

Figure 8.8: The time constants τ for the different dilution jumps against the difference in the initial and final lengths of the micelles $L_\infty - L_0$. Increase in τ per increase in difference between the final and initial lengths is 10.2Ås^{-1}

The fact that τ is proportional to the change in the length of the micelles suggests that the growth proceeds in the same way throughout the process, so that independently of the size of the micelles and the concentration of the sample the growth proceeds in the same way. This is

very suprising, but as the length and concentration are linked it is difficult to differentiate the contributions which might balance so as to produce this linear behaviour.

Apart from the overall growth time τ, the early rate of growth of the micelles $\delta L/\delta t$ can be studied. The early growth is linear in time for times $t_0 \ll t \ll 2\tau$ [29]. A linear fit to the early growth times gives us a measure of $\delta L/\delta t$. For all the different dilution jumps studied (with different L_0 and number densities of micelles) $\delta L/\delta t$ are constant with an average of 5.6 ± 0.4 Ås^{-1}, and as such independent of L_0 and concentration. This would indicate that $\delta L/\delta t$ should be constant throughout the process, until saturation (where the equilibrium length is reached). The fact that τ is linearly dependant on $L_\infty - L_0$ (see figure 8.8) is in agreement with this result, suggesting a constant rate of growth throughout the process.

However, due to the relationship between length and concentration the discussion is complicated. We will now explore some of the different contributions to $\delta L/\delta t$ and τ which might offer some insight to the apparent linearity.

To aid the discussion we will define $n(t)$ as the number density of micelles per m^3 at time t in the system. $n(t)$ is calculated (as in section 7.2), assuming that λ (number of lecithin molecules per length of cylindrical part of micelle) is constant and there is no lecithin in bulk solution. Here we will only use the one value for λ of 0.7 Å^{-1} [43] as it is only a constant in the equation and so the absolute value does not change the trends observed.

This means that the molar concentration of lecithin [LEC] in the system and the length of the middle part of the micelles L_{mid} ($= L - L_{end}$, where $L_{end} = 2R$ and R is the radius of the cross-section) can be used to calculate n:

$$n(t) = \frac{[\text{LEC}]N_A}{d\lambda L_{mid}(t)}, \tag{8.2}$$

where [LEC] here it is 37mM, N_A is Avogadro's number and d the dilution of the sample.

The rate of coalescence of the micelles $\tau_{coal}^{-1}(t)$ s^{-1}m^{-3} is given by:

$$\tau_{coal}^{-1}(t) = \frac{n(t)\frac{\delta L}{\delta t}}{L(t)}. \tag{8.3}$$

As $\frac{\delta L}{\delta t}$ is constant throughout the growth we have

$$\tau_{coal}^{-1}(t) \propto \frac{n(t)}{L(t)}. \tag{8.4}$$

Further explanations are complicated due to the relationship between $n(t)$ and $L(t)$, and their time dependence. As effectively $n(t)$ depends on $L(t)/L_0$, this would lead to the suggestion that in fact $\tau_{coal}^{-1}(t)$ is independent of L and t and only depends on L_0, leading to a constant $\tau_{coal}^{-1}(t)$ defined simply by L_0, which indeed would produce the constant $\delta L/\delta t$ observed. We will now suggest a reason for the $n(t)$ and $L(t)$ dependence of τ_{coal}^{-1}.

We can start by examining the diffusion of the micelles, where faster diffusion should lead to a higher τ_{coal}^{-1}. According to polymer dynamics in the dilute regime (where we are using the Rouse model, as the samples are dilute with a short Debye length $\kappa^{-1} \approx 10$ Å so it is reasonable to assume that when far away they do not really feel each other) the self diffusion constant D for a short worm–like micelle (more like elliptical micelle) is proportional to L^{-1} [70]. This could explain the L^{-1} dependence of τ_{coal}^{-1}. It will be shown in the section 8.3 that there are both an electrostatic and a topological barrier to the growth of the micelles, however it could be imagined that when these barriers are constant diffusion would play a role in the kinetics.

Now we will look more closely at the way in which the micelles fuse, we could also think that the growth depends on the reaction surface i.e. the surface through which reaction can occur. Whether the micelles coalesce through endcaps only or whether they can coalesce anywhere along their bodies, the reaction surface S depends on n.

We will estimate S simply by the surface area of the micelle. If the micelles can coalesce through their whole bodies the reaction surface will be given by:

$$S_{body} \propto n(4\pi R^2) + 2\pi R L_{tot}, \tag{8.5}$$

where R is the radius of the cross-section and L_{tot} the total length of the middle parts, which is constant for a given experiment as [LEC] is constant. However, if the micelles can only grow

through coalescence through the endcaps we should have the following reaction surface:

$$S_{ends} \propto n(4\pi R^2). \tag{8.6}$$

For both cases $S \propto n$, this means that as there are fewer micelles in the system S decreases linearly with n.

This means that if τ_{coal}^{-1} depends linearly on both S and D, this could explain the apparent linearity in the growth $L(t)$, i.e. constant $\frac{\delta L}{\delta t}$ and no dependence on the size or concentration is detected.

8.3 Effect of Ionic Strength

Three different salt concentrations were studied, all with the TC-lecithin system (at the PSI). The dilutions were all from 2.5 to 5, which again is within the mixed micelle region for TC close to the phase boundary with micelle-vesicle coexistence region. TC has a higher CMC than TCDC, and hence the transformation from mixed micelles to micelle-vesicle coexistence occurs at lower dilutions for a given lecithin to bile salt ratio. The lecithin to bile salt ratio was kept constant at 0.9.

The ionic strength of the solution c_S consists of the component from the buffer, the added NaCl and the ions from the bile salt itself (see section 5.3). The different salt concentrations (initial concentration c_{Si} and final concentration c_{Sf}), the time resolution used and the total measurement times are shown in table 8.3.

c_{Si} [mM]	c_{Sf} [mM]	t_R[ms]	no. averaged	meas. time [s]
97	62	950	20	19
145	136	1000	20	20
97	362	950	28	26.6

Table 8.3: Initial and final ionic strength of the solution, time resolution, number of averaged experiments and total acquisition time per time resolution step for kinetic experiments with TC-lecithin system with R_{tot} = 0.9 and dilution step from 2.5 to 5.

The initial size of the micelles is the same for the two transitions where the initial ionic strength is the same, at 97mM. However, the initial size of the micelles will be smaller for the experiments where the initial ionic strength was 145mM.

The data presented for c_{Sf} = 62mM was not taken with the stopped flow setup, but due to the very long relaxation time, a series of longer equilibrium measurements were used. The measurement time for each scattering curve was 100s, with 11s between measurements for the computer to store the data.

The data is fitted using the worm–like micelle model, where again only the length of the micelles was fitted for, and b and σ_L/L kept constant at 400Å and 1.0 respectively. The data is all in the small q-range and hence the cross–sectional information is not available and thus R was fixed at 18.1 Å and ϵ at 1.57 (the values for R and ϵ were found not to affect the fitted length of the micelles). Hence it was only the length L of the micelles that was fitted.

The resulting time dependent lengths of the micelles were averaged to obtain a smooth line, where care was taken not to loose any of the detail of the data. The resulting graphs of length in time are shown in figure 8.9.

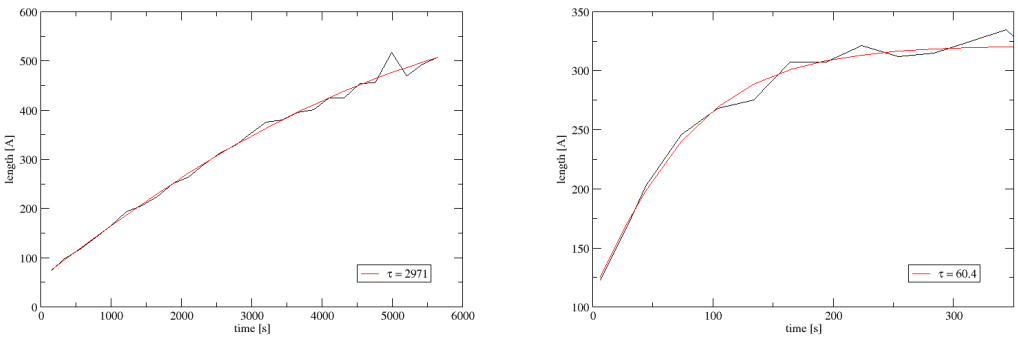

Figure 8.9: The growth of the micelles for TC-lecithin system at R_{tot} = 0.9 for dilution jump 2.5 - 5. On the left 97mM to 62mM and on the right 145mM to 136mM . The fit using equation 8.1 is shown as the dashed line.

The length dependence in time can be fitted using equation 8.1 to obtain the relaxation time τ for the growth of the micelles, where data along with the fits are shown in figure 8.9.

There is no equilibrium measurement at dilution 2.5 and c_S = 97mM to obtain the initial size

of the micelles for two of the experiments. Hence the initial length L_0 was found through extrapolating to zero time and for c_{Sf} = 62mM was found to be 58 $\pm$ 4 Å. The final length L_∞ was not reached during the measurement time (as seen in figure 8.9), due to the very long equilibriation time and L_∞ was used as a fit parameter along with the relaxation time τ.

For the ionic strength difference data from 145mM to 136mM the initial size, as found from the equilibrium measurements, of 80 Å could not be used, because there σ_L/L was 0.5, and here the value of 1.0 was used (in agreement with the data treatment of all other kinetic data and it was not possible to refit the equilibrium result with such large polydispersity). This means that extrapolating to zero time gave L_0 of 114 $\pm$ 6 Å. The final size was found (as for the TCDC-lecithin samples) from the final average size once the growth had levelled off (i.e. equilibrium was reached) and is 321 $\pm$ 5 Å.

The initial and final sizes as well as the resulting relaxation times τ are summarised in table 8.4, where the fits from are shown in figure 8.9.

c_{Si} [mM]	c_{Sf} [mM]	L_0 [Å]	L_∞ [Å]	τ [s]
97	62	58	651	2970
145	136	114	321	60

Table 8.4: The initial and final sizes of the micelles L_0 and L_∞ for the two different salt concentrations studied and the relaxation time τ

The difference in the two relaxation constants for c_{Sf} of 62mM at 2970s and for c_{Sf} 136mM of 60s is enormous. For the samples where the salt concentration was kept constant and the initial and final dilutions were varied τ ranged from 3.5 to 53.9 (for the jumps from 102Å to 157Å and from 102Å to 620Å respectively), whereas here the difference between the two relaxation times is almost two orders of magnitude.

Assuming, as was found in the experiments at constant ionic strength (section 8.2), that the relaxation is linearly dependent on the length that the micelles have to grow. We can again plot $L_\infty - L_0$ vs. τ (as the initial and final sizes of the micelles are different), to obtain a length independent measure of the growth of the micelles, as shown in figure 8.10.

As can be seen from figure 8.10, the resulting slope of $\delta\tau/\delta(L_\infty - L_0)$ is much greater for the

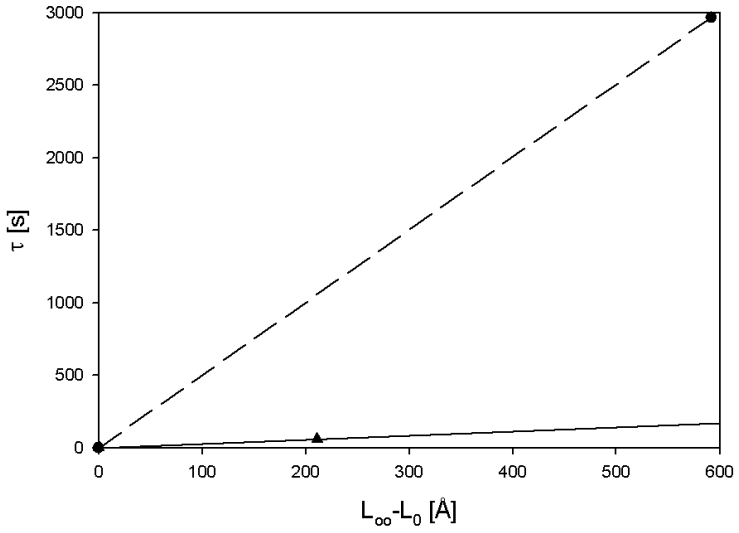

Figure 8.10: TC-lecithin system R_{tot} = 0.9, time constants for dilution from 2.5 to 5 for two different salt concentrations as a function of $L_\infty - L_0$. Triangle and solid line c_{Sf} = 136mM and circle with dashed line c_{Sf} = 62mM.

low ionic strength sample, beyond the experimental errors. Although here there exists only one sample for each of the salt concentrations a straight line through the origin has been drawn (as done in section 8.2). This gives a measure of the increase in the time constant per increase in the change in length, for c_{Sf} = 136mM it is 0.3 sÅ^{-1} and for c_{Sf} = 62mM it is 5.0 sÅ^{-1}.

Again looking at the initial rates of growth $\frac{\delta L}{\delta t}$, which were found to be the same for all the samples at 75mM added NaCl in section 8.2, for the sample with c_{Sf} = 136mM it is 1.8Ås^{-1} and for c_{Sf} = 62mM it was found to be 0.1Ås^{-1}.

The strong effect that c_S has on the growth rates of the micelles implies that electrostatic interactions are important during the growth process, suggesting an electrostatic barrier to coalescence.

As shown in table 8.3, a third salt concentration was also investigated, from 97mM to 362mM. It could be imagined that the the growth of the micelles would be even faster than that for c_{Sf} = 136mM. However, the results are very different. There are changes in the scattered intensity up to the latest times studied at 380s. Some of the resulting q-dependent intensities at different time steps were averaged to remove some of the noise in the data and are shown in figure 8.11.

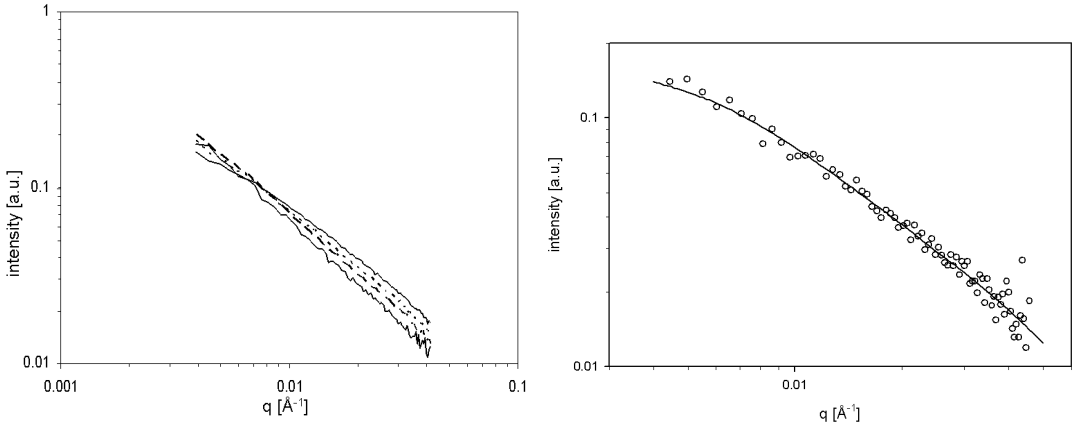

Figure 8.11: On the left data from dilution 2.5-5 with c_{Sf} of 362mM with scattered intensity as a function of q, starting from the bottom (at small q) solid line 7.5s after mixing, dashed line 125s after mixing, dotted line 225s after mixing and continuous line 375s after mixing. On the right data and resulting fits using worm–like micelle model for 350s after mixing.

The resulting intesity distributions at early times from the experiments could not be fitted with the worm–like micelle model, as the overall size of the micelles is not accessible. However, at later times I(q) can again be fitted using the worm–like micelle model, resulting in fitted lengths of 330Å $\pm$ 40, after about 350s. The resulting data and a fit for t = 350s are shown on the right in figure 8.11. It is possible that this is not the final size of the micelles.

What exactly is happening within the sample is difficult to say from the data, it might be that the bile salt concentration in bulk is greater at dilution 5 at c_S = 362mM, than at dilution 2.5 with c_S = 97mM. This would lead to the bile salt initially leaving the solution for the micelles, which might end up larger than their equilibrium size, but due to the very hydrophobic nature of lecithin the break up of these micelles would be very very slow, resulting in a long relaxation time.

Meyhas *et al* [62] did experiments on the aqueous bile salt concentration and the lecithin to bile salt molar ratio in micelles at the phase boundary between mixed micelles and micelle-vesicle coexistence, as a function of the ionic strength of the solution. For an ionic strength change of 97mM to 362mM, they found that the bile salt in bulk decreases from 5.2mM to 2.8mM $\pm$ 0.2mM. Their experiments were carried out with lecithin and cholate, so one would expect the absolute values to vary slightly and it is possible that a dilution of 2, with an increase of the

ionic strength of the solution from 97mM to 362mM might indeed decrease the concentration of bile salt in solution.

8.4 Cross–section during growth

Kinetic experiments monitoring the cross-section of the micelles during the growth were carried out for both the TCDC– and TC–lecithin systems. The data is at the large q range, thus information on the overall size and flexibility of the micelles is not available. The data was fitted using the worm–like micelle model, where σ_L/L was fixed at 1.0, b at 400 Å and the length was fixed by inspection although it was found that even differences in the length of $\approx$ 20% did not make a noticeable difference to the values found for the cross–sectional parameters. Thus the data was fitted for the cross–sectional radius R and the ellipticity of the cross–section ϵ only.

In figure 8.12 data and fits are shown for TCDC-lecithin sample for dilution 6.6-20 at 100mM added NaCl and R_{tot} = 0.9.

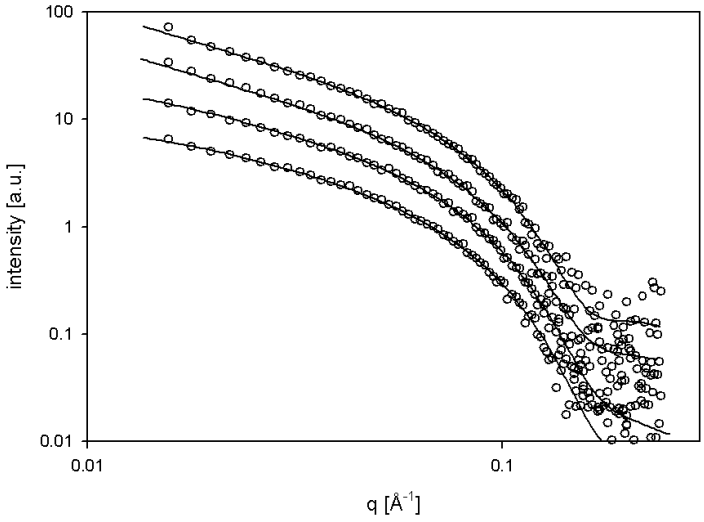

Figure 8.12: Data and fits for dilution 6.6-20, R_{tot} = 0.9, 100mM added NaCl; starting from bottom with 3s, 10s, 100s and 300s after mixing of the sample.

It was not possible to fit the cross–sectional data using the program designed for fitting the

kinetic data, where all 400 data sets are fitted one after another automatically. This is possibly because there are two parameters to be fitted R and ϵ. As each of the data sets had to be fitted manually, not all of the data sets were fitted. However the resulting parameters for a few of the data sets are shown in figure 8.13.

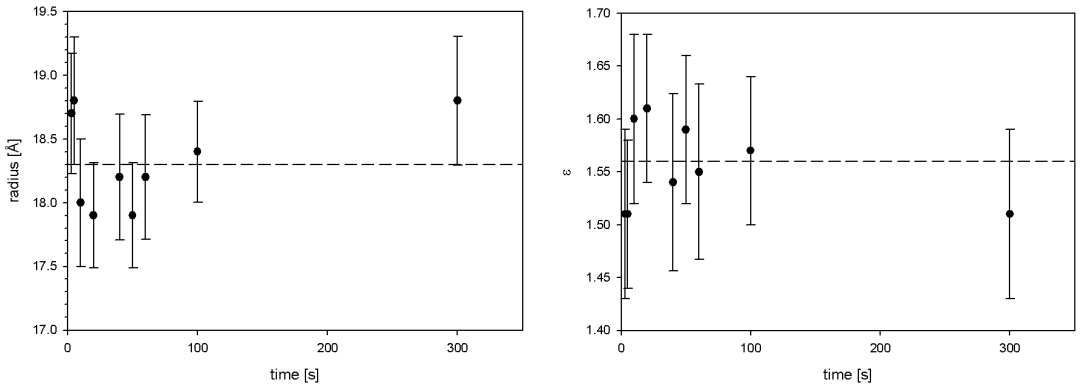

Figure 8.13: Dilution 6.6-20, R_{tot}=0.9, [NaCl]=100mM. On the left cross–sectional radius R in time and on the right the ratio of the major to minor axis ϵ as a function of time. The dashed line indicates the average values.

Within the errors of the fits the cross–section of the micelles does not change during the transition, resulting in averages of R = 18.3 Å $\pm$ 0.1 and ϵ = 1.56 $\pm$ 0.01.

Experiments carried out using TC-lecithin system for dilution 2-6 with 100mM added NaCl and R_{tot} = 0.8, also found that there was no change in the cross–section of the micelles during the transition. The average values found were R = 18.3 Å $\pm$ 0.1 and ϵ = 1.58 $\pm$ 0.02.

The cross–section of the micelles remains constant throughout the growth process. This suggests that the composition of the endcaps and the cylindrical parts of the micelles remain constant throughout the growth process, resulting in constant cross–sectional size. It could also be that the cross–section of the micelles changes slightly during the growth, for example if the equilibration of bile salt between the micelles and the bulk occurs very fast, as the micelles grow the amount of bile salt in the cylindrical parts of the micelles would increase as there are less endcaps to create.

8.5 Discussion on the growth of the micelles

Summarising the results from the three different sets of experiments on the growth of the worm–like micelles. Firstly, the relaxation time was found to be independent of the initial and final lengths of the micelles and only dependent on the difference between the two. $\frac{\delta L}{\delta t}$ was found to be constant for all the different experiments with constant ionic strength.

It was found that the constant $\frac{\delta L}{\delta t}$ could be explained by simple arguments on the diffusion constant and the reaction surface of the micelles. This is only a tentative model for the growth process, as the interdependency of n and L complicates the analysis considerably. This would imply that the electrostatic and topological barriers would be constant for a given ionic strength, meaning that the composition of the micelles does not change during the growth process.

Secondly, the relaxation time was found to be strongly dependent on the ionic strength of the solution, with increased ionic strength of the solution resulting in shorter relaxation times, indicating the importance of the electrostatic interactions within the system and suggesting an electrostatic barrier to coalescence. Thirdly, the cross–section of the micelles remains constant throughout the growth, either meaning that the lecithin to bile salt ratio along the cylindrical part of the micelles is constant, or that the change in this ratio is not sufficiently large to result in a change in the cross–section of the micelles (within the errors of the experiments). This is consistent with the first finding.

The approximate aggregation times for spherical particles at the given initial number densities n are given by $3\nu/4kTn$ [66]. For the number densities in our experiments ($\approx 10^{-25}$ m^3) and with the viscosity of water ν = 10^{-3}Pa s, we obtain aggregation times of $\approx 10^{-9}$s, which is much faster than the experimentally observed timescales. This means that the coalescence of the micelles is not diffusion limited, but there exists a barrier to coalescence.

The strong ionic strength dependence of the growth process indicates an electrostatic barrier to the growth, where at higher ionic strengths the electrostatic interactions are screened and the growth of the micelles is much faster. There is also a topological barrier to the coalescence of the micelles, as the amphiphiles have to form a neck before coalescence, and such bending of the micelles is energetically costly [67]. There exists no model for the topological barrier

for worm–like micelles, but calculations on the size of the barrier for the fusion of two disc–like lecithin-bile salt micelles, found that the size of the topological barrier is much larger than the electrostatic barrier. It was found for disc–like micelles that energetically it was most favourable to fuse edge-to-edge only, although this was the only part of the micelle that was charged.

It is possible to calculate the DLVO interaction energy E for the two approaching worm–like micelles, similarly to the DLVO interaction energy for the two disc–like micelles [57]. The DLVO interaction energy combining the van der Waals attraction and electrostatic repulsion will be calculated for flat monolayers, and the curvature will be taken into account using the Deryaguin approximation [4, 68]. The theoretical details are in section 3.3.1.

We perform the calculation only for the fusion of two endcaps for the two limiting cases of constant potential and constant charge. In figure 8.14 the DLVO potential as a function of the ionic strength of the solution is shown.

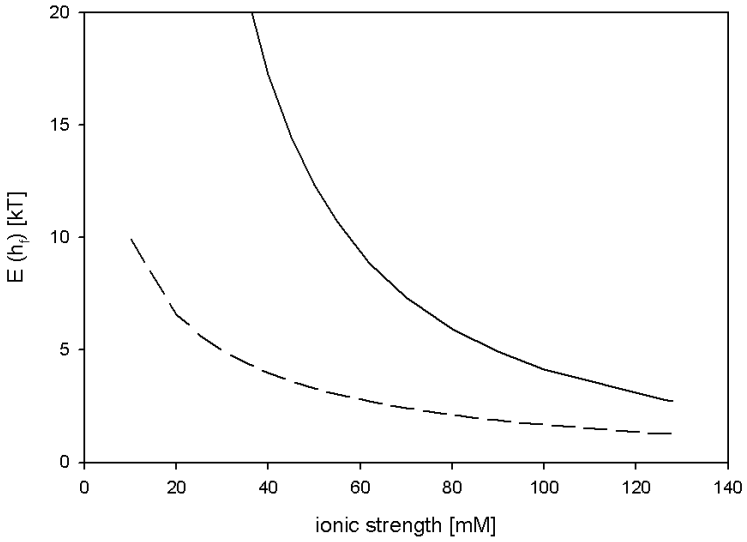

Figure 8.14: The interaction distance at a typical fusion distance of 10 Å based on constant charge (solid line) and based on constant potential (dashed line) as a function of the ionic strength of the solution.

The topological barrier to fusion is more difficult to calculate. Estimates from the amount of amphiphile that needs to bend for the different orientations of the coalescences of two disc–

like micelles [57] i.e. face-to-face, edge-to-face and edge-to-edge resulted in values of 25kT, 17kT and 8kT. Continuing in similar fashion it could be imagined that the topological barrier for the worm–like micelles for middle-to-middle would be between 8 - 17kT, for end-to-end orientation less than 8kT, and for end-to-middle somewhere between these two values.

At the lowest ionic strength examined, 62mM the electrostatic interaction is calculated to be between 2.7 and 8.9kT, which is comparable to the size of the topological barrier. However for the experiments at $c_S \approx$ 100mM or more E is expected to be between 1.6 and 4kT, which is already much lower than the topological energy barrier. This would suggest that apart from the lowest ionic strength examined, it is the lowest topological barrier that controls the way the micelles fuse (similarly as for disc–like micelles). However, at the lowest ionic strength the micelles might fuse in a different way as the electrostatic and topological barriers are of equivalent size, but as the growth can be fitted with the expression from equation 8.1 it would seem that the growth process is the same as for the other ionic strengths studied.

The calculations of the electrostatic interaction energies and comparisons with possible topological interaction energies, suggest that the growth of the worm–like micelles occurs end-to-end.

It seems that the growth of the micelles follows the same process independently of L, as the micelles get longer and n decreases τ_{coal}^{-1} decreases accordingly. This can be explained by the change in D which is proportional to L^{-1} and the change in S leading leading to a constant rate of growth in the length of the micelles. It is believed that the process remains the same with varying c_S i.e. of constant $\frac{\delta L}{\delta t}$, but the rate of growth (value of $\frac{\delta L}{\delta t}$) changes dramatically.

Chapter 9

Future Work

It is hoped that the work in the thesis has highlighted the complexity of the studied system, where the results presented should be regarded more as a new outlook on the system rather than producing definitive answers.

A model, which allows the calculation of the equilibrium composition of mixed lecithin–bile salt micelles, has been presented and compared with existing data. It is found to be in agreement with most of the available data, however there are still many open questions and the model awaits further experiments.

The composition of the micelles has been calculated in the dilute regime for several different R_{tot} and over a wider concentration regime for one R_{tot}. The most easily accessible (although not simple) experimental verification of the different input parameters (and the model itself) could be made by measuring the bulk concentration of bile salt for the samples where the size has been measured.

Most of the work has been on the very dilute regime close to the micelle to micelle-vesicle coexistence boundry, and there is still little data in the concentrated regime. It would be interesting to know how the growth in the concentrated regime changes with R_{tot} for example, to allow for further development of the model for the composition of the micelles.

The stopped flow setup that was designed and constructed has allowed for the measurement of the growth of the micelles to start 200ms after mixing. However the setup will be continued

to be improved to achieve faster mixing times, to be able to study even faster processes. The setup can obviously be used for many other experiments where the mixing of two fluids results in a rapid change in the structure or interactions in the samples.

The work on the growth of the micelles has answered some questions but there are many more that have opened up. It seems that the growth of the micelles is through coalescence where the growth depends only on the difference between the initial and final sizes. However, why this is so is still unclear as the explanation of the results is complicated due to the relationship between the concentration and the length of the micelles. Although we have seen that there is an electrostatic barrier to the coalescence, it is still not certain how the micelles grow; whether the coalescence occurs only through the endcaps or through the whole body of the micelle.

If indeed the growth of the micelles is linear, one would expect that even if the final equilibrium structure would be in the vesicular region the micelles should grow in their worm–like state until they reach their maximal size and collapse into discs, before forming vesicles. However, this is difficult to realise experimentally, as conclusively analysing neutron experiments on two different populations of objects, both of which change their number and size in time is very complicated.

There are many more questions, even within the kinetics in the micellar region. It is known that there are two different regimes, but all the kinetic experiments presented were in the dilute regime where the composition of the micelles at equilibrium seems to be roughly constant. It is expected that the kinetics would be quite different if the starting concentration would be in the concentrated regime, where in particular the fact that there are simple micelles in the solution should change the kinetics. The breakup of micelles is also of interest, and has not even been touched during the thesis.

Understanding both the equilibrium behaviour and the kinetics of the growth of the micelles is of interest from a biological point of view. The lecithin–bile salt micelles studied are used as model systems for the biliary micelles, which transport lipids around the digestive system, and understanding how they function is important. There have also been some attempts at using mixed micelles as carriers for drugs, where it would be of importance to understand how these micelles form and also break up when subjected to a change in external conditions. Once the

growth and break up of the mixed micelles is understood it will be easier to understand what is happening when other molecules (such as proteins) are introduced into the micelles.

Chapter 10

Summary and Conclusions

The thesis has concerned itself with the study of the lecithin–bile salt system in water, where together the amphiphiles can form mixed micelles or mixed vesicles, or a mixture of both at high water contents. The phase behaviour of the system is well understood; the phase boundaries between mixed micelles, coexistence of mixed micelles and vesicles and the mixed vesicle region are known [40, 43, 47]. The positions of the phase boundaries for the TCDC-lecithin system are shown in figure 10.1.

Although the existence and positions of the phase boundaries is well known, details of micellar composition are yet to be understood as well as the kinetics and pathways of transitions between different aggregates.

10.1 Equilibrium

One of the aims of the thesis has been to further understand the structure and composition of the mixed micelles in the micellar region (I in figure 10.1).

In simple micelle systems (i.e. composed of only one type of surfactant) the length of the micelles increases with concentration. However, for mixed micelles there are two distinct regimes in the size of the micelles; concentration induced growth and dilution induced growth [46]. At high concentrations of amphiphile the micelles grow through concentration induced

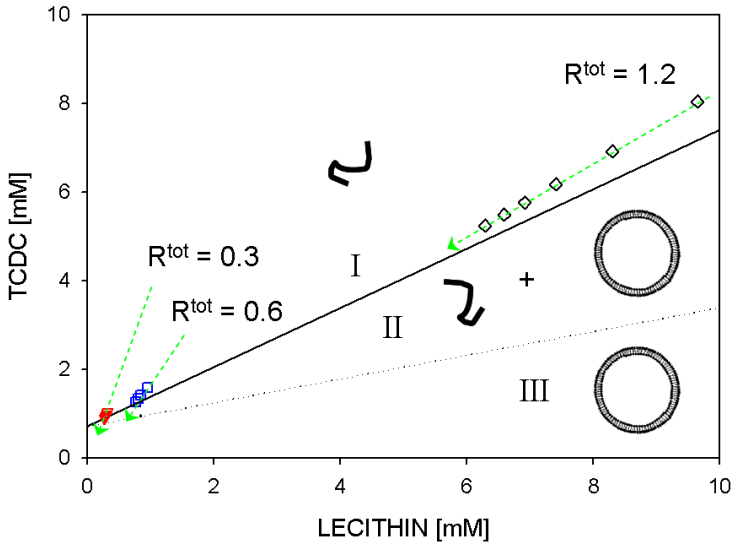

Figure 10.1: Phase diagram for TCDC-lecithin system. I Mixed micelle region, II Micelle-vesicle coexistence, III Vesicles. Experimental data points for the TCDC-lecithin system on the phase diagram, all the points are in the mixed micelle region I. Different data series are shown with R^{tot} = 1.2 diamonds, R^{tot} = 0.6 squares and R^{tot} = 0.3 triangles. The dashed line shows the line of dilution. The phase boundary between the micellar region and the coexistence region is indicated by the continuous line given by [TCDC] = 0.67 [LEC] + 0.71mM. The phase boundary between the coexistence region and the vesicular region is approximate and shown by the dotted line.

growth (similarly to simple micelles), whereas at decreasing concentrations the growth of the micelles is driven through the loss of bile salt from the micelles into the bulk solution. Bile salt has high spontaneous curvature and is required to make the highly curved endcaps of the worm–like micelles, hence loss of bile salt forces the micelles to grow longer (to have fewer endcaps). In figure 10.2 the phase diagram for GCDC-lecithin system is shown, with data extending over the two different regimes (data from [46]).

A model for the composition of the mixed micelles (region Ia and Ib) has been developed, where the partitioning of bile salt between the bulk solution and the micelles can be calculated. It is assumed that all the lecithin is in the middle parts of the micelles, where the number of lecithin molecules along the length of the cylindrical part (λ) is constant i.e. there is a constant surface cover by lecithin along the cylindrical part independent of the amount of bile salt in the middle. Using the length of the micelles as an input parameter the partitioning of bile salt between bulk solution and micelles are calculated, where the amount of bile salt in the endcaps

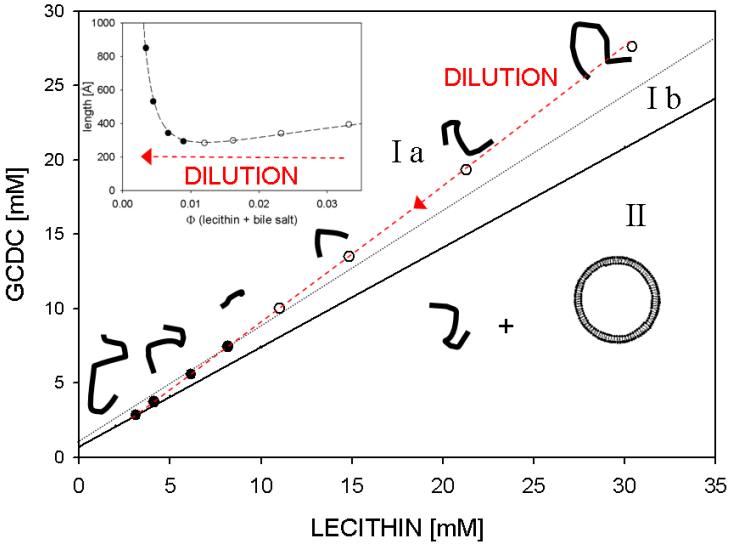

Figure 10.2: Phase diagram for GCDC-lecithin system data from [46], concentration induced growth regime empty circles and dilution induced growth regime filled circles. The dotted line is intended as a guide to the eye to show a possible position of the change from concentration induced growth I a to dilution induced growth I b.

and middle parts are treated separately.

Depending on the choice of the input parameters different behaviour can be observed. Here only the results from one choice of input parameters are summarised, where the agreement with theory and literature data is most complete.

The model shows the difference between the two micellar regions (Ia and Ib) clearly. It is found that in region in the region of dilution induced growth (Ib), the composition of the micelles remains constant i.e. the bile salt surface cover of the endcaps ϕ_e and the middle parts of the micelles ϕ_m are constant, at ϕ_e = 0.8 and ϕ_m = 0.66 (for λ = 0.7 Å^{-1} [43]). The amount of bile salt in the bulk solution remains constant at the CMC; for TCDC this is at 0.71mM. This implies that as the sample is diluted (see dashed line on figure 10.2) some of the bile salt leaves the micelles to maintain a constant bulk concentration, there is less bile salt available for the creation of the endcaps and the micelles have to grow. Effectively, the lecithin to bile salt ratio along the middle part of the micelles is at its maximum for the cylindrical shape, any further loss of bile salt would lead to the formation of vesicles. However as the endcaps are more bile

salt rich, with increased length (and hence fewer endcaps), there is enough bile salt to keep the worm–like shape.

We now consider an increase in the total concentration of lecithin and bile salt (still within the region of dilution induced growth). As the amount of bile salt in the system continues to increase, the micelles initially get shorter. The decrease in the length of the micelles is due to the extra bile salt, which due to entropic (and spontaneous curvature) reasons prefers to sit at the endcaps creating many shorter micelles than to pack into the longer micelles. The micelles continue to get smaller, until a minimum size is reached (defined by packing constrictions of lecithin and bile salt). As the amphiphile concentration continues to increase moving to region of concentration induced growth, the mixed micelles start to grow through concentration induced growth, with simple bile salt micelles forming in solution. The formation of simple micelles at higher surfactant concentrations has been experimentally observed through dialysis experiments [80].

10.2 Kinetic experiments

Although the kinetics of simple micelles has been the subject of some study, the kinetics of mixed micelle systems have received little attention. The dilution of a sample (in the mixed micelle region with dilution induced growth) results in the growth of the worm–like micelles, as shown in figure 10.3.

There existed no suitable stopped flow setup for time resolved SANS experiments (requiring to mix relatively large volumes), which is why I specifically designed and constructed one. The stock solution (with concentrated lecithin and bile salt in buffer) is mixed with buffer in the stopped flow setup, allowing for measurements to start 200ms after initial contact of the two solutions. The setup has been used to follow the growth of the micelles upon dilution, where different initial and final dilutions (and hence sizes) are studied (e.g. in figure 10.3 6.6 - 13.3). In addition to the dilution dependence, experiments were carried out into the effects of changing ionic strength.

Simple micelles (with appreciable CMC) can grow either through monomer exchange through

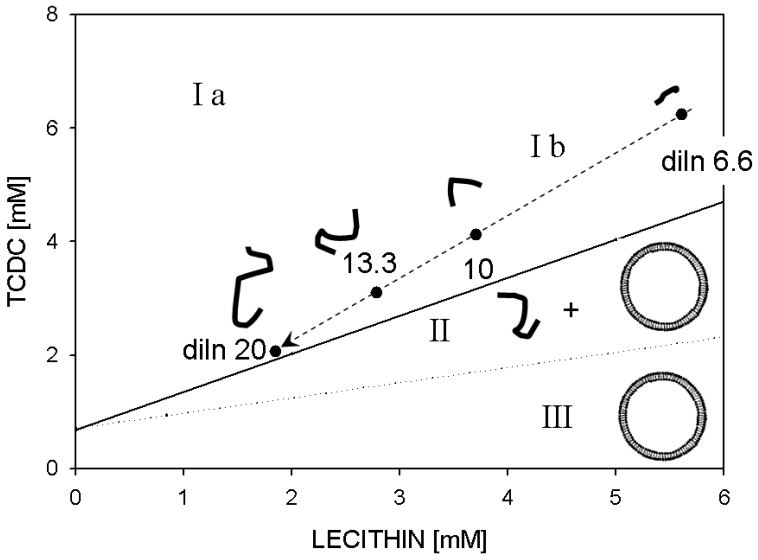

Figure 10.3: The dilution of a sample from dilution 6.6 to 10, 13.3 or 20 is shown by the dashed line on the phase diagram. All the start and end dilutions are within the micellar region in the dilution induced growth part (I b).

the bulk solution or through coalescence. However, due to the low solubility of lecithin it was found that the mixed micelles chiefly grow through coalescence.

It is known that if a sample is diluted as far as into the vesicular region (see figure 10.3 region III), before forming vesicles the worm–like micelles form disc–like micelles as a kinetically metastable structure [64, 57]. However experiments presented in this thesis on the kinetics of worm–like micelles show that these micelles retain the worm–like shape throughout the growth process, with a constant cross–section of the cylindrical parts. This indicates a constant composition of the micelles as changes in the ratio of lecithin to bile salt along the cross–section should change the curvature of the cross–section.

There exists no theory for the growth of mixed worm–like micelles, so the theory developed for single component worm–like micelles was used to analyse the growth in the length of the micelles [29]. This is the first time, that instead of an exponential growth the theoretically predicted tanh behaviour has been used to obtain the time constants τ for the growth of the micelles with good success.

It was found that τ depends only on the difference between the final and initial lengths of

the micelles i.e. it only depends on the length the micelles need to grow to achieve the new equilibrium size. This length dependence combined with a constant initial rate of growth $\delta L/\delta t$ (for a given bile salt species), indicates that the growth process remains the same throughout the growth. This agrees with the constant composition throughout the growth process, where changes in the composition would lead to changes in the electrostatic interactions between the micelles due to the charge on the bile salt.

Using a different bile salt (TC) the growth of the micelles was studied using different amounts of added salt, where it was found that the growth of the micelles is strongly influenced by the ionic strength of the solution as expected for a system with significant electrostatic interactions. The growth can also be fitted with the predicted tanh behaviour with τ increasing dramatically with decreasing ionic strength of the solution. This confirms the importance of electrostatic interactions in the coalescence process.

Appendix A

Wiring Instructions for the Stopped Flow

These instructions are for the wiring of the stopped flow setup for the motors and controllers, switches and communication with PSI software.

This is a summary of the instructions from Baldor manuals, which can be found in the entirety on their website www.supportme.net (to find the full documents go to Documents then Installation Manuals and find *FlexDrive and Flex+Drive Installation Manual*, *NextMove PCI MintMT Installation Manual* and *MN1800 Linear Motors Installation and Operation Manual*).

A schematic wiring diagram is shown in figure A.1.

All the wiring should be done with shielded wires.

A.0.1 Motor Connections

The motors are Baldor motors with Renishaw RG22 linear encoders. The power connections from the motor to the flexdrive are explained in manual MN1902 (page 3-7 and 3-17). The blue and orange wires which are for thermal connections should not be connected to anything only the ends need to be trimmed and covered up. The motors will be disconnected from the

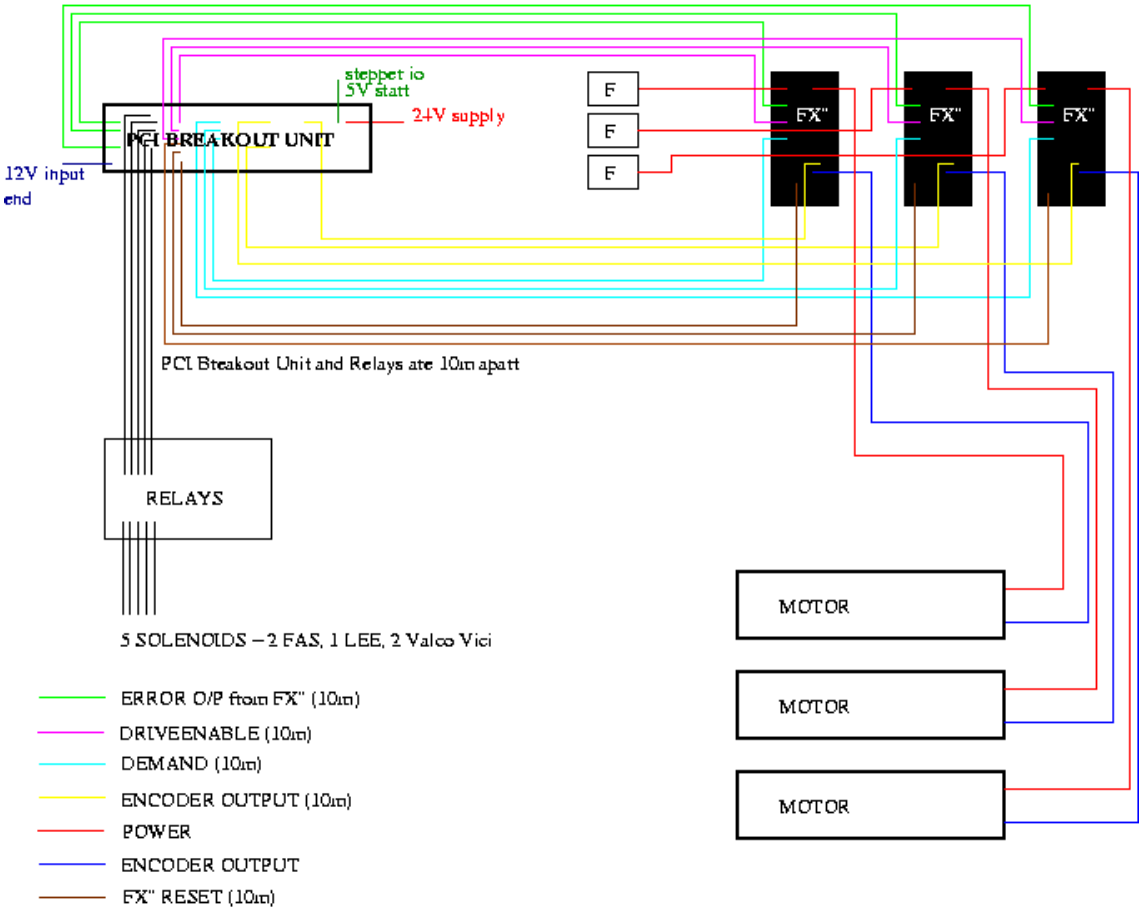

Figure A.1: Schematic diagram for the electric wiring for the stopped flow setup.

FlexDrive units during transport so suitable fittings should be made such that connection and disconnection is simple.

The encoder and feedback connections are detailed in manual MN1902 (pages 3-21 and 3-26). MN1800 (page 2-24) shows signal connections onto the FlexDrive and A5 explains the wire colours from the motor. The wires should be about 2m long.

A.0.2 Power to the Flexdrive

The Flexdrive we have is a single phase model with external AC filters provided. Fuses are installed in the on/off switch box. The connections and accompanying notes refer to MN1902

pages (pages 3-9, 3-11, 3-12 and 3-13), all the power wiring must be screened and earthed.

A.0.3 Encoder output from Flexdrive to Nextmove PCI

These are connected from X7 on the flexdrive to X12, X13 and X14 on the nextmove. The connections for wiring and shielding are detailed in MN1902 (page 4-11). The cables must be 10m long.

A.0.4 Demand Signal

The demand signal should be wired from Nextmove X7 to Flexdrive X3 pins 1&2 for each of the motors. These connections are shown in figure A.2 and should be made such that connection and disconnection are easy, manuals MN1903 (page 4-7) and manual MN1902 (pages 4-2 and 4-3) show details. These wires will also be 10m long. NB Demand 0 (X7-1&2) corresponds to the encoder connection A (X12), Demand 1 (X7-4) for encoder B (X13)and so on.

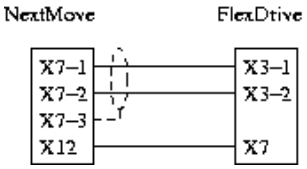

Figure A.2: Demand signal from Nextmove to the Flexdrive encoders.

A.0.5 Drive Enable and Error Output Connections

The drive enable pins on the Flexdrive need to be connected to a 24V supply for the motor to be enabled. This is done by connecting one of the digital outputs (X5) on the nextmove directly to pins 7 & 9 on the flexdrive X3. An example configuration for these connections along with those required for the error output are shown in the figure A.3. Note that the nextmove and flexdrive will be 10m apart.

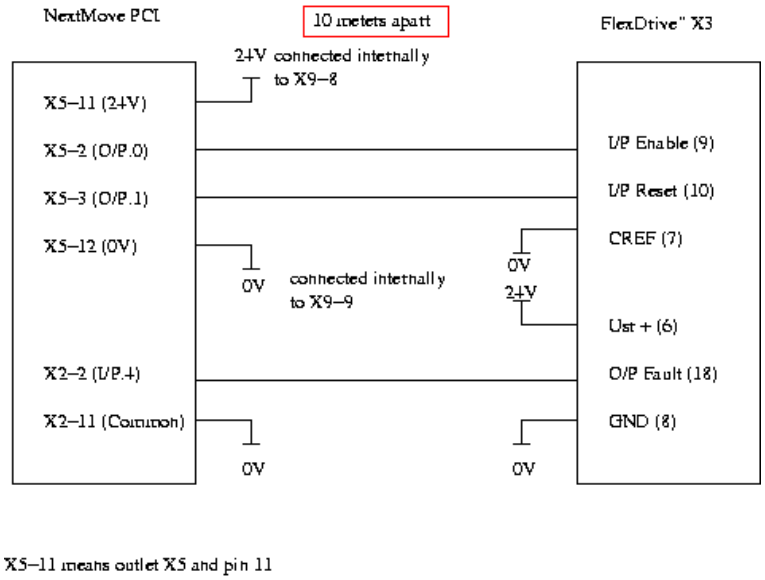

Figure A.3: Connections from NextMove to a single Flexdrive.

In figure A.4 the digital input and output connections from the nextmove are detailed. These will also be used for the control of solenoids and for communication with the PSI control system.

A.0.6 Control of Switches

Only two of the old Fluid Automation Systems' solenoids will be used, and these will be switched using the digital outputs (as shown in earlier diagram) on the nextmove via a relay (as previously). A new 2-way solenoid will arrive from LEE Products and this should be fitted such that it can be controlled using another digital output from the NextMove (through a relay).

There will also be two high pressure switches arriving from Valco Vici and these will be controlled using the NextMove digital outputs.

The relays and the NextMove PCI Board are 10m apart.

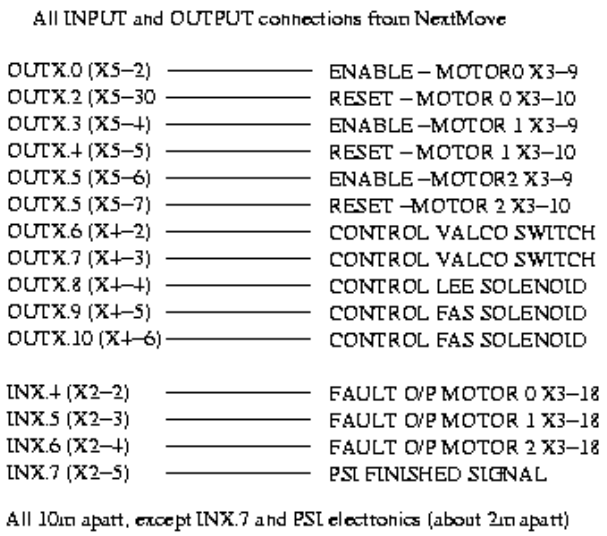

Figure A.4: All inputs and outputs from NextMove.

A.0.7 Communication Between NextMove and PSI Electronics

The stepper output (X10) on the Nextmove will be used for the communication between the Nextmove and PSI Electronics. The stepper output can be be used as a simple 5V output. From the NextMove X10-1 is +5V and X10-3 is GND connect these to standard communications wiring (similar to one on X1-9 and X1-12).

There will also be a 24V signal from the PSI software when the measurement is finished. This will be connected also to one of the digital inputs, INX.19 (connections X1-9 and X1-12).

A.0.8 Power to the NextMove PCI Board

A 24V supply must be attached across X9 pins 8 and 9 as detailed in manual MN1903 (page 4-17). The supply is internally connected to the digital outputs X4 and X5. The external supply ground and the pc ground must be connected together, i.e. pin 9 or 10 to pin 4 or 5.

A.0.9 Earthing

All the parts should be earthed in a suitable way.

Appendix B

Program for running the stopped flow setup

Program used to run the stopped flow setup written in Mint™programming language as provided with the Baldor linear motors. The inputs to the program are the volume of the syringes, the time required for the movement and the number of repeats of the measurement.

There are three motors in the system 0, 1, 2 where 0 and 1 are used for the filling of the cell and 2 is used for the cleaning part. The different switches are controlled using commands OUTX.N, where N is the number of the switch.

The program consists of four parts, the main body of the program, where the input parameters are defined. The shooting section, where the two syringes used for the sample and buffer are filled and emptied into the cell. The cleaning section, where the cell is emptied and cleaned. The final part is the startup block, which is read at the beginning of any program and the motors and controllers are initialised.

```
CANCELALL

Define ALL = 0,1,2
```

```
Define SHOOT = 0,1
’with scale factor 14 working in ul
Dim in_vol1 = 1000
Dim in_vol2 = 1000
Dim in_move_time = 1000
Dim in_cycle = 10
Dim vol_clean = 1800
Dim home_offset = -250

Loop

’set system parameters
Repeat
  Input "Volume syringe 1: ", in_vol1 Using 4,1
Until in_vol1 > 0 And in_vol1 < 1200

Repeat
  Input "Volume syringe 2: ", in_vol2 Using 4,1
Until in_vol2 > 0 And in_vol2 < 1200

Repeat
  Input "Move time: ", in_move_time Using 3,0
Until in_move_time > 10

Repeat
  Input "Number of cycles: ", in_cycle Using 3,0
Until in_cycle < 200

OUTX.9 = 1 ’somewhere for the water to go from syringe 2
OUTX.6 = 1 ’ connected to the bottle
```

```
’OUTX.7 = 0 ’ connected to the bottle

Wait = 2000

DRIVEENABLE[ALL] = 1;
HOME[ALL] = _hmNEGATIVE_INDEX;
Pause IDLE[ALL]
MOVER[ALL] = home_offset;
’MOVER.2 = -500
GO[ALL]
Pause IDLE[ALL]
POS[ALL] = 0;
DRIVEENABLE[ALL] = 0;

OUTX.9 = 0
OUTX.6 = 0
’OUTX.7 = 0

Dim i
For i = 1 To in_cycle
  Inject in_vol1, in_vol2, in_move_time
  Pause INX.18 =0
  Clean
  If InKey = ’S’ Then Exit For
    Next i
  OUTX.6 = 1
  OUTX.9 = 1
  Wait = 2000
    SPEED[SHOOT] = 140.00, 140.00
    ACCEL[SHOOT] = 500.00, 500.00
```

```
    DECEL[SHOOT] = 500.00, 500.00
  DRIVEENABLE[ALL] = 1;
  MOVER[ALL] = 400;
  GO[ALL]
  Pause IDLE[ALL]
  DRIVEENABLE[ALL]=0;
  OUTX.9 = 0
  Wait = 2000
  End Loop

  ’Fill syringes
  Sub Inject (vol1, vol2, move_time)
    Print "Start filling syringes"

    ’Fill cycle - constant speed
    OUTX.6 = 1
    ’outx.7 = 0
    Wait = 3000
    SPEED[SHOOT] = 140.00, 140.00
    ACCEL[SHOOT] = 500.00, 500.00
    DECEL[SHOOT] = 500.00, 500.00

    DRIVEENABLE[SHOOT] = 1;

    MOVER[SHOOT] = vol1, vol2
    GO[SHOOT]
    Pause IDLE[SHOOT]

    ’Empty syringes
    OUTX.6 = 0 ’connected to cell
```

```
’OUTX.7 = 1
Wait = 3000

Print "about to shoot"
SPEED[SHOOT] = 2000*vol1/move_time, 2000*vol2/move_time
ACCEL[SHOOT] = SPEED.0*2000/move_time, SPEED.1*2000/move_time
DECEL[SHOOT] = SPEED.0*2000/move_time, SPEED.1*2000/move_time

CAPTUREMODE.0 = _cpMEASURED_SPEED
CAPTUREMODEPARAMETER.0 = 0
CAPTUREMODE.1 = _cpFOLLOWING_ERROR
CAPTUREMODEPARAMETER.1 = 0
CAPTUREMODE.2 = _cpMEASURED_SPEED
CAPTUREMODEPARAMETER.2 = 1
CAPTUREMODE.3 = _cpFOLLOWING_ERROR
CAPTUREMODEPARAMETER.3 = 1

CAPTUREDURATION = 500
CAPTURE = _capDURATION

MOVER[SHOOT] = -vol1, -vol2
STEPPERIO.0 = 1
GO[SHOOT]
Pause IDLE[SHOOT]

Wait = 500 ’MAYBE MAKE LONGER TO AVOID BOUNCE BACK

DRIVEENABLE[SHOOT] = 0;
OUTX.6 = 1
’OUTX.7 = 0
```

```
    STEPPERIO.0 = 0

    Wait = 10000
  End Sub

  'Clean the cell

  Sub Clean( )
    Print "Start Cleaning"
    DE.2 = 1
    Dim a
    For a = 1 To 1 Step 1

      Dim b
        For b = 1 To 7 Step 1

      'first empty cell
      OUTX.7 = 0 'switch at the top is open
      OUTX.8 = 0 ' solenoid for dirty
      OUTX.9 = 0 'solenoid for clean
      OUTX.10 = 1 'solenoid under the cell
      Wait = 500

      'For 2 accel, decel, speed set to slow in startup
      'can keep the same all the time

      MOVER.2 = vol_clean/2
      GO.2
      Pause IDLE.2
```

```
Wait = 1000

’now empty contents into dirty bottle
OUTX.8  = 1
OUTX.9 = 0
OUTX.10 = 0

Wait = 500

MOVER.2 = -vol_clean/2
GO.2
Pause IDLE.2
Wait = 1000

Next b

Dim c
  For c = 1 To 7 Step 1

’now fill syringe with water
OUTX.8 = 0
OUTX.9 = 1
OUTX.10 = 0

Wait = 500

MOVER.2 = vol_clean/2
GO.2
Pause IDLE.2
```

```
  Wait = 1000

  ’empty water into the cell
  OUTX.8 = 0
  OUTX.9 = 0
  OUTX.10 = 1
  Wait = 500

  MOVER.2 = -vol_clean/2
  GO.2
  Pause IDLE.2

  Wait = 1000

  Next c

Next a

  Dim d
    For d = 1 To 2 Step 1

’after last time filling with water want to just empty and leave it

  OUTX.8 = 0
  OUTX.9 = 0
  OUTX.10 = 1

  Wait = 500
  MOVER.2 = vol_clean/2
  GO.2
```

```
    Pause IDLE.2

    Wait = 1000

    OUTX.8 = 1
    OUTX.9 = 0
    OUTX.10 = 0

    Wait = 500

    MOVER.2 = -vol_clean/2
    GO.2
    Pause IDLE.2

    Wait = 1000

  Next d

  DE.2 = 0
  OUTX.8 = 0
  OUTX.9 = 0
  OUTX.10 = 0
  'outx.7 = 0


End Sub
```

```
Startup


Rem Wednesday, August 13, 2003

'Define ALL = 0, 1, 2
Define SELECTED = 0, 1, 2
Define SERVOS = 0, 1, 2
Define DINBANKS = 0
Define DOUTBANKS = 0
Define ADCS = 0, 1, 2
Define DACS = 0, 1, 2
Define ENCODERS = 0, 1, 2
Define AUXENCODERS = 0

Rem Abort any motion currently in progress

ABORT:Wait = 10
CONFIG[ALL] = _cfOFF;
AXISCHANNEL[ALL] = 0, 1, 2

Rem Define loop times

LOOPTIME = 1000
PROFILETIME = 2000

Rem Define config modes for all axes

CONFIG[SELECTED] = _cfSERVO, _cfSERVO, _cfSERVO
```

```
Rem Initialize the axes

CANCELALL
DRIVEENABLE[SELECTED] = 0;

Rem Digital input configuration

INPUTMODE[DINBANKS] = 0x0
INPUTACTIVELEVEL[DINBANKS] = 0xfffff
INPUTPOSTRIGGER[DINBANKS] = 0x0
INPUTNEGTRIGGER[DINBANKS] = 0x0

Rem Analog input configuration

ADCMODE[ADCS] = 0, 0, 0

Rem Digital output configuration

GLOBALERROROUTPUT = -1
OUTPUTACTIVELEVEL[DOUTBANKS] = 0xfff

Rem Analog output configuration

DACMODE[DACS] = 16, 16, 16

Rem Axis scaling

SCALE[SELECTED] = 11.70, 11.70, 11.70

Rem Axis Error parameters
```

```
ADCERRORMODE[SELECTED] = _emCRASH_STOP_DISABLE, _emCRASH_STOP_DISABLE, _emCRASH_
ERRORINPUTMODE[SELECTED] = _emCRASH_STOP_DISABLE, _emCRASH_STOP_DISABLE, _emCRAS
ABORTMODE[SELECTED] = _emCRASH_STOP_DISABLE, _emCRASH_STOP_DISABLE, _emCRASH_STO
LIMITMODE[SELECTED] = _emCRASH_STOP_DISABLE, _emCRASH_STOP_DISABLE, _emCRASH_STO
SOFTLIMITMODE[SELECTED] = _emIGNORE, _emIGNORE, _emIGNORE
STOPINPUTMODE[SELECTED] = 0, 0, 0
SOFTLIMITFORWARD[SELECTED] = 499321.00, 499321.00, 499321.00
SOFTLIMITREVERSE[SELECTED] = -499321.00, -499321.00, -499321.00
FOLERRORMODE[SERVOS] = _emIGNORE, _emIGNORE, _emIGNORE
FOLERRORFATAL[SERVOS] = 100.00, 100.00, 100.00

Rem Axis Digital input events

ERRORINPUT[SELECTED] = -1, -1, -1
HOMEINPUT[SELECTED] = -1, -1, -1
STOPINPUT[SELECTED] = -1, -1, -1
LIMITFORWARDINPUT[SELECTED] = -1, -1, -1
LIMITREVERSEINPUT[SELECTED] = -1, -1, -1

Rem Axis Drive Output Enables

DRIVEENABLEOUTPUT[SELECTED] = 0, 2, 4

Rem Axis Tuning Parameters

KDERIV[SERVOS] = 0.00, 0.00, 0.00
KINT[SERVOS] = 0.00, 0.00, 0.00
KINTLIMIT[SERVOS] = 100.00, 100.00, 100.00
KINTMODE[SERVOS] = 1, 1, 1
```

```
KPROP[SERVOS] = 0.30, 0.30, 0.30
KVEL[SERVOS] = 0.00, 0.00, 0.00
KVELFF[SERVOS] = 1.46, 1.46, 1.46
KACCEL[SERVOS] = 0.00, 0.00, 0.00

Rem Axis Parameters

PROFILEMODE[SELECTED] = 0, 0, 0
SPEED[SELECTED] = 238.00, 238.00, 238.00
ACCEL[SELECTED] = 1786.00, 1786.00, 1786.00
DECEL[SELECTED] = 1786.00, 1786.00, 1786.00
ERRORDECEL[SELECTED] = 178668.00, 178668.00, 178668.00
ACCELJERK[SELECTED] = 178668.00, 178668.00, 178668.00
DECELJERK[SELECTED] = 178668.00, 178668.00, 178668.00
MOVEBUFFERSIZE[SELECTED] = 2, 2, 2
HOMEBACKOFF[SELECTED] = 1.00, 1.00, 1.00
HOMESPEED[SELECTED] = 59.00, 59.00, 59.00
IDLEPOS[SERVOS] = 59.00, 59.00, 59.00
IDLEVEL[SERVOS] = 298.00, 298.00, 298.00
BACKLASHMODE[SERVOS] = 0, 0, 0
BACKLASH[SERVOS] = 0.00, 0.00, 0.00, 0.00
BACKLASHINTERVAL[SERVOS] = 50, 50, 50, 50

Rem Encoder configuration

ENCODERSCALE[ENCODERS] = 1.00, 1.00, 1.00
ENCODERWRAP[ENCODERS] = 0.00, 0.00, 0.00
ENCODERMODE[ENCODERS] = 0, 0, 0

Rem Aux Encoder configuration
```

```
AUXENCODERSCALE[AUXENCODERS] = 1.00
AUXENCODERWRAP[AUXENCODERS] = 0.00
AUXENCODERMODE[AUXENCODERS] = 0

End Startup
```

List of Figures

List of Tables

Bibliography

[1] C. Tanford. *The hydrophobic effect: Formation of micelles and biological membranes*. Krieger Publishing Company, 2nd edition edition, 1991.

[2] H. Diamant D. Andelman. Kinetics of surfactant adsorption at fluid-fluid interfaces. *J. Phys. Chem*, 100:13732–13742, 1996.

[3] J. T. Davies. Adsorption of long-chain ions. I. *Proc. R. Soc. London, Ser. A*, 245:417, 1958.

[4] J. Israelachvili. *Intermolecular and Surface Forces*. Academic Press, 2nd edition edition, 1992.

[5] D. Fennell Evans H. Wennerström. *The colloidal domain where physics, chemistry, biology, and technology meet*. VCH Publishers Inc, 1994.

[6] P-G. de Gennes. *Scaling concepts in polymer physics*, chapter 8. Cornell University Press, 1979.

[7] M. E. Cates S. J. Candau. Statics and dynamics of worm-like surfactant micelles. *J. Phys. Cond. Matt.*, 2:6869–6892, 1990.

[8] A. Bernheim-Groswasser R. Zana Y. Talmon. Sphere-to-cylinder transition in aqueous micellar solutuion of dimeric (gemini) surfactant. *J. Phys. Chem. B*, 104:4005–4009, 2000.

[9] T. Kato M Kanada T Seimiya. Measurements of lights scattering intensitites on extremely dilute solutions of nonionic surfactant. *Langmuir*, 11:1867–1869, 1995.

[10] P. van der Schoot. Equilibrium charge distribution on linear micelles. *Langmuir*, 13:4926–4928, 1997.

[11] F. Mackintosh S. A. Safran P. A. Pincus. Self-assembly of linear aggregates: the effect of electrostatics on the growth. *Europhys. Lett.*, 12:697–702, 1990.

[12] G. Porte J. Appell Y. Poggi. Experimental investigations on the flexibility of elongated cetyopyridinium bromide micelles. *J. Phys. Chem*, 84:3105–3110, 1980.

[13] G. Porte P. Marignan P. Bassereau R. May. Shape transformations of the aggregates in dilute surfactant solutions: a small-angle neutron scattering study. *J. Phys. France*, 49:511–519, 1988.

[14] J. Appell J. Marignan. Structure of giant micelles: a small angle neutron scattering study. *J. Phys. 2 France*, 1:1447–1454, 1991.

[15] M. E. Cates C. M. Marques J-P. Bouchaud. Dynamic relaxation of rodlike micelles. *J. Chem. Phys.*, 94:8529–8536, 1991.

[16] R. J. Hunter, editor. *Foundations of Colloid Science*. Oxford University Press, New York, 1987.

[17] J. Lang C. Tondre R. Zana. Chemical relaxation studies on micellar equilibria. *J. Phys. Chem*, 79:276–283, 1975.

[18] T. Telgmann U. Kaatze. On the kinetics of the formation of small sicelles. 1. Broadband ultrasonic absorption spectrometry. *J. Phys. Chem. B*, 101:7758–7765, 1997.

[19] T. Telgmann U. Kaatze. On the kinetics of the formation of small micelles. 2. Extension of the model for stepwise association. *J. Phys. Chem. B*, 101:7766–7772, 1997.

[20] C. Trachimow L. De Meyer U. Kaatze. Extremely slow reaggregation processes in micelle solutions. a dynamic light scattering study. *J. Phys Chem B*, 102:4483–4487, 1998.

[21] E. A. G. Aniasson S. N. Wall. On the kinetics of step-wise micelle association. *J. Phys. Chem*, 78:1024–1030, 1974.

[22] E. A. G. Aniasson S. N. Wall. Correction and improvement on: "On the kinetics of step-wise micelle association". *J. Phys. Chem*, 79:857–858, 1975.

[23] E. A. G. Aniasson S. N. Wall M. Almgren H. Hoffmann I. Kielmann W. Ulbricht R. Zana J. Lang C. Tondre. Theory of the kinetics of micellar equilibria and quantitative interpretation of chemical relaxation studies of micellar solutions of ionic surfactants. *J. Phys. Chem*, 80:905–922, 1976.

[24] L. De Meyer C. Trachimow U. Kaatze. Simulation study to model extremely slow reaggregation processes in micelle solutions. *J. Phys Chem B*, 102:8024–8028, 1998.

[25] E. Lessner M. Teubner M. Kahlweit. Relaxation experiments in aqueous solutions of ionic micelles. 1. Theory and experiments on the system H2O-sodium tetradecyl sulfate-NaCIO4. *J. Phys. Chem*, 85:1529–1536, 1981.

[26] M. Kahlweit. Kinetics of formation of association colloids. *J. Coll. Int. Sci.*, 90:92–99, 1981.

[27] E. Lessner M. Teubner M. Kahlweit. Relaxation experiments in aqueous solutions of ionic micelles. 2. Experiments on the system H_20-NaDS-$NaClO_4$ and their theoretical interpretation. *J. Phys. Chem*, 85:3167–3175, 1981.

[28] M. S. Turner M. E. Cates. The relaxation spectrum of polymer length distributions. *Journal de Physique*, 51:307–316, 1990.

[29] C. M. Marques M. E. Cates. Nonlinear thermodynamic relaxation of living polymers. *J. Phys. 2 France*, 1:489–492, 1991.

[30] D. M. Small. *The physical chemistry of cholanic acids. In The Bile Acids - Chemistry, Physiology and Metabolism*, chapter 8. Plenum Press, New York, 1973.

[31] M. C. Carey D. M. Small. Physical chemistry of cholesterol solubility in bile. relationship to gallstone formation and dissolution in man. *J. Clin. Invest.*, 61:998–1026, 1978.

[32] M. C. Carey. *Bile acids in health and disease*, chapter Lipid solubilisation in bile. Kluwer Academic Publishers, 1988.

[33] W. Taylor. The biliary system. *J. Phys Chem*, 96:165, 1965.

[34] F. D. Gunstone J. L. Harwood F. B. Padley, editor. *The Lipid Handbook*. Chapman and Hall, 1994.

[35] A. Kuksis. The biliary system. *Biochim. et Biophys. Acta*, 1124:205, 1992.

[36] B. A. Cornell J. Middlehurst F. Separovic. The molecular packing and stability within highly curved phospholipid bilayers. *Biochim. Biophys. Acta*, 598:405–410, 1980.

[37] D. M. Small. Phase equilibria and structure of dry and hydrated egg lecithin. *J. Lipid Res.*, 8:551–557, 1967.

[38] W. Känzig P. Schurtenberger N. Mazer. Static and dynamic light scattering studies of micellar growth and interactions in bile-salt lecithin solutions. *J. Phys. Chem*, 87:308–315, 1983.

[39] M. Janich J. Lange H. Graener R. Neubert. Extended light scattering investigations on dihydroxy bile salt micelles in low-salt aqueous solutions. *J. Phys Chem B*, 102:5957–5962, 1998.

[40] D. M. Small M. C. Bourgès D. G. Dervichian. The biophysics of lipid associations 1. The ternary systems lecithin-bile salt-water. *Biochim. et Biophys. Acta*, 125:563–580, 1966.

[41] B. Angelov M. Ollivon A. Angelova. X-ray diffraction study of the effect of the detergent octyl glucoside on the structure of lamellar and nonlamellar lipid/water phases of use for membrane protein reconstitution. *Langmuir*, 15:8225–8234, 1999.

[42] L. Arleth M. Bergström J. S. Pedersen. Small-angle neutron scattering study of the growth behaviour, flexibility, and intermicellar interactions of wormlike SDS micelles in NaBr aqueous solutions. *Langmuir*, 18:5343–5353, 2002.

[43] S. U. Egelhaaf P. Schurtenberger. Shape transformations in the lecithin-bile salt system: From cylinders to vesicles. *J. Phys. Chem.*, 98:8560, 1994.

[44] M. Ollivon S. Lesieur C. Grabielle-Madelmont M. Paternostre. Vesicle reconstitution from lipid-detergent mixed micelles. *Biochim. et Biophys. Acta*, 1508:34–50, 2000.

[45] W. Känzig P. Schurtenberger N. Mazer. Micelle to vesicle transition in aqueous solutions of bile salt and lecithin. *J. Phys. Chem*, 89:1042–1049, 1985.

[46] L. Arleth R. B. Bauer L. H. Øgendal S. U. Egelhaaf P. Schurtenberger J. S. Pedersen. Growth behaviour of mixed wormlike micelles: A small-angle scattering study of the lecithin-bile salt system. *Langmuir*, 19:4096–4104, 2003.

[47] Y. Roth E. Opatowski D. Lichtenberg M. M. Kozlov. Phase behaviour of dilute aqueous solutions of lipid-surfactant mixtures: effects of finite size of micelles. *Langmuir*, 16:2052–2061, 2000.

[48] D. Andelman M. M. Kozlov W. Helfrich. Phase transitions between vesicles and micelles driven by competing curvatures. *Europhys. Lett.*, 25:231–236, 1994.

[49] D. Lichtenberg. Characterization of the solubilization of lipid bilayers by surfactatnts. *Biochim. et Biophys. Acta*, 821:470–478, 1985.

[50] E. Opatowski M. M. Kozlov D. Lichtenberg. Partitioning of octyl glucoside between octyl glucoside phosphatidylcholine mixed aggregates and aqueous media as studied by isothermal titration calorimetry. *Biophys. J.*, 73:1448–1457, 1997.

[51] D. Lichtenberg E. Opatowski M. M. Kozlov. Phase boundaries in mixtures of membrane-forming amphiphiles and micelle-forming amphiphiles. *Langmuir*, 16:6431–6437, 2000.

[52] J. S. Pedersen S. U. Egelhaaf P. Schurtenberger. Formation of polymerlike mixed micelles and vesicles in lecithin - bile salt solutions: A small-angle neutron scattering study. *J. Phys Chem*, 99:1299–1305, 1995.

[53] R. P. Hjelm Jr. P. Thiyagarajan H. Alkan-Onyuksel. Organization of phosphatidylcholine and bile salt in rodlike micelles. *J. Phys. Chem.*, 96:8653–8661, 1992.

[54] S. A. Safran P. Pincus D. Andelman. Theory of spontaneous vesicle formation in surfactant mixtures. *Science*, 248:354–356, 1990.

[55] S. A. Safran P. Pincus D. Andelman F. C. MacKintosh. Stability and phase behaviour of mixed surfactant vesicles. *Phys. Rev. A*, 43:1071–1078, 1991.

[56] J. Leng S. U. Egelhaaf M. E. Cates. Kineticpathway of spontaneous vesicle formation. *Europhys. Lett.*, 59:311–317, 2002.

[57] J. Leng S. U. Egelhaaf M. E. Cates. Kinetics of the micelle-to-vesicle transition: Aqueous lecithin-bile salt mixtures. *Biophys. J.*, 85:1624–1646, 2003.

[58] P. Lesieur M. A. Kiselev L. I. Barsukov D. Lombardo. Temperature-induced micelle to vesicle transition: kinetic effects in the DMPC/NaC system. *J. App. Cryst.*, 33:623–627, 2000.

[59] J. Ulmius G. Lindblom H. Wennerström L. B-Å. Johansson K. Fontell O. Söderman G. Arvidson. Bdkaljlkj. *J. Coll. Int. Sci.*, 21:1553–1560, 1982.

[60] J. W. Nichols J. Ozarowski. Sizing of lecithin-bile salt mixed micelles by size-exclusion high-performance liquid chromatography. *Biochemistry*, 29:4600–4606, 1990.

[61] M. C. Carey D. M. Small. Micelle formation by bile salts. Physical-chemical and thermodynamic considerations. *Arch. Intern. Med.*, 130:506–527, 1972.

[62] D. Meyuhas A. Bor I. Pinchuk A. Kaplun Y. Talmon M. M. Kozlov D. Lichtenberg. Effect of ionic strength on the self-assembly in mixtures of phosphatidylcholine and sodium cholate. *J. Coll. Int. Science*, 188:351–362, 1997.

[63] M. Gradzielski. Kinetics of morphological changes in surfactant systems. *Current Opinion in Colloid and Interface Science*, 8:337–345, 2003.

[64] S. U. Egelhaaf P. Schurtenberger. Micelle-to-vesicle transition: A time-resolved structural study. *Phys. Rev. Lett.*, 82:2804–2807, 1999.

[65] St. Schmölzer D. Gräbner M. Gradzielski T. Narayanan. Millisecond-range time-resolved small-angle X-ray scattering studies of micellar transformations. *Phys. Rev. Lett.*, 88:art. no. 258301, 2002.

[66] W. B. Russel D. A. Saville W. R. Schowalter. *Colloidal Dispersions*. Cambridge University Press, 1991.

[67] Y. Kozlovsky M. M. Kozlov. Stalk model of membrane fusion: solution of energy crisis. *Biophys. J.*, 82:882–895, 2002.

[68] R. L. White. On the deryaguin approximation for the interaction of macrobodies. *J. Coll. Int. Science*, 95:286–288, 1983.

[69] P. Hänggi P. Talkner M. Borkovec. Reaction-rate theory: fifty years after Kramers. *Reviews of Modern Physics*, 62(2):251–341, 1990.

[70] P. Lindner Th. Zemb, editor. *Neutrons, X-rays and Light, Scattering Methods Applied to Soft Condensed Matter*. Elsevier Science, 2002.

[71] J. S. Higgins H. C. Benoit. *Polymers and Neutron Scattering*. Oxford University Press, 1994.

[72] J. S. Pedersen P. Schurtenberger. Scattering functions of semiflexible polymers with and without excluded volume interactions. *Macromolecules*, 29:7602–7612, 1996.

[73] T. Yoshizaki H. Yamakawa. Scattering functions of wormlike and helical wormlike chains. *Macromolecules*, 13:1518–1525, 1980.

[74] V. M. Garamus J. S. Pedersen H. Kawasaki H. Maeda. Scattering from polymerlike micelles of tdao in salt/water solutions at semidilute concentrations. *Langmuir*, 16:6431–6437, 2000.

[75] J. S. Pedersen P. Schurtenberger. Static properties of polystyrene in semidilute solutions: A comparison of monte carlo simulations and small-angle neutron scattering results. *Europhys. Lett.*, 45:666–672, 1999.

[76] M. C. Carey D. M. Small. Studies on simple and mixed bile salt micelles by nuclear magnetic resonance spectroscopy. *Biochim. et Biophys. Acta*, 176:178–189, 1969.

[77] C. Huang J. T. Mason. Geometric packing constraints in egg phosphatidylcholine vesicles. *Proc. Natl. Acad. Sci. USA*, 75:308–310, 1978.

[78] H. Matsuoka J. P. Kratohvil N. Ise. Small-angle x-ray scattering from solutions of bile salts: sodium taurodeoxycholate in aqueous electrolyte solutions. *J. Colloid Interface Sci.*, 118:387–396, 1987.

[79] K. S. Schweizer J. G. Curro. PRISM theory of the structure, thermodynamics, and phase-transitions of polymer liquids and alloys. *Advances in Polymer Science*, 116:319–377, 1994.

[80] W. C. Duane. Taurocholate- and taurochenodeoxycholate-lecithin micelles: The equilibrium of bile salt between aqueous phase and micelle. *Biochem. Biophys. Research Communications*, 74:223–229, 1977.

[81] W. Shankland. The equilibrium and structure of lecithin-cholate mixed micelles. *Chem. Phys. Lipids*, 4:109–130, 1970.